DESIGN OF FUNCTIONAL MATERIALS VIA EMULSION TEMPLATING:

ENERGY AND BIOMEDICAL APPLICATIONS

DERYA AYDIN

KOC UNIVERSITY

JUNE, 2017

Design of Functional Materials via Emulsion Templating

Energy and Biomedical Applications

by

Derya Aydın

A Thesis Submitted to the

Graduate School of Sciences and Engineering

in Partial Fulfillment of the Requirements for

the Degree of

Doctor of Philosophy

in

Chemical and Biological Engineering

June 22, 2017

Design of Functional Materials via Emulsion Templating:

Energy and Biomedical Applications

Koc University

Graduate School of Sciences and Engineering

This is to certify that I have examined this copy of a doctoral dissertation by

Derya Aydın

and have found that it is complete and satisfactory in all respects,

and that any and all revisions required by the final

examining committee have been made.

Committee Members:

Assoc. Prof. Seda Kızılel (Advisor)

Prof. Burak Erman

Prof. M. Levent Demirel

Prof. Ebru Toksoy Öner

Assoc. Prof. Başak Kayıtmazer

Date: 22.06.2017

To my family &

To the memory of my grandmother

ABSTRACT

Incorporating functional materials into immiscible mediums has been a conventional challenge in materials science. Solid structures are formed via templating stable liquid emulsions to overcome this challenge. In the first part of thesis, we designed a composite membrane via Pickering Emulsion templating, which integrates a hydrophobic styrene-butediene-styrene (SBS) polymer phase and hydrophilic agar phase that incorporates ionic salts for anti-icing property on bitumen surfaces. We demonstrated significant freezing delay with composite-modified bitumen compared to base bitumen in different temperature controlled chambers with temperatures of -14 and -2 °C. In addition, we investigated morphological and salt release properties of composite modified bitumen and observed potassium formate release for 67 days. Furthermore, we investigated altered ionic salts consisting of potassium formate, sodium chloride or magnesium chloride. These results are promising and suggest the potential of this polymer composite-modified bitumen for anti-icing functionality and for industrially relevant applications.

In seond part of thesis, we synthesized polyethylene glycol (PEG) nanospheres via water-in-water emulsion templating method based on phase separation of dextran and PEG prepolymer and achieved the synthesis of nano-scale PEG hydrogel particles for biomedical applications. Next, we investigated the release kinetics of a model drug, pregabalin from PEG nanospheres. In the last part, we synthesized photocrosslinked SBS network and designed SBS-PEG hybrid gels for sustained drug release purposes. We achieved extended release of anti rheumatoid arthritis drug from SBS-PEG gels up to 28 days. Cell-survival assay suggested that PEG nanospheres and SBS-PEG gels are non-toxic, and can be considered for controlled drug/molecule delivery.

ÖZET

İşlevsel malzemeleri birbiriyle karışmadığı ortamlara karıştırmak malzeme biliminde alışılagelmiş bir zorluktur. Bu durumla başa çıkmak için kararlı emülsiyonlar kalıp olarak kullanarak katı yapılar oluşturulabilir. Tezin ilk kısmında, Pickering emülsiyon kalıplama yoluyla, asfalt yüzeylerde buzlanma-karşıtı özellik için hidrofobik stiren-bütadien-stiren (SBS) polimerini iyonik tuzları içeren hidrofilik agar fazına entegre eden bir bileşim membran tasarladık. Bileşim modifiye bitümde -2 ve -14 °C sıcaklıklardaki farklı sıcaklık kontrollü odalarda normal bitüme nazaran önemli derecede buzlanmada gecikme olduğunu ispatladık. Ayrıca bileşim modifiye bitümün biçimsel ve tuz salım özelliklerini inceledik ve 67 gün boyunca potasyum format salımı gözlemledik. Dahası magnezyum klorür ve sodyum klorür içeren değişik iyonik tuzları da inceledik. Bu sonuçlar umut vericidir ve bu bileşim modifiye bitümüm buzlanma karşıtı ve endüstriyle alakalı uygulamalardaki potansiyelini gösterir.

Tezin ikinci kısmında, biyomedikal uygulamalar için su-içinde-su (s/s) emülsiyon kalıplama yöntemiyle, dekstran ve polietilen glikol (PEG)'in faz ayrımına dayanarak nanoküre PEG sentezini araştırdık ve biyomedikal uygulamalar için nano-skala PEG nanoküresi sentezini başardık. Bundan sonra, model ilaç pregabalinin nanokürelerden salım kinetiğini araştırdık. Tezin son kısmında, çaprazbağlı SBS ağı sentezledik ve sürdürülebilir ilaç salımı için SBS-PEG hibrit jelleri tasarladık. Eklem iltihabı ilacının SBS-PEG hibrit jellerden 28 güne kadar uzatılmış olan salımını başardık. Hücre canlılığı testleri PEG nanokürelerin ve SBS-PEG hibrit jellerin toksik olmadığını ve kontrollü ilaç/molekül dağıtımında kullanılabileceğini gösterdi.

ACKNOWLEDGEMENT

Firstly, I would like to thank my advisor Assoc. Prof. Seda Kızılel for her continous guidance and support during my Ph.D. studies. It is an honor and great pleasure for me to meet and work with her.

I owe special thanks to my thesis commitee Prof. Burak Erman, Prof. A. Levent Demirel, Prof. Ebru Toksoy Öner, and Assoc. Prof. Başak Kayıtmazer for sparing their precious time for me.

I would like to thank the Koç University, Vehbi Koç Foundation, TÜPRAŞ and GENERALI for their financial support during my Ph.D. studies.

I am thankful to Selin Kanyas, Doğan Gidon, M. Birgul Akolpoglu and Ramazan Oğuz Canıaz for their contributions to my Ph.D. studies. I am also grateful to my colleagues Tuğba Bal, Rubab Batool, Pelin Erkoç, Dilem Ceren Oran, Uğur Bozüyük and Onur Özer for their friendships and accompanying me in good and bad. I thank to Vahid Pour Reza Ghoushchi, Murat Gözüm, Amirreza Aghakhani, Orkun Önal, Günce Ezgi Cinay, Seyhan Uçar and other friends in Koç University has also made available their precious friendship. Gizay Büyükdoğanay, Kaan Büyükdoğanay and Fatma Tatar has made their support available during my education as a good and trustworthy friend.

Last but definitely not the least, I wish to thank my mother, my father and my brothers for the endless support they have given. Without them, I could not be what I am today.

TABLE OF CONTENTS

List of Tables **x**

List of Figures **xi**

Nomenclature **xvi**

Chapter 1: Introduction 1

Chapter 2:Literature review 5

2.1. Synthesis of Materials via Emulsion templating 5

2.1.1 Definition and classification of emulsions 5

2.1.2. Emulsion templating 5

2.1.3 Emulsion Stabilization Methods 6

2.1.4 Water in water emulsions 10

2.2. Approaches for anti-icing surfaces 11

2.2.1. Morphological approach 12

2.2.2 Chemical approach 14

2.3. Anti-icing functionality on asphalt roads 16

2.4. Polymer Modification of Asphalt binders 18

2.4.1. Rheological characterization of bitumen 20

2.5. Synthesis of PEG nanogels via water-in-water emulsions for drug delivery applications 22

2.5.1 Hydrogel microspheres 22

2.5.2. Synthesis of hydrogel micro/nanospheres for drug delivery purposes 24

2.5.4. Micro-nanospheres for controlled drug delivery 27

2.5.5. Factors that affect drug release rates 27

2.6. Consideration of SBS for biomedical applications 28

2.6.2. SBS for biomedical applications 29

2.6.3. Crosslinking of SBS 29

2.6.4. Photo-initiated thiol-ene reactions 30
Chapter 3: Synthesis and Characterization of Functional Polymer Composite 32
3.1. Introduction 32
3.2. Materials and Methods 34
3.2.1. Materials 34
3.2.2. Preparation of Functional polymer Composite 34
3.2.2.5. Salt release characterization 36
3.2.6. Anti-icing property characterization 36
3.3. Results and Discussion 37
3.3.1. Comparison of emulsion stabilization methods 38
3.3.2 Dynamic Mechanical Analysis 40
3.3.2. Salt release measurements of functional dry composite membranes 42
3.3.3. Anti-icing properties of functional dry composite membranes 44
3.4. Conclusion 45
Chapter 4: Design of Functional Polymer Composite Modified Bitumen 47
4.1. Introduction 47
4.2. Materials and Methods 49
4. 2.1. Materials 49
4.2.2. Preparation of composite-modified bitumen 50
4.2.3. Surface characterization of composite-modified bitumen 51
4.2.4. Dynamic mechanical analysis 51
4.2.5. Characterization of Functional Properties 52
4.3. Results and Discussion 52
4.3.1. Dynamic Mechanical Analysis 52
4.3.2. Morphological characterization of modified bitumen 57
4.3.3. Characterization of anti-icing properties 61
4.3.4. Characterization of salt release from composite-modified bitumen 66
4.3.5. Characterization of rheological properties in repeating temperature oscillations 68
4.4. Conclusions 69
Chapter 5: Comparison of different ionic salts for composite-modified bitumen 71
5.1. Introduction 71
5.2. Methods and Results 72
5.2.1. Materials 72

5.2.2. Preparation of Composite Modified Bitumen 72
5.2.3. Surface characterization of composite-modified bitumen 74
5.2.4. Rheological Characterization of composite-modified bitumen 79
5.2.5. Anti-icing property characterization 80
5.5. Conclusion and Futurework 83
Chapter 6: Water-in-water emulsion based synthesis of nanospheres with tunable drug release properties 85
6.1. Introduction 85
6.2.1. Materials 87
6.2.2. Synthesis of Nanospheres 87
6.2.3. Structural, chemical and physical characterization of nanospheres 89
6.2.4. Pregabalin loading and release experiments 90
6.2.5. Model Fitting 90
6.2.6. Biocompatibility tests 92
6.3. Results and Discussion 92
6.3.1 PGB loading into PEG nanospheres 97
6.3.2. PGB release from PEG nanospheres 98
6.3.3. Model Fitting Results 100
6.3.4. Biocompatibility test of PEG nanospheres 103
6.4. Conclusion 105
Chapter 7: Cross-linked SBS-PEG hybrid gels for sustained drug release purposes 106
7.1 Introduction 106
7.2. Materials and Methods 108
7.2.2. Synthesis of PEG particles and SBS-PEG gels 108
7.3. Results and discussion 112
7.3.1. Synthesis and characterization of PEG particles 112
7.3.2. Synthesis and characterization of SBS-PEG hybrid gels 114
7.3.3. Nano-indentation tests 120
7.3.4. AZ11657312 release from PEG particles and SBS-PEG gels 122
Chapter 8: Conclusion and Futurework 127
Bibliography 131
Vita 142

LIST OF TABLES

Table 2 1: Solubilities of different salts at 25 °C [68]. 15
Table 3. 1: Concentrations of potassium formate in water released from dry composite membranes with geltaion of the internal phase in different time periods…… 42

Table 3. 2: Initial amounts of potassium formate encapsulated in the dry composite membranes with gelation of the internal phase. 44
Table 4. 1: Description of the sets studied for characterization of mechanical and anti-icing properties. 53
Table 5. 1: Expected freezing point decrease values of aqueous phase in emulsions with 0.3 g/ml concentration according to Equation 2.7. 82
Table 6. 1: Description of the sets studied for characterization of size and morphology of PEG hydrogel particles. 95
Table 6. 2: PGB loading efficiencies of the samples. 98
Table 6. 3: Model fit results of PGB release data estimated from stretched exponential model (equation 6.4). 102
Table 7. 1: Average modulus and average hardness of SBS and SBS-PEG gels calculated from load-displacement curves by using Oliver-Pharr method. 122

LIST OF FIGURES

Figure 2. 1: Schematic of SDS and surfactant stabilization. 7
Figure 2. 2: Contact angle (up) and corresponding probable spherical particles positioning (down) of at the oil-water interface when contact angle θ<90° and θ>90° adapted from [32]. 9
Figure 2. 3: Definition of different contact angles a) Contact angle on ideal surface called as Young contact angle, b) Contact angle on rough surface called as Wenzel contact angle and c) Contact angle called Cassie- Baxter 13
Figure 2. 4: Behaviour of water molecules in a) absence and b) presence of salt. 15
Figure 2. 5: Number of accidents happened in different wet road conditions according to Turkish Traffic Accident Statistics of 2013. 16
Figure 2. 6: Morphologies of SBS modified bitumen (5 %wt.) with a) different heating termal histories and b) different types of bitumen (magnification = 50x). Reprinted from [88] with permisson from NRS Annual Transaction. 19
Figure 2. 7 Isochronal plots of a) complex modulus and b) phase angle at 0.02 Hz for SBS modified bitumens. Reprinted from [89] with permisson from Elsevier. 21
Figure 2. 8: Schematic of synthesis of polymer microspheres water-in-water emulsion method. 25
Figure 2. 9: Schematic of synthesis of polymer microspheres Pickering emulsion method. 27
Figure 2. 10: Schematic representation of SBS triblock copolymer. 28
Figure 3. 1: Measurement of K+ ions released from dry composite membranes immersed in water. 36
Figure 3. 2: Monitoring of freezing delays on composite membranes in temperature and humidity controlled chamber. 37
Figure 3. 3: Schematic representation of the steps for casting of solutions prepared with aqueous KCOOH solution suspended in SBS polymer with particle stabilization. 38
Figure 3. 4: Optical microscope images of wet emulsions and their macroscopic appearance with internal volume fraction Q =25% (v/v) prepared by different stabilization methods for immediately after and 3 minutes after preparation of emulsions. (a) Wet emulsions without stabilizing agent, (b) wet emulsions prepared with SDS surfactant as the

stabilizing agent, (c) wet emulsions prepared by nanoparticle stabilization. Scale bar is 500 mm. 39
Figure 3. 5: Optical microscope images of dry membranes of emulsions prepared a) without agar gel in the dispersed phase, b) with agar gel in the dispersed phase. Scale bar is 100 μm. 40
Figure 3. 6: Dynamic mechanical analysis of emulsions prepared with or without agar. Plots of a) Complex modulus, b) Phase angle and c) Dynamic viscosity with temperature ramp at 1 Hz. d) Plots of dynamic viscosity with angular frequency ramp at 25 °C..... 41
Figure 3. 7: Effect of internal phase volume fraction and nanoparticle concentration on profile of potassium formate release from dry composite membranes with gelation of the internal phase. 43
Figure 3. 8: Average freezing times of 10 water droplets on dry composite membranes with gelation of the internal phase, SBS (control) and SBS with 1.0 % nanoparticle concentration (control).The inset figure is from one of the experiments after 60 minutes where the composite with 1 % (w/v) nanoparticle concentration (left, ϕ =0.25) and 0.7 % (w/v) nanoparticle concentration (right, ϕ =0.25) are monitored in humidity and temperature controlled chamber (plate temperature: -14 °C, ambient temperature: 5 °C). 44
Figure 4. 1: A schematic of the preparation of composite polymer-modified bitumen. 51
Figure 4. 2: Isochronal plots of the complex modulus, G* at 0.02 Hz for SBS and composite-modified bitumen. 55
Figure 4. 3: Isochronal plots of the phase angle at 0.02 Hz for SBS and composite-modified bitumen. 57
Figure 4. 4 Morphological analysis of SBS and composite-modified bitumen with fluorescence microscopy (scale bar: 100 μm). 58
Figure 4. 5: AFM phase difference (left) and topographic image (right) of a) base bitumen b) dry composite (with agar)-modified bitumen (5% (wt/wt)) c) dry composite (without agar)-modified bitumen (5% (wt/wt)) d) SBS polymer modified bitumen (5% (wt/wt)). 60
Figure 4. 6: Surface images of base bitumen and composite (with agar)-modified bitumen (7.5% (wt/wt)) in a humidity and temperature controlled chamber at different time points (Plate temperature: -14 °C, medium temperature: 5-6 °C and relative humidity: 50%). 62

Figure 4. 7: Freezing delays on surfaces of base and composite-modified bitumen (5% (wt/wt)) with different salt content in humidity and temperature controlled chamber (Plate temperature: -14 °C, medium temperature: 5-6 °C and relative humidity: 50%). 63
Figure 4. 8: Freezing delays on the surfaces of base, composite (with agar) and composite (no agar)- modified bitumen (5% (wt/wt)) in a humidity and temperature controlled chamber (Plate temperature: -14 °C, medium temperature: 5-6 °C and relative humidity: 50%). 65
Figure 4. 9: Time dependent release of HCOOK from composite-modified bitumen samples. 67
Figure 4. 10: Fluorescent images of a) composite (no agar)-modified bitumen (5% (wt/wt)), b) composite (with agar)-modified bitumen (5% (wt/wt)), c) composite (no agar)-modified bitumen (7.5% (wt/wt)) (scale bar: 100 μm). 67
Figure 4. 11: Change of complex modulus of composite modified bitumen with three cycle of temperature changes between -10, 25 and 70 °C. 69
Figure 5. 1: Schematic of composite coating of bitumen surfaces……. 74
Figure 5. 2: Images of emulsion, composite and composite modified bitumen for different salts. a) Macroscopic appearance of composite membrane b) Microscopic image of emulsions c) Fluorescence microscope images of composite-incorporated bitumen and d) SEM images of composite-coated bitumen. 76
Figure 5. 3: EDX analysis of composite-coated bitumen surfaces prepared with different salts. a) SEM image, b) EDX spectra for inside and c) EDX spectra for outside of domains on bitumen surface. 77
Figure 5. 4: AFM phase difference images of a) base and composite-incorporated b)SBS and composite-coated bitumen surfaces with a topoghraphic zoomed image of bee shaped structures. 79
Figure 5. 5: Isochronal plots of a) complex modulus and b) phase angle at 0.02 Hz base and composite-incorporated bitumen for different type of salts 80
Figure 5. 6: Freezing experiments in cold chamber with a -2 °C plate and ambient temperature a) Camera-attached cold chamber b) Monitoring of freezing of droplets on composite-incorporated and composite-coated bitumen samples in cold chamber. 81
Figure 5. 7: Freezing delays on surfaces of base, composite-incorporated and composite-coated bitumen with different types of salt in temperature controlled chamber (Medium temperature: -2°C). 83

Figure 6. 1: Structures of the components a)PEGDA b)TEA c)dextran d) NVP e) eosinY f) PGB……...88
Figure 6. 2: Schematics for the synthesis of PEG nanospheres [12]..... 89
Figure 6. 3: FTIR spectra of PEG hydrogel, PEG nanosphere, PEGDA and dextran. 93
Figure 6. 4: a) Two-phase separation of dextran-PEG polymer b) Light microscope image of dextran-PEG w/w emulsion (scale bar: 20 μm) c) SEM image of dried PEG (scale bar: 1 μm) [12]..... 94
Figure 6. 5: SEM images of PEG nanospheres showing the differences in morphology of a) P100-40s (scale bar: 2 μm) b) P100-20s (scale bar: 1 μm) c) P50-40s (scale bar: 1 μm) and d) P50-20s (scale bar: 2 μm) [12]. 96
Figure 6. 6: Size distribution of PEG nanospheres a) P100-40s b) P100-20s c) P50-40s d) P50-20s obtained from DLS characterization [12]..... 97
Figure 6. 7: Percent cumulative PGB release from PEG nanospheres [12]. 100
Figure 6. 8: Experimental percent cumulative release of PGB from PEG nanospheres and model fit (solid curves) provided by the model (equation 6.4) [12]. 102
Figure 6. 9 Percent cell viability of fibroblast cells cultured with a) 0.1 b) 0.5 and c) 1 mg/ml concentration of PEG nanospheres [12]. 104
Figure 7 1: Schematic for synthesis of SBS-PEG gels…….. 109
Figure 7 2: Light microscope images of PEG-cyclohexanone (ϕ= 0.25) water in oil silica nanoparticle (1.5 %) stabilized pickering emulsions prepared by vortexing times of a) 30 s b) 60 s c) 2 min d) 8 min. 113
Figure 7. 3: Structural characterization of PEG particles. a) SEM image of powder PEG particles (scale bar: 1 μm) b) SEM image of casted PEG particles (scale bar: 10 μm) c) FTIR spectra of PEGDA, PEG bulk hydrogel and PEG microgel. 114
Figure 7. 4. a) Mechanism of UV-light mediated thiyl-ene photopolymerization. Schematic representation of; b) the photocrosslinked SBS triblock copolymer network including DTT, c) the photocrosslinked SBS/DTT polymer network formed in the elastomeric phase. 116
Figure 7. 5: Storage and loss moduli of SBS versus photopolymerization time. 117
Figure 7 6: Schematics of the components and the PEG particles incorporated photo-crosslinked SBS polymer network structure. 118
Figure 7 7: SEM images of a) SBS membrane (scale bar 1 μm) b) SBS gel (scale bar 1 μm) c) SBS membrane+PEG (scale bar 2 μm) and d) SBS gel+PEG (scale bar 2 μm). SBS

membrane-PEG gels were prepared by casting SBS solution after incorporation of PEG particles. SBS SBS gel+PEG were prepared by crosslinking of SBS solution after incorporation of PEG particles. Hybrid gels were dried in vacuum oven overnight before analysis with SEM. 119
Figure 7 8 Water contact a) images and b) angles (Θ) of SBS membrane, SBS gel, SBS membrane+PEG and SBS gel+PEG surfaces. 10 µl of deionized, triple distilled water was injected on surfaces to obtain water droplets for measurement of contact angles. 120
Figure 7 9: Nano-indentation load-displacement curves for SBS and SBS-PEG gels. Maximum indentation depth applied was 22 µm. 122
Figure 7 10: Cumulative percent release of AZ11657312 from PEG particles. 123
Figure 7 11: Cumulative percent release of AZ11657312 from SBS-PEG membrane and gels 124
Figure 7 12: Percent cell viability of SBS and SBS-PEG gels. 126

NOMENCLATURE

SBS	Styrene-butadiene-styrene
NPs	Nanoparticles
PGB	Pregabalin
PMB	Polymer modified bitumen
PEG	Polyethylene Glycol
SDS	Sodium Dodecyl Sulfate

Chapter 1

INTRODUCTION

Composite polymeric membranes are good for any application in which hydrophilic functional agents should be homogeneously dispersed and controllably released such as anti-icing agents for surfaces, biomolecules or drugs for therapeutic applications, etc. The technique we introduce here involves incorporation of aqueous phase consisting of a hydrophilic functional domains into hydrophobic styrene-butadiene-styrene (SBS) block copolymer medium using Pickering emulsion templating method and stabilization of the mixture with slightly hydrophobic nanoparticles. Partially hydrophobic nanoparticles are used to form Pickering emulsion in order to have stable emulsions. In addition, we used water-in-water emulsion as template for synthesis of nanospheres for tunable drug release purposes. We aimed to fabricate functional materials with controlled molecule delivery properties using different emulsion templating and polymerization methods for energy and biomedical applications.

In the first part of thesis, we designed a composite membrane, which integrates a hydrophobic polymer phase and hydrophilic aqueous phase that incorporates anti-icing agent. We incorporated an ionic salt potassium formate (KCOOH), into SBS polymer by using particle stabilized emulsion templating method. We observed that potassium formate encapsulated in SBS polymer medium is released from casted membranes depending on the internal volume fraction of hydrophilic phase and nanoparticle concentration used in stabilization of the emulsions. Dry composite membrane delayed freezing of water droplets for about 70 minutes in a temperature and humidity controlled chamber [1]. The

hydrophobicity and thermoplastic nature of SBS polymer allows for incorporation of this composite into other mediums, thus opens up the possibility of delivering anti-icing agents through bitumen. Hence, we investigated incorporation of this polymer composite into bitumen for winter maintenance of the pavements.

Usage of anti-icing agents such as ionic salts to eliminate the ice on surfaces is mostly used approach in winter maintenance. However, these ionic salts are wasted due to washing away by water which necessitates frequent salt feeding and causes economical cost due usage of equipment and human in asphalt road applications. Moreover, these salts have numerous side effects to mechanical properties of roads and harm living organisms and environment. Thus, integrating these hydrophilic salts into bitumen which is a hydrophobic asphalt binder is an effective solution for both anti-icing functionality and sustained mechanical properties of the pavements. For this purpose, we investigated modified bitumen with polymer composite and showed the proper distribution of the composite with morphological analysis. After that, we investigated anti-icing and salt release properties of modified bitumen surfaces and demonstrated significant increase in freezing delay of composite modified bitumen compared to base bitumen in humidity and temperature controlled chamber without sacrificing mechanical properties. This work presents potency of the functional polymer composite for bitumen modification with anti-icing surface functionality [2]. Next, we investigated effect of different salts on functional, morphological and mechanical properties of composite incorporated or coated bitumen. We conducted freezing experiments of composite modified and coated bitumen surfaces in camera-integrated cold chamber where the temperature (-2 ^{o}C) was uniformly distributed. These results suggested that freezing delay could be tuned with the type and amount of anti-icing agent incorporation into the composite. This approach is promising for development of polymer composite-modified bitumen with anti-icing function and for industrially relevant applications.

In second part of this thesis, we worked on synthesis and characterization of PEG hydrogel micro-nanogels using emulsion methods. The design and preparation of hydrogel microgels have attracted a great deal of interest in biomedical engineering, pharmaceutical applications, and biomaterials science because of their tunable chemical and three-dimensional (3D) physical structure, good mechanical properties, high water content, and biocompatibility [3-6]. Macroscopic PEG-based hydrogel, suffers from the disadvantages of

being relatively hard to surface modification, small surface area-to volume, low encapsulation efficiency of payload in drug-release system [7, 8]. To prepare PEG-based hydrogel microspheres both the solvent evaporation method and the emulsification method have been widely used, in which organic solvent or surfactant is needed, and the resulting microspheres are limited for extensive and further applications in the biomedical field [9-11]. However, these methods can have some limitations in case of retrieving and biocompatibility of microgels due to organic solvents used during w/o emulsion synthesis. On the other hand, w/w emulsions are synthesized based on polymer–polymer immiscibility in aqueous solutions without using surfactants, nanoparticles and organic solvents. Therefore, usage of w/w emulsions is more promising for biomedical applications. So, we investigated synthesis and characterization of nano scale size particles based on w/w emulsion system which includes PEG and dextran. We investigated the tunable drug release kinetics of a model drug from these particles and fitted experimental data to a stretched exponential function that described experimental data with high correlation [12].

In the third part of thesis, we considered SBS for biomedical applications [13] and investigated synthesis and characterization of cross-linked SBS-PEG gels for sustained drug delivery purposes. The reasons for wishing to achieve slow release are to decrease the number of daily administrations, improve compliance and minimize side effects [14, 15]. Sustained drug release is important for efficacious treatment of diseases such as periodontitis and severe bacterial infections since these physiological processes require repeated administration of drugs. Sustained release of drugs from gel network depends on hydrophilic-hydrohobic nature of the drugs and the gel matrix, network properties of gel matrix and degradability of the components [14]. While hydrogels have been widely studied as biomaterials due to their controllable swelling, molecule loading and release properties, their hydrophobic counter parts have not received the same attention, especially in relation to biomaterials research [16]. In literature, SBS was used in few biomedical applications [17] and drug release kinetics of this rubber elostomer is unknown. We designed a novel hybrid gel for sustained release of a model drug with amphiphilic property, by using styrene-butadiene-styrene (SBS) hydrophobic polymer network as matrix where hydrophilic polyethylene glycol (PEG) hydrogel particles were embedded. For synthesis of SBS-PEG hybrid gels, we firstly synthesized PEG particles via particle stabilized emulsion method to be able to distribute hydrophilic PEG particles in

hydrophobic SBS polymer uniformly. We characterized surface properties of SBS-PEG gels via SEM and contact angle measurements. The mechanical properties of gels were investigated with nanoindentation tests. Next, we investigated release of an anti-rheumatoid arthritis drug from PEG particles and SBS-PEG hybrid gels prepared with normal SBS and crosslinked SBS. The results showed that SBS-PEG gels have potential for sustained drug delivery applications.

In this thesis, a general overview about emulsion templating, anti-icing strategies and bitumen modification for energy applications is given in chapter 2. Emulsion methods used for synthesis of micro-nanospheres for biomedical applications is also presented. Subsequently, cross-linking of SBS copolymer and its consideration for biomedical applications is briefly reviewed in Chapter 2

Methods and results of design of functional polymer composite modified bitumen are presented in Chapter 3, 4 and 5. Synthesis and characterization of functional properties of nanoparticle and gelation stabilized functional composites of an ionic salt in a hydrophobic polymer matrix are presented in Chapter 3. Effect of stabilization methods, salt release and anti-icing properties of composite membranes are discussed in this chapter. Investigation of composite-modified bitumen for anti-icing purposes is given in Chapter 4. Morphological, mechanical and functional properties of composite modified bitumen are presented in this chapter. Comparison of different ionic salts for composite-modified bitumen is given Chapter 5. Effect of salt type on morphological, mechanical and anti-icing properties of functional bitumen is presented in this chapter.

Synthesis of PEG nanospheres using water-in-water emulsion templating method for biomedical applications is given in Chapter 6. Methods and results about synthesis, characterization of nanospheres and investigation of drug release from nanospheres is presented.

Results of synthesis and characterization of crosslinked SBS-PEG gels for drug delivery purposes is presented in Chapter 7.

Conclusions and further insights about the future of the projects are given in Chapter 8.

Chapter 2

LITERATURE REVIEW

2.1. Synthesis of Materials via Emulsion templating

2.1.1 Definition and classification of emulsions

Emulsion is the mixture of two immiscible liquids where one phase is dispersed in other phase. In emulsions there is a continuous or external phase that suspends the droplets of the other phase which is called the dispersed or internal phase [18]. Emulsions are used in many areas such as cosmetics, foods or in the oil industry [19]. They are also used as templates in synthesis of materials such as polymer foams, composites, capsules and microgels [18, 20-22]. Emulsions can be classified based on the agent used to stabilize them such as surfactant or particle stabilized emulsions. They are also classifed based on the distribution of liquid phases, such as water-in-oil, oil-in-water (w/o), water-in-water (o/w) or multiple emulsions (w/o/w, o/w/o). There is another type of emulsion called water-in-water emulsion (w/w) which is obtained based on immiscibility of two-phase aqueous systems. Moreover, emulsions can be classified according to the internal phase ratio such as Low, medium and high internal phase emulsions (LIPE/MIPE/HIPE). Emulsions can be prepared by stirring, vortexing, ultrasonication or shaking of immsicible liquids [18, 23, 24].

2.1.2. Emulsion templating

Incorporating functional materials into immiscible mediums has been a conventional challenge in materials science. This can be overcomed by formation of stable liquid emulsions and using them as templates to form solid structures. Emulsion templating is a

technique which makes use of the stability of emulsion droplets. [20-22, 25-29] [1-11] This method requires drying of the emulsion without deforming the interfacial borders between the dispersed and the continous phases. The microstructure and morphology of materials obtained with emulsion templating are determined by the parent emulsion [21, 22, 29]. This technique has been described as a tool for the two main approaches. In first approach, the continuous phase is mechanically set by polymerization and crosslinking. After, the internal phase which is composed of volatile droplets is being evaporated and a cross-linked macro-porous polymer structure is obtained with the voids left behind. Therefore, the internal droplets serve to create the pores in the final structure [20-22, 26, 28]. The size of pores changes depend on the characteristics of the emulsion system [22]. Such macroporous materials can be used for many applications such as catalytic storages, filtering materials and optical band-gaps. [20, 21, 26] In the second approach, emulsion template method involves precipitation or coating of a target material around the internal phase droplets in order to form core-shell structure. The continuous phase which is a selected volatile liquid is washed and evaporated to obtain individual micro-capsules. The resultant capsules are subsequently isolated from the continuous phase and dried. These capsules can be used for delivery systems for functional materials for food processing or drug delivery [25, 27, 29].

2.1.3 Emulsion Stabilization Methods

Mixture of two immiscible liquids results in phase separation due to the interfacial energy if any stabilization agent is not used. Because the contact between an oil and water phase is not energitically favourable and increases the free energy of the system. This phenomena results in decreasing the interfacial area and phase seperation finally. Emulsion template method requires a robust and long-term stability of the emulsion droplets to preserve the structure throughout the following templating processes.

Emulsion droplets tend to coalesce and phase separate before the templating process, unless sufficient emulsion stabilization is used. [22, 23, 26]. Phase seperation may be delayed or prevented by use of stabilizing agents which attach in the interphase of the phases and increases the interfacial area by decreasing the interfacial tension energy. There are two types stabilizing agents for stabilization of emulsions; surfactant and particle stabilization [24].

2.1.3.1. Surfactant Stabilization

Surfactants are amphiphilic molecules which have functional groups within the same molecule that have a hydrophobic and hydrophilic character. Surfactants are the mostly used molecules for emulsion stabilization. They localize in the interface of two mediums due to having both hydrophilic and hydrophobic parts and prevent coalescence by decreasing the interfacial tension energy [18, 24]. Schematic of Sodium Dodecyl Sulfate (SDS) and surfactant stabilization is illustrated in Figure 2.1.

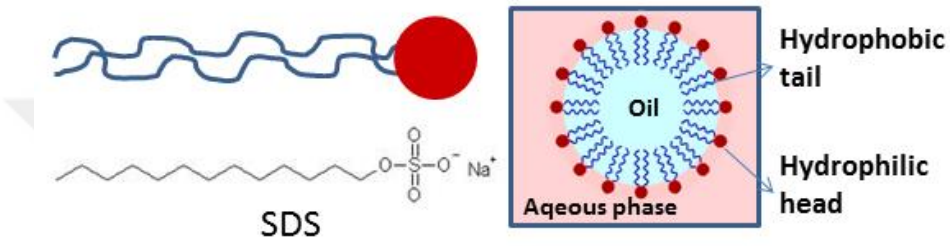

Figure 2. 1: Schematic of SDS and surfactant stabilization.

2.1.3.2 Particle Stabilization (Pickering Emulsions)

Another emulsion stabilization method is Pickering emulsions where small solid particles attach at interfaces of two immiscible mediums, since the particles are partially wettable by both mediums [30-32]. Recently, Pickering emulsions have attracted more interest for the stabilization of emulsion templates due to their strong stability [31, 32]. Self assembly of pickering particles at the interface is thermodynamically favorable. This phenomena is based on the decrease of interfacial tension energy. When particle attach at an interface, entropy decreases and the total free energy is reduced. The interfacial energies of the particle oil interface ($\gamma_{P/O}$), the particle-water interface ($\gamma_{P/W}$), the oil-water interface ($\gamma_{O/W}$) and the effective radius of the particle (R) contribute to the free energy change due to a single particle attachment (Equation. 2.1). [30, 31]

$$\Delta E = -\frac{\pi R^2}{\gamma_{O/W}}(\gamma_{O/W} - \gamma_{P/W} + \gamma_{P/O})^2 \qquad (2.1)$$

This energy favor is higher than the thermal energy of particles coming together with the kinetic energy of the Brownian motion for Pickering particles. Thus, once a particle is attached, it is not delocalized. This results in irreversible attachment to the interface. Possible spontaneous tendency of detachment of extremely small particles is also reported in literature. [31] The reason is that because energy change in Eqn. 1 increases with radius so that thermal energy is sufficient to detach small particles from the interface when the particles are too small. So, in Pickering emulsions larger particles are more stable than the smaller ones. [31] However, Pickering particles consist of a range from nanometer up to micrometer size and their attachment to the interface is principally irreversible [32]. The irreversibility of the attachment is an important difference and an advantage compared to usage of surfactant molecules for stabilization. The very high energy of attachment of particles to interfaces yields significant stability against coalescence which surfactant molecules do not perform. Unlike Pickering particles, surfactant molecules are held at the interface by dynamic equilibrium; they rapidly adsorb and desorb at the interface, which makes their stabilization weaker [33, 34]. Particle stabilization have another advantages over surfactans such that they do not have solubility requirement. Particles can be dispersed in one of the phases that participate in the emulsion. Beside particles localized in the interface can contribute to permeability of molecules between phases.

2.1.3.3 Stability of Pickering Emulsions

Similar to surfactants' behaviour according to hydrophilic-lipophylic-balance (HLB), particle's wettability at the oil water interface determines the adsorption behavior at the interface [35, 36].

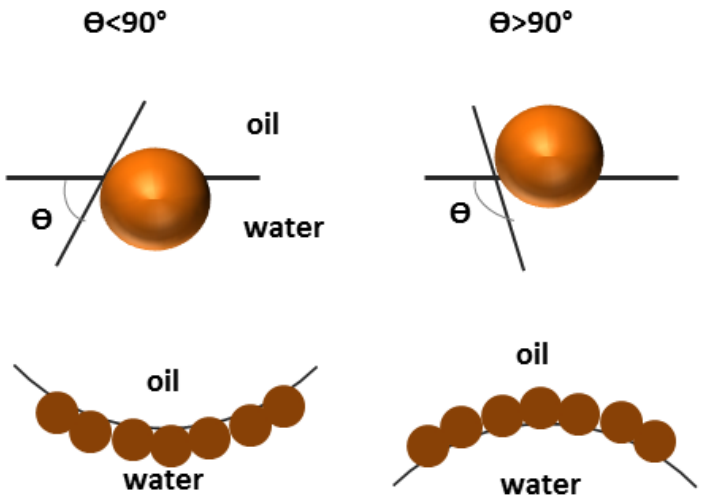

Figure 2. 2: Contact angle (up) and corresponding probable spherical particles positioning (down) of at the oil-water interface when contact angle θ<90° and θ>90° adapted from [32].

When two phase are mixed in the presence of the partially hydrophilic particles They tend to localize the majority of the particles' surface in the aqueous phase and the interfacial contact angle θ obtained in the water is θ<90°. Therefore, this behaviour of these particles results in oil-in-water (o/w) emulsion formation, while partially hydrophobic particles with θ>90°[3] results in formation of water-in-oil (w/o) emulsions. However, strongly hydrophilic (θ<30°) or hydrophobic (θ>150°) particles tend to form unstable emulsions since they prefer to be fully in one phase. Therefore, the particles need to be partially wettable by both phases in order to have stable emulsions. [3][33]. Particles with an angle of 90° at the oil-water interface have the maximum desorption energy, *E*, according to Equation 2.2 [35].

$$E = \pi R^2 \gamma_{o/w} (1 + \cos\theta)^2 \quad (2.2)$$

In Equation 2.2, $\gamma_{o/w}$ represents the tension of the interface and *R* represents the radius of a single spherical particle. This is why, strongest stabilization is obtained with particles with θ=90.

Since wettability of particles is critical in pickering emulsion stabilization, several studies were done to investigate the wettability of particles [32, 35, 37, 38]. Effect of wettability of SiO2 particles on the stability of water-toluene system was investigated by

Binks group. They altered the wettability of particles with silanization systematically and observed that the pickering emulsion prepared with highly hydrophilicor hydrophobic particles were unstable [35]. Furthermore, material characteristics such as the particle size, shape and hydrophobicity are also important in stability of emulsions. The emulsion stabilization performance of particles with different shapes such as rods, fibers, and cubes were investigated [32]. Besides, experimental parameters such as shear rate and temperature in emulsions are others factors in Pickering emulsion stabilization. It is reported that high temperatures tend to form more stable emulsions and low temperatures stimulate droplet coalescence [39] In another study needle like Polyaniline (PANI) particles as have been found to be more effective polymeric stabilizers than spherical particles. Noble and colleagues could obtain stable w/o emulsions with rodlike polymeric, as well [40].

Since the wettability of particles is important in Pickering emulsions, many studies were done to determine the wettability of particles [32, 37]. In one of them sinking time of particles from surface to bottom were measured to see how wettability is related to floating [32].

Size of particles also affect the stability of Pickering emulsions [41, 42]. Binks group demonstrated that emulsion stablity increased with increasing the particle size to 0.21 to 2.7 μm range [42]. Another group prepared stable Pickering emulsions using chitosan-coated alginate particles with different sizes of 230 nm, 550 nm, and 1100 nm[41]. On the other hand, this strong stability have disadvantages in applications where controlled destabilization of emulsions are required. For example, coatings and adhesives are obtained with breaking down of emulsions by evaporating the volatile components to form a film on a solid surface [43].

2.1.4 Water in water emulsions

Water-in-water (w/w) emulsions are prepared based on polymer–polymer immiscibility in aqueous solutions without the need of surfactants, nanoparticles and organic solvents [1, 44-47]. W/W emulsions can be obtained with two-phase aqueous systems, where interfaces occurs between the phases of thermodynamically incompatible aqueous domain [44-47]. Commonly, phase separation is observed between aqueous

polymer solutions, such as polysaccharides and proteins. Phase separation occurs due to changes in polymer molecular weight solvent composition and temperature, which can be characterized by the free energy of mixing (ΔF_{mix}) with at least two minima [45, 48]. Phase separation occurs and ΔF_{mix} changes with composition according to free energy of mixing equation of Flory-Huggins theory as follows in Equation 2.3:

$$\Delta F_{mix} = kT\left[\frac{\phi}{N_A}\ln\Phi + \frac{1-\Phi}{N_B}\ln(1-\Phi) + \chi\Phi(1-\Phi)\right] \qquad (2.3)$$

where k is Boltzmann's constant, T is temperature, Φ is the volume fraction of polymer A, χ is the Flory interaction parameter, N_A is the degree of polymerization of polymer A, and N_B is the degree of polymerization of polymer B. For polymer A dissolved in B, N_B becomes equal to 1. This aqueous polymer immiscibility occurs with many combinations of water-soluble polymers (e.g. combinations of dextran, poly(ethylene glycol) (PEG), poly(vinyl alcohol), poly(vinylpyrrolidone), gelatin or soluble starch). The polymers may remain solution; however, above a certain concentration they separate into two aqueous phases [49].

Colloidal instability and wide size distribution of w/w emulsion are important considerations that make optimization of synthesis of these particles difficult for further applications [45]. For this reason, it is observed that these emulsions are stabilized by particles in some cases [50, 51]. Even though the forces take place in particle stabilized water-in-water emulsions are same with the ones in water-in-oil, stability of water-in-water emulsions are influenced by many conditions such as ionic strength, pH and thermal energy. Beside these, type, chemistry and softness of the particles affect the stability of the resultant emulsions. [52, 53]. It has become clear that there are important differences in these systems and interactions of particles are crucial important in stability of water-in-water emulsions [50, 51, 53].

2.2. Approaches for anti-icing surfaces

Anti-icing functionality is needed to delay the reformation of ice, or to prevent adhesion of ice up to a certain period of time on surfaces. This is required on various

surfaces such as infrastructural components, mechanisms and machines, including aircraft, ships, offshore oil platforms, wind turbines, electrical power plants, power transmission lines and telecoms equipment, heat pumps, refrigerators and air conditioners [54, 55]. Ice and wet-snow adhesion and excessive accumulation on these structures and equipment is well known to cause serious problems in espeacially in cold-climate regions [56]. Atmospheric icing occurs when super-cooled water droplets come into contact with the surface of exposed structures, which may lead to material damage and social-economic costs in these sectors [54, 56, 57]. It is reported that several failures happened because of ice accumulation in Iceland, Norway, Canada, Russia, Finland, the US and China each year [57].

Many challenges are experienced due to the diversity of icing related problems. Systems designed to fight icing can control icing in certain environments. Because icing occurs in a widerange of conditions such as temperatures, humidity levels. Depending on this conditions, different forms of precipitaion occur such as frost formation, snow, freezing rain or fog icing[58].

Various deicing and anti-icing strategies have been developed over the past few decades such as active heating, chemical deicing fluids, mechanical removal and development of icephobic surfaces [54, 55, 57-61]. Among those, chemical and morphological approaches are the mostly preferred approaches to counter this problem:

2.2.1. Morphological approach

One of the most promising approaches to achieve anti-icing property on surfaces is the creation of icephobic surfaces which also known as passive anti-icing. Icephobic surfaces can be obtained via modification of surfaces in micro-nano scale. The aim is to change the roughness of the surface to decrease the wettability of the surfaces which is generally measured with increase in water contact angle of water droplet on a surface.

The contact angle of the water drop on absurface is related to surface energies through Young's equation as follow in Equation 2.4 [58, 62]:

$$\cos\theta = (\gamma_{SV} - \gamma_{SL}) / \gamma_{LV} \qquad (2.4)$$

Where, Θ is the contact angle of water droplet, γ_{SV} is the solid-vapour interfacial energy, γ_{SL} is the solid-liquid interfacial energy and γ_{LV} is the liquid-vapour interfacial energy.

Surfaces are normally rough and a modification is done to create those surfaces. Only cleaved surfaces are smooth down to atomic scale. When a water drop places on such a surface then the contact angle is modified. In case of roughness on surface, the contact angle will be modified as in Wenzel equation (Equation 2.5) [58, 62]:

$$\cos\theta^* = r\cos\theta \qquad (2.5)$$

Where r is the roughness factor which is ratio of the actual surface area to project area. r is greater than 1 for rough surfaces and about 1.2 to 1.3 for fractured surfaces. In nature lotus leaves have hair like structures which provides high roughness.

The contact angle is higher than the Young's contact angle if the surface is hydrophobic. Air gets trapped between the surface and droplet when the water does not penetrate the roughness of the surface. Then contact angle is given by Cassie- Baxter relation as follows in Equation 2.6:

$$\cos\theta^* = \varphi_S(\cos\theta + 1) - 1 \qquad (2.6)$$

Where, φ_s is the fraction of surface in contact with water. If φ_s is smaller than 1, θ^* will be greater than θ. For example, lotus leaves have hairy structures which provide trapped air between them which results in higher contact angle. When the contact angle is greater than 140^o then the surfaces may be called as superhydrophobic.

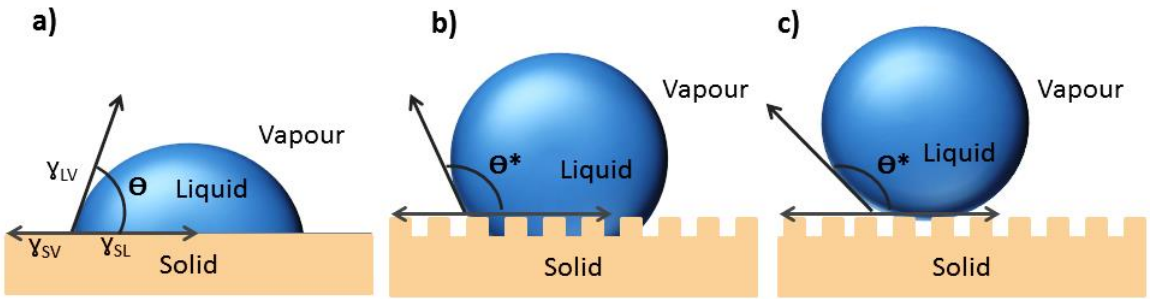

Figure 2. 3: Definition of different contact angles a) Contact angle on ideal surface called as Young contact angle, b) Contact angle on rough surface called as Wenzel contact angle and c) Contact angle called Cassie-Baxter.

Icephobic surfaces can decrease ice or snow accumulation on material surface due to their physicochemical properties. The efficiency of this approach is related to water-repelling surface properties which decrease accumulation of water on the surface [54, 59, 63]. Icephobic surfaces require water repellency for low water wettability. Beside water repellency, ice nucleation suppression and ice adhession force reduction is also required for icephobic surfaces [58]. This research area geneally involves the development and preparation of superhydrophobic coatings on the surfaces of protected materials [54, 59]. In recent strategies, additional to surface roughness, surface is treated with hydrophobic agents to decrease the surface energy. Besides, appropriate choose of texturig element is important for increasing the contact angle [54, 63].

Although studies about anti-icing surfaces are mostly related with the aim of achieving super-hydrophobicity on surfaces, superhydrophobicity is not necessarily applicable to all surfaces that require anti-icing property. Because superhydrophobic surfaces can promote slippness due to reducing drag between the surface and the liquid because of gas bubbles in a microscopic texture [64]. So, superhydrophobicity may not be suitable in cases where the main aim is decreasing slipperness. Furthermore, surface geometry modification at nano-level is economically not feasible in most cases.

2.2.2 Chemical approach

Another approach to eliminate ice formation on surfaces is the use of freezing point depressant agents. Freezing-point depression is the process in which a solute is added to to a solvent to decrease the freezing point of the solvent. Salty water, alcohol in water or mixture of two solids such as impurities in a powder drug are exmaples for this process. The resulting solution or solid-solid mixture has a lower freezing point than the pure solvent or solid. This approach is widely used to reduce the icing of airplanes, wind turbines, helicopters, runways and road management to remove icing from sidewalks and roads [54, 65-67].

Ionic salts are the mostly used agents for this purpose [65, 68]. In pure water, water molecules come together and start ice nucleation with decrease of temperature. As ions are dissolved in water, ionic molecules which localize between water molecules as schemtized in Figure 2.4 to prevent the gathering of water and delays the crystallization

process. Therefore, water remains in liquid phase at lower temperatures than its normal freezing point

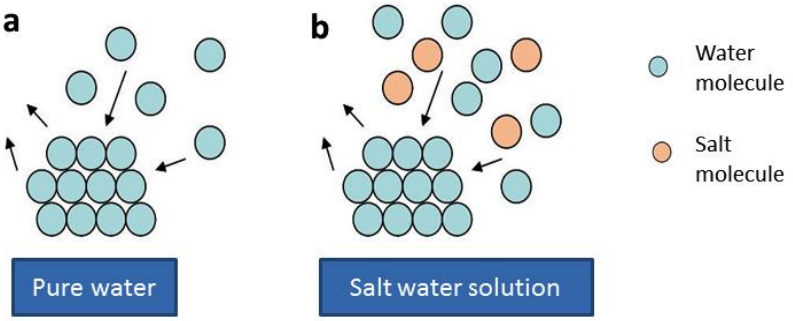

Figure 2. 4: Behaviour of water molecules in a) absence and b) presence of salt.

The degree of freezing point depression of water when an ionic salt is dissolved is determined by the Equation 2.7 below:

$$\Delta T_F = K_F \cdot b \cdot i \qquad (2.7)$$

Where, ΔT_F is the decrease in the freezing temperature (°C), K_F is the cryoscopic constant which is an intrinsic property of the solute, b is the molality of the salt solution (mol/kg) and i is the van't Hoff factor which is the number of ions per solute molecule. According to this relation, freezing point depression performance of salts in water changes based on the amount of salt solved in solution and ionization degree of salt molecule. Thus, solubility of salts in water is a critical parameter for freezing point depression purposes. Solubility of some of ionic salts that are used for de-icing or anti-icing solutions on surfaces are given in table [69].

Table 2 1: Solubilities of different salts at 25 °C [68].

	Solubility (g/L) at 25 °C
NaCl	359
KCOOH	3310
$CaCl_2$	811
$MgCl_2$	543
HCOONa	972

Road salting is a general approach which uses advantage of this phenomena to decrease the freezing point of the ice on roads to allow the ice to melt at lower temperatures and prevents the accumulation of ice. Sodium chloride, calcium chloride, magnesium chloride, potassium formate, sodium acetate, potassium acetate or a mixture of many are generally used for this purpose [70]. However, this de-icing application has also many disadvantages on roads, environment, economy and living organisms which will be discussed in the following section.

2.3. Anti-icing functionality on asphalt roads

Anti-icing functionality has urgent need on asphalt roads and vehicle transportation. Snow and ice control technology in winter has been an important issue in many countries currently, since too many accidents are resulted from the snow and ice on the pavement surface [70]. For example, among many exceptional road conditions, icy roads lead to the largest number of accidents, based on the traffic accident statistics of 2013 for Turkey Figure 2.5.

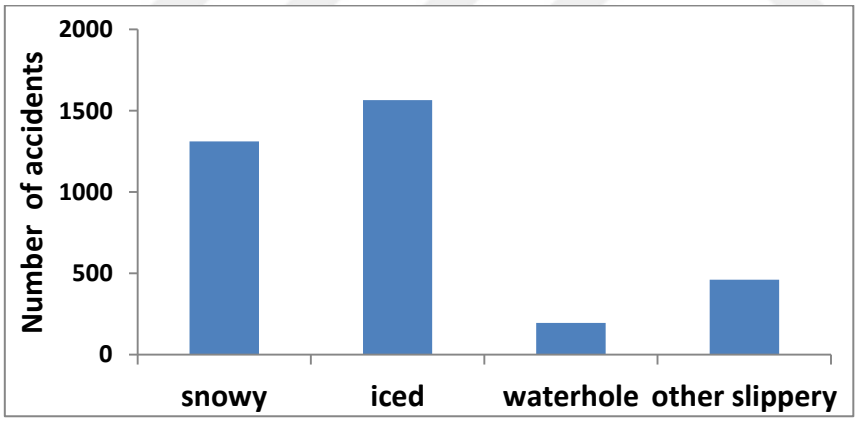

Figure 2. 5: Number of accidents happened in different wet road conditions according to Turkish Traffic Accident Statistics of 2013.

According to *ten-year averages of* National Highway Traffic Safety Administration statistics *from 2005 to 2014*, 43% of crashes that happen on wet roads occur during snow or on slippery roads.

Although achieving superhydrophobic surfaces is mostly used strategy for anti-icing solutions on surfaces, it is not suitable for all surfaces that require anti-icing functionality. Because superhydrophobicity can promote slippness with the exposure of

water as mentioned in previous sections. Furthermore, surface morphology modification is costly applications which will be not feasible for asphalt roads. Another method is electricity systems integrated on roads to prevent icing on roads. However, this application is also demanding high costs.

Chemical approach is the mostly used approach among the strategies used for anti-icing surfaces. Freezing point depression is appealed in this approach where ionic salts are used to decrease the freezing point of water. Sodium chloride, calcium chloride, potassium formate, magnessium chloride are the mostly used ionic salts for winter maintanence on asphalt roads.

Ionic salts are generally directly applied on road which have some economical, social and environmental disadvantages. According to statistics in USA, salt production for winter maintanence was a $2.2 billion cost in 2014 in USA, which causes high economical charge. Bulk application of salts on asphalt roads has also negative effects on mechanical strength of mastic which results in cracks on roads. Furthermore, these excess salts applied on roads cause damages to environment such as vehicles, plants and other living organisms. Because of these disadvantages of applying salts to asphalt surfaces for de-icing puposes, studies were conducted to replace this de-icing technology with anti-icing.

Many methods were studied to prevent icing on roads [71-74]. It is reported that graphite and carbon fiber reinforced conductive asphalt concrete was designed for preventing and melting icing [72]. In another study, rubber nanoparticles were incorporated into asphalt concrete for anti-icing functionality[73]. Geothermal energy is also used to prevent icing on tunnels and bridges [74]. Additionally anti-icing fillers have been suggested as alternatives to the conventional usage of anti-icing agents [65, 68, 75, 76]. One of those strategies involves the addition of levulinic salts into the asphalt mixture to eliminate the need for the common anti-icing agents and to obtain pavements with an anti-icing property [75]. In another study, researchers evaluated the potential of synthetic fillers such as sodium chloride, calcium carbonate, magnesium carbonate in an asphalt mixture to promote an anti-icing property. A delay in frost formation and a decrease in adhesion between ice and the pavement were reported [77]. However, these fillers include high concentrations of salt (70-75 % (w/w)) which can have negative impacts on mechanical and morphological properties of mastic which

were not considered in these studies. Moreover, Marshall tests which were conducted for evaluating engineering performance of asphalt mixtures demostrate that composition and content of anti-icing fillers affect the properties of asphalt mixtures and it is presented that the amount of anti-icing filler should be in the range of 3- 6% (w/w) [78].

Previous studies are important for the development of anti-icing strategies; however, the influence of these synthetic fillers on the morphological and thermomechanical properties of the binder in asphalt mixtures still needs to be investigated.

2.4. Polymer Modification of Asphalt binders

Bitumen is a semi-solid hydrocarbon material, generally produced from certain crude oils by distillation (atmospheric/vacuum) units in oil refineries. It is the heaviest part obtained from crude oil distillation process. The majority of bitumen has been used as a binder in asphalt road pavements [79]. The chemical composition and mechanical properties of bitumen has important effect on its performance as a paving material. Binders for road paving requires a variety of thermomechanical demands such as thermomechanical resitance and viscoelasticity [80]. Some pavement defects occur in asphalt roads in time due to traffic loads and thermomechanical properties of asphalts. These are rutting in high temperatues, cracks and propagation in low temperatures. Bitumen is modified with bitumen in order to improve its thermomechanical resistance, elasticity and adhesivity [81, 82]. Modification with polymers has significant effects on the engineering and processing properties of bitumen [83]. Most of the polymers are insoluble in the bitumen matrix that results in separation of both phases. Morphological, structural and chemical changes are observed during the processing of modified and neat bitumen. Chemical compatibility such as bitumen and polymer type and processing conditions, such as type of mixing device, time and temperature are important for obtaining stable polymer modified bitumen with desired properties [84]. Higher stiffness at high temperatures, higher cracking resistance at low temperatures, better resistance to moisture, İmproved elastic recovery, higher softening point, higher viscosity and higher cohesive strength are desirable properties obtained for polmeyr modified bitumen [85, 86].

Bitumen has been modified with different plastomers and thermoplastic elastomers such as ethylene-vinyl acetate (EVA), polypropylene (PP) styrene-butadiene-styrene (SBS), ethylene-butyl acrylate (EBA) polyethylene (PE), styrene-ethylene/butylene-styrene (SEBS) and styrene-isoprenestyrene (SIS). Although these polymers can enhance bitumen properties to some extent, there are still some drawbacks need to be addresssed such as high cost, low ageing resistance and poor storage stability of polymer modified bitumen [83]. Polymer modified binders are utilized at locations with high stress, such as airports, busy streets and race tracks [85].

Continous dispersion and the compatibility of polymer within the bitumen are the most important criteria in polymer modified bitumen manufacturing. Compatibility and morphological properties of PMBs depend on gaestal index (GI) of base bitumen (GI = (saturates + asphaltenes)/(aromatics + resins), polymer type and content and sample preparation history such as sample preparation temperature and time [87]. Figure 2.6 shows the results of a study which investigate the effects of bitumen type and samle preparation on polymer modified bitumen morphology [88]. Figure 2.6 a shows the effect of heating temperature and rate on morphology of SBS modified bitumen. Morphology of different type of bitumen samples modified by 5% (w/w) SBS is seen in Figure 2.6 b.

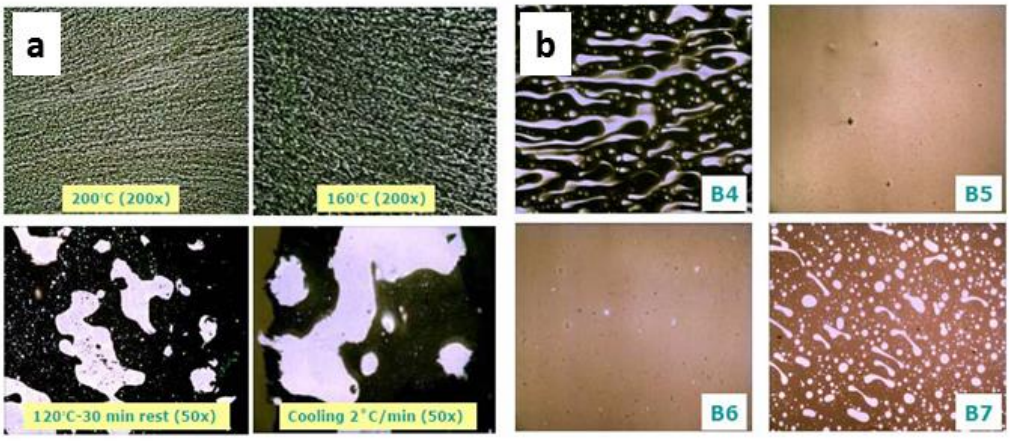

Figure 2. 6: Morphologies of SBS modified bitumen (5 %wt.) with a) different heating termal histories and b) different types of bitumen (magnification = 50x). Reprinted from [88] with permisson from NRS Annual Transaction.

2.4.1. Rheological characterization of bitumen

Bitumen is generally modified with polymers for improvement of mechanical properties suh as viscoelasticity, thermomechanaical resistance and viscosity. This is why, rheological characterization for polymer modified bitumen has been the most intensively studied topic in bitumen research. Rheological properties of PMBs is measured by dynamic shear rheometers and bending beam rheometer. Rheologicacal properties of PMBs is related with morphology and sample preparation of PMBs. Rheological properties also depend on the type of bitumen, polymer properties, polymer content and manufacturing parameters.

Dynamic mechanical tests are usually conducted to investigate the viscoelastic properties of bitumen. The viscoelastic parameters measured in the oscillatory tests are the complex modulus (G*) and the phase angle (δ). G* is defined as the ratio of maximum stress to maximum strain and provides a measure of the total resistance to deformation under shear loading. It contains elastic and viscous components, which are the storage modulus (G') and loss modulus (G''), respectively. These two parameters are related to each other through the phase angle (δ), which is the phase lag between the applied shear stress and the shear strain during an oscillatory test. The phase angle is a measure of the viscoelastic balance of the material behavior and is equal to the arctangent of the ratio of loss modulus (G'') to storage modulus (G') [89].

Several studies were done to characterize rheological properties of polymer modified bitumen [80, 82, 84, 86, 88-90]. In one of these studies, dynamic mechanical tests show that a plateau region is established at high temperatures as a an evidence of polymeric modification in G* meaurements as presented in Figure 2.7 a [89]. This region indicates a dominant polymer network establishment throughout the bitumen. Phase angle (phase angle (δ) measurements also gives information about improvement in rheological properties with polymer modification. It is observed that δ decreases at SBS modified bitumen as shown in Figure 2.7 b which can be attributed to the improvement in elastic property. δ of base bitumen is around 90° at high temperatures which is indication of

viscous behavior, while δ of SBS modified bitumen decreases at low high temperatures as aresult of improved elastic behaviour [89].

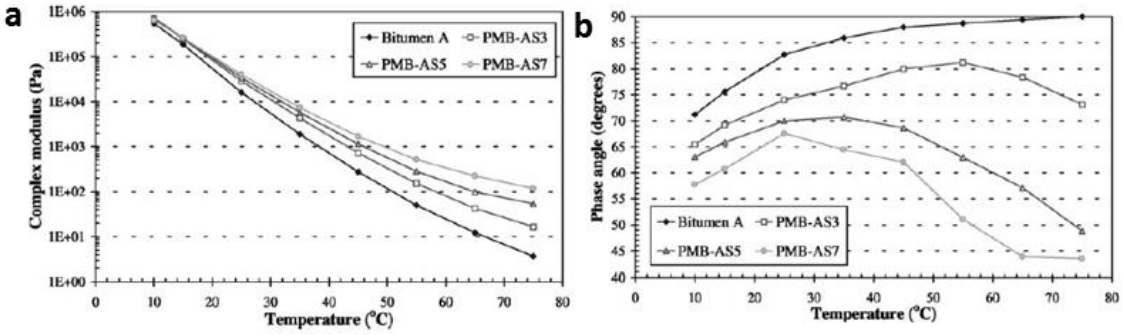

Figure 2. 7 Isochronal plots of a) complex modulus and b) phase angle at 0.02 Hz for SBS modified bitumens. Reprinted from [89] with permisson from Elsevier.

2.4.2. Morphological characterization of bitumen

2.4.2.1 Atomic Force Microscopy

Bitumen is generally known to be composed of a continous and a dispersed phase. The size of the dispersed phase is in the range of 1-6 μm [91]. In literature, there are different conclusions about the relation between the morphology and the components of the bitumen. Another research showed the observation of different morphologies and classified asphalt bitumen within three main groups with AFM microscopy. These are fine dispersion in range of 0.1-0.7 μm in continous matrix, domains with 0.1 μm, and four different phases which are called as catana-, per-, para-, and sal-phases. However, they did not define a relation between the four components (saturates, asphaltenes, resins, and aromatics) and the AFM morphology and in bitumen [92].

Another important phase observed in bitumen is "bee-shaped structures" which are generally observed with AFM micrsocopy. These structures look like strings which are immersed and emerged in bitumen surface. Bee-shaped structures were correlated to different phase and components of the bitumen as a result of different studies. Some of these studies suggest that bee-shaped structures are related to crystalline waxes in bitumen [93-95]. Mc Carron et al. Also conclude that increasedin processing temperature

decreases the height of the bee-shaped structures [93]. Another hypothesis is that these structures occur as a result of a latter process which is indication modification of bitumen[91]. Our observations is also consistent with this theory which we discuss them in following chapters.

Researchers showed that there is relation between the bee structures and the mechanical properties of bitumen. They state that there is difference in continous phase and the bee structures in terms of elasticity, stifness and adhesive properties. It is reported that bee structures show higher stifness and less adhesive property [96]. They also show that elastic recovery of bitumen is also related to distribution of bee structures [97].

2.4.2.2. Flourescence Microscopy

Morphology of SBS modified bitumen can be investigated under flourescence microscopy [87, 88, 98]. When SBS was mixed to bitumen, elastomer phase of copolymer swelled up to nine nine times of the initial volume and formed a polymer network throughout the bitumen [98]. Swollen polymer gives flourescence under flourescence micrsocopy which enables imaging of distribution of polymer in SBS modified bitumen. Polymer structures appear as bright domains with a dark (bitumen) background [87].

A continous polymer or bitumen network is obtained in PMB depending on polymer content, bitumen type and the thermal and mixing history.

2.5. Synthesis of PEG nanogels via water-in-water emulsions for drug delivery applications

2.5.1 Hydrogel microspheres

Design and characterization of hydrogels have attracted significant attention in tissue engineering and pharmaceutical applications because of their tunable chemical and three-dimensional physical structure, good mechanical properties, high water content, and biocompatibility [3-6, 99]. These properties offer great potential for use of hydrogels in tissue engineering, biomedical applications, drug delivery systems, and bionanotechnology [100-103]

Hydrogels can be in the form of macroscopic gels or smaller dimensions such as microgels and nanogels. When the size of microgels is in submicron range, they are known as nanogels. Microgels/nanogels have many advantages for polymer-based drug delivery systems (DDS) such as tunable size from nanometers to several micrometers, colloidal stability, high surface area/volume ratio, facile synthesis, and control over particle size [10, 104]. Among them large surface area is important for multivalent bioconjugation. Besides they have an interior network for incorporation and delivery of biological molecules [105, 106].

PEG hydrogel are highly hydrophilic, nonimmunogenic, and biocompatible.[102, 107-109] Their high hydrophilicity comes from the ethylene oxide linkages in the polymer backbone. They are nonimmunogenic because they resist cell adhesion and recognition from the immune system. Therefore, they are used as scaffolds for tissue engineering, as drug delivery carriers, surgical barriers, in tissue repair, in cell encapsulation for transplantation and as coatings in biosensors [102, 110-114].

PEG-based micro/nano-scale hydrogels have been considered to overcome the problems associated with macroscopic gels, such as small surface area-to-volume ratio, low encapsulation efficiency and longer response time to external stimuli [7, 8, 115]. PEG hydrogel particles still maintain desired characteristics of macroscopic PEG-based hydrogels, such as swelling capacity and biocompatibility [106]. Furthermore they offer advantages such as a tunable size from nanometers to micrometers, a large surface area for bioconjugation, and an interior network for incorporation and controlled release of molecules [10, 104, 116]. However, several limitations exist for design and development of effective hydrogel-based particles as drug delivery carriers for *in vivo* applications [105]. One important requirement involves control over the dimension to be less than 200 nm in diameter, which can improve cellular uptake of particles through cell membranes and reduce nanoparticle uptake through mononuclear phagocytic system [117]. This property can significantly increases the circulation time of particles in blood [9, 10].

2.5.2 Synthesis of hydrogel micro/nanospheres for drug delivery purposes

For the synthesis of hydrogel micro/nanospheres, solvent evaporation, simple emulsion, double emulsion, coacervation (phase separation) and spray drying methods are generally used. However, in recent years, pickering emulsions and water-in-water emulsions are getting more interest for synthesis of micro-nanospheres due to their advantages over use of conventional emulsion methods. Pickering emulsions enable permeability control through the domains and they do not require surfactant and solubility. Beside they form very stable emulsions which is desired for templating of emulsion. Only disadvantage of this method is that it still requires organic solvent similar to other conventional microsphere synthesis methods. This problem can be overcomed with use of water-in-water emulsions which are prepared based on aqueous solution of polymers which is important for biocompatibility of synthesis process and resultant microspheres. Because water-in-water emulions do not require surfactants, nanoparticles and organic solvents [1, 44-47]. However, colloidal instability and wide size distribution of w/w emulsion are important considerations that make optimization of synthesis of these particles difficult for further applications [45].

2.5.2.1 Water-in-water Emulsion Method

Very few studies were conducted to use water-in-water emulsion method for synthesis of microparticles [44-47, 118, 119]. Completely aqueous w/w emulsion technique was first used by Okke et al. as a novel technique for preparation of PEG hydrogel microparticles [46]. In this technique, two aqueous solution of polymers form a two-phase aqueous system due to immsicibility of polymer solutions. Next, this two phase system is mixed by stirring to obtain an emulsion where the polymer in the dispersed phase was crosslinked to form hydrogel microspheres. Finally, crosslinked microparticles are retrieved by washing the continous phase and filtering anddrying the microspheres. Schematic of synthesis of polymer microspheres water-in-water emulsion method is shown in Figure 2.8.

In previous studies, only few reports exist, where the synthesis of micron-size hydrogel particles via w/w emulsion was considered. In previous report by Murphy and colleagues, dynamic network properties of hydrogel microspheres were characterized and release of proteins such as VEGF and BMP-2 from these microspheres were investigated,

where hydrogel microspheres were prepared via w/w emulsion of dextran and PEG prepolymer [44, 47, 118].

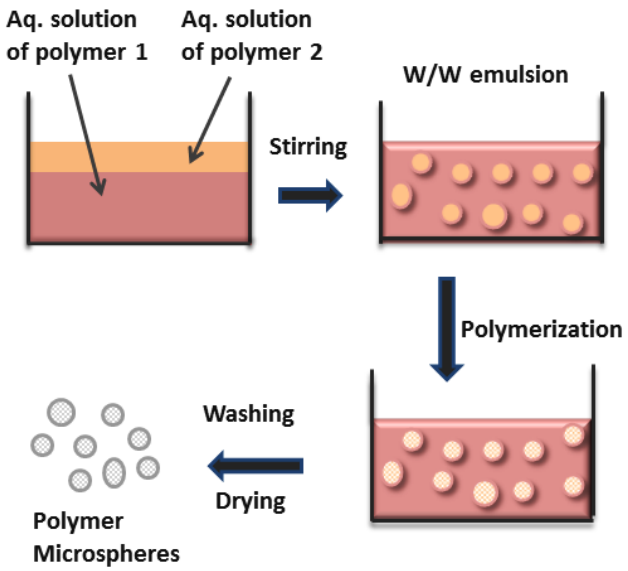

Figure 2. 8: Schematic of synthesis of polymer microspheres water-in-water emulsion method.

Size of the particles obtained in a dispersed phase of w/w emulsion would change depending on the molecular weight and concentrations of polymer used in each phase, volume fraction of both phases, stirring rate and time used for emulsification [45, 46, 119]. In previous studies, micron size spheres (2.5 to 25 µm) were obtained by emulsification of dimethacrylated PEG (PEG-MA_2; molecular weight: 3400 Da) and dextran (molecular weight: 40 kDa) with a vortex time of 1 min. It was also observed that dispersed PEG hydrogel particles in micron-scale size range would increase with decreased concentration of dextran (from 23 to 15% (w/w)) in continuous phase, probably due to the lower viscosity obtained for the continuous phase [46].

2.5.2.2 Pickering Emulsion Method

Pickering emulsions have many advantages over conventional methods that use surfactants. They are intrinsically suitable for synthesis of core-shell stuctures and hallow particles [120-125]. In one of these studies, Pickering emulsions were used for synthesis of micron-size polyaniline/nano-Fe_3O_4 composites for the first time [123]. Pickering

emulsions were formed with self-assmebly of Fe_3O_4 nanoparticles in toluene-water interface in which Aniline monomers were absorbed on the surface of nanoparticles. Fe_3O_4 nanoparticles formed the shell structure and Polyaniline/nano-Fe_3O_4 composites were obtained with polymerization of aniline inside the shell. In another study, raspberry-like PMMA/SiO2 nanocomposite particles were synthesized via Pickering emulsion method [124].

Another group prepared Silica nanoparticle-armored polyaniline microspheres (SNAPMs) using Pickering emulsions. This group also synthesized different nanostructures such as polyaniline/nano-CeO_2 composites, polyaniline nanofibers, and nano-sized CdS hollow particles using different types of nanoparticle as stabilizers [125].

Although having many advantages such as permeability control, superior stability, size control, feasibilty for core-shell structure and surfactant-free property, very few studies have been reported for use of Pickering emulsions for biomedical applications. A general schematic of synthesis of polymer microspheres Pickering emulsion method is presented in Figure 2.9. Aqueos solution of polymer is mixed with an organic solvent including nanoparticles via vortex which leads to water/oil emulsion. Then, polymer solution of dispersed phase is polymerized to obtain microspheres. Finally, the mixture is washed and dried to remove the organic solvent and retrieve the microparticles.

In one of these studies, hydroxyapatite/poly-l-lactide (Hap/PLLA) interconnected porous materials were prepared using g-HAp nanoparticle-stabilized Pickering emulsions as templates. Porous structure was obtained with evopration of W/O Pickering emlusions [126]. In another study Ibuprofen (IBU) loaded poly(lactic-co-glycolic acid) (PLGA) microspheres were synthesized via SiO_2 nanoparticles stabilized O/W emulsions which were prepared with water and dichloromethane [127]. Release of Ibuprofen from PLGA microphere were investigated in this study. Best to our knowledge, Pickering emulsions have not been reported for synthesis of nano-sized PEG hydrogel particles for drug delivery purposes.

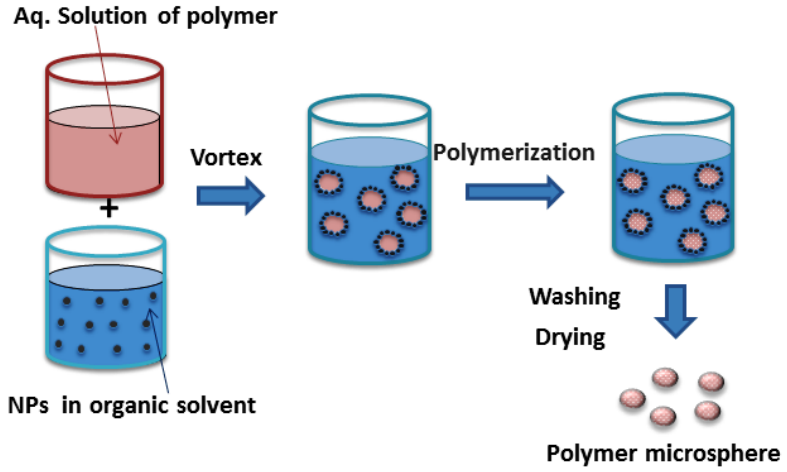

Figure 2. 9: Schematic of synthesis of polymer microspheres Pickering emulsion method.

2.5.3 Micro-nanospheres for controlled drug delivery

Although various drug delivery systems are used for controlled drug delivery, polymer microspheres are the mostly used types due to their several advantages as discussed in previous sections. Micro-nanospheres can be used for encapsulation and delivery of variety of drugs such as small molecules, peptides, nucleic acids and proteins. [8, 10, 12, 104, 105, 116, 119, 128, 129]. Understanding drug relase rates and mechanisms is the most important point for improvement of systems for controlled drug delivery.

2.5.4 Factors that affect drug release rates

Drug encapsulation and release rates are governed with many factors such as polymer type, molecular weight, nature of drug, composition of polymers, stabilizing agents and the size of microspheres. Type of polymer effects drug release rate depending on degradation and hydrolysis rate of polymer and the diffusion mechanism [10, 104].

Polymer molecular weight also affects the release rates depending on degradation and diffussion. Decrease in polymer molecular weight can yield to more quickly degradation of polymers which increase the drug release rates. On the other hand, decrease in molecular weight of polymer can also increase the diffusivity which results in decrease in drug release rate [10, 130].

Size and size distribution of microspheres also affect the drug release rates [10, 131]. Increase in microsphere size decreases the surface-per-volume ratio and drug

release rate. Increase in size also delay the water penetration from surface to the center of particle which results in slower drug release, as well [131, 132].

2.6 Consideration of SBS for biomedical applications

2.6.1 Properties of SBS

SBS is a synthetic triblock copolymer, commonly used as a rubber substitute due to its high tensile strength, high elongation and resilience [133, 134]. Due to its desirable properties, SBS has been used in a variety of industries, ranging from construction (as an additive to bitumen to enhance road resilience) to biomedicine.

Physical properties and phase separation behaviour of SBS have been well studied, and these can be manipulated through modifications of size and ratio of styrene to butadiene blocks, as well as the type solvent used in the system [134, 135]. As a result of phase separation, SBS remains within the network structure, where flexible poly(butadiene) domains act as physical crosslinks between the rigid polystyrene domains (Figure 2.10) [134].

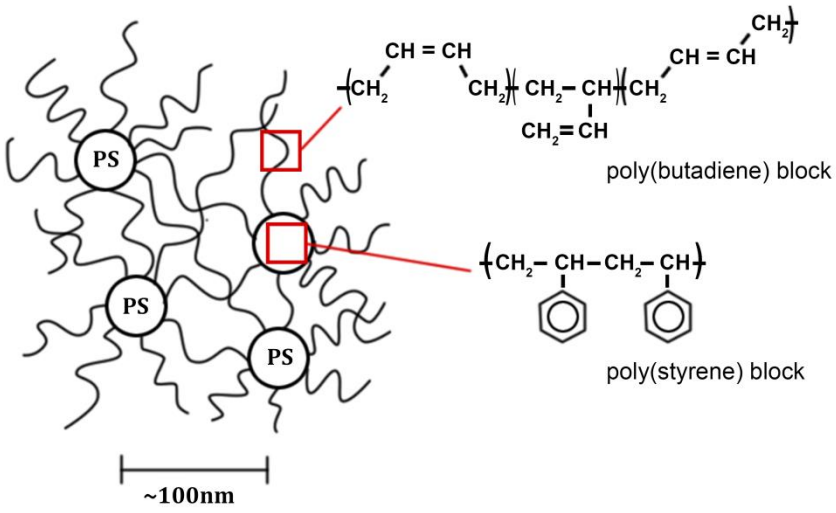

Figure 2. 10: Schematic representation of SBS triblock copolymer.

Tacticity of styrene and butadiene chains affect the crystallinity, thermal and mechanical behavior of SBS copolymer. Tactic polymers are partially crystalline, while

atactic polymers are amorphous. Tacticity makes a big difference in polystyrene. Atactic polystyrene is a hard plastic, and completely amorphous while tactic has more crystalline structure which has higher glass transition temperature (Tg). Free radical vinyl polymerization normally can only produce atactic polymers. Atactic 1,2-polybutadiene is also amorphous and used in rubber industry [136, 137]. Syndiotactic (which is tactic) 1,2-polybutadiene can be prepared using various cobalt catalysts. Commercial SBS are generally composed of atactic styrene and butadiene which has amorphous structure and low Tg [137].

2.6.2. SBS for biomedical applications

SBS has a long-standing use in biomedical devices including surgical drapes, blood bags and catheters [138]. The microstructure of SBS has also been exploited for specific cell response. Due to its phase separable nature, the topology of casted SBS membranes can be modified to create tuneable cell polymer interfaces [135]. Moreover, unsaturated carbons within butadiene blocks allow for a wide range of modifications in SBS structure, including grafting, crosslinking, and epoxidization with tunable properties. [17, 133, 139, 140] For example, Yang et. al. used vinyl pyridine (VP) grafting onto SBS structure to create heparin (HEP)-loaded membranes for potential use in biomedical applications. The authors investigated the influence of the amount of VP and HEP on the biocompatibility of SBS-g-VP and SBS-g-HEP membranes through characterization of fibrinogen and albumin adsorption on those membranes. The researchers observed decreases in the adsorption of albumin and fibrinogen with increases in VP grafting, and heparin on SBS membranes [17]. Previously, we designed polymer composite dispersed in SBS matrix and investigated the release of an anti-icing agent, potassium formate (KCOOH), through this polymer matrix [1]. In another study, our group developed the synthesis of pH responsive composite hydrogel gel network incorporating crosslinked SBS network for the delivery of an epileptic drug [141].

2.6.3. Crosslinking of SBS

Crosslinking of SBS triblock copolymer was considered to improve physical properties [142, 143]. In an earlier report, Mateo et al. prepared crosslinked SBS using hexanediol dimethacrylate to increase transmittance through visible light region, while retaining the regular structure [142]. Morphological and mechanical properties of SBS

can also be modified through crosslinking of SBS copolymers or blends with Low Density Polyethylene (LDPE) [144-146]. For example, shape memory behaviour and other mechanical properties can be improved by chemical crosslinking of SBS/LDPE blends[146].

SBS can also be used to create slightly hydrophobic networks analogous to hydrogels such as poly ethylene glycol (PEG). While hydrogels have been widely studied as biomaterials due to their controllable swelling, molecule loading and release properties, their hydrophobic counter parts have not received the same attention, especially in relation to biomaterials research [16]. However, it is also possible to obtain covalently crosslinked hydrophobic networks, such as SBS, through appropriate use of crosslinking molecules [133, 139, 145, 147]. For example, Decker et. al used thiol-ene chemistry and demonstrated that it was possible to use multi-functional thiol and a UV photo initiator to create an insoluble SBS network within toluene [133, 148]. The authors used photoinitiated thiol/ene polymerization to obtain a crosslinked structure of a triblock SBS polymer of low vinyl content (8%), with concentrations of less than 1 wt % in the trifunctional thiol crosslinker. The effect of thiol and photoinitiator concentrations on UV polymerization of both low-vinyl SBS and commercial SBS rubber were also tested in the same study. For these experiments, trimethylolpropane mercaptopropionate (TRIS) was used as a crosslinking agent, and Lucirin TPO was a photoiniator in the system [133]. Thiol-ene chemistry was also used in photoinitiated step-growth polymerization of Poly(ethylene glycol)-tetra-norbornene (PEG4NB) to form PEG-based hydrogels [128, 149].

2.6.4. Photo-initiated thiol-ene reactions

Upon UV or visible light exposure, eosin Y can be excited to abstract hydrogen from thiol-containing crosslinkers, such as DTT, thus forming thiyl radicals. These radicals propagate through norbornene moieties on multi-arm PEG macromers to form thioether bonds and create gel network [128, 149]. Step-growth thiol-ene hydrogels with multilayer structures can also be formed by visible light mediated photo-click reactions between macromer PEG-norbornene and cross-linker dithiothreitol (DTT) [150]. Crosslinked SBS network can be synthesized through the addition of radicalized thiol groups onto the double bonds found in the poly(butadiene blocks). This mechanism, also

known as “click chemistry”, is relatively simple, versatile and has been extensively studied and used to control molecular weight in radical polymerization reactions [151]. Thiol-ene chemistry is advantageous, since it does not require a catalyst, and the radicals can be formed through a variety of methods such as thermal, visible light and UV initiation. The eosin Y and TEA initiator system has also been widely used in the crosslinking of poly(ethylene glycol) (PEG) hydrogels and is capable of producing radicals to drive the crosslinking under visible (wavelength ~500nm) or UV light [3, 152, 153]. In our study, we combined these two systems for the first time, where SBS polymer was crosslinked via UV photoinitiated thiol-ene reactions using dithiothreitol (DTT) as crosslinker, and eosin Y-TEA photoinitiation system to initiate crosslinking reactions with TEA radicals.

Chapter 3

SYNTHESIS AND CHARACTERIZATION OF FUNCTIONAL POLYMER COMPOSITE

3.1. Introduction

Incorporation of hydrophilic functional agents within a hydrophobic polymer matrix has been a conventional challenge in materials science. This challenge can be addressed by forming stable liquid emulsions and using them as templates to form solid composites [25-28, 154-166]. The liquid emulsion droplets need to be robust and have long-term stability, so that the structure of the emulsion droplets throughout the drying process will be maintained [161]. As an alternative to surface active molecules, small solid particles attach at interfaces of two immiscible mediums when the particles are partially wettable by both mediums.[38, 167, 168] This mechanism, which is preferred approach for use in emulsion templates due to their strong stability, is known as "Pickering emulsions"[169, 170].

Templates of emulsions have been used for the two main approaches. The first of these approaches yields to porous monolith materials.[26, 155, 160, 161] This approach requires transformation of the continuous phase of an emulsion into a solid matrix. Subsequently, dispersed droplets are removed by evaporating or dissolving in a suitable liquid, leaving spherical pores behind [160, 161]. Such porous monoliths are attractive

potential materials for filtering aerosols. Such porous monoliths are also proposed to be used as adsorbents, catalytic supports, light-weight structural materials, insulators besides their potential application as filters [155, 160, 161, 163]. The second approach involves precipitation or coating of a target material around the droplets in order to form core-shell structure [25, 27, 165]. Such capsules are promising to be used as delivery vehicles for controlled-release encapsulation, drug delivery, protection of biologically active agents [27, 165].

In general, these two approaches of emulsion templating method have been considered for different application. We combined the two approaches through particle stabilization to design a functional polymer composite that includes an anti-icing agent. Ionic salts are widely used agents for this purpose. We designed a composite membrane coating, which integrates a hydrophobic polymer adhesive base and hydrophilic aqueous phase that incorporates anti-icing agent. The functional membrane consists of a base which is non-polar SBS block copolymer, and can be compatible with most non-polar surfaces. The hydrophilic domains include spherical droplets that store and induce controlled release of the anti-icing agent, KCOOH. In order to avoid destructed shapes, to enhance restricted permeability, and to reinforce rheological properties, we included functional domains in agarose gel within the designed material. We used Pickering emulsion droplets as templates for the functional domains, which encapsulate anti-icing KCOOH in the functional membrane coating.

The effects of experimental design parameters on the salt release and anti-icing properties of dry membranes are described and discussed in detail. The main thrust of this study is the unique functionality of SBS based emulsions with anti-icing agents, and possibility of release of this water soluble agent into the surrounding medium upon incorporation of SBS into various compatible mediums to attain anti-icing property. Different from other previous studies where oil or hydrophobic solvent have been used, a hydrophobic block copolymer (SBS) has been used here to form the continuous phase of nanoparticle stabilized emulsions. One of the advantages of retaining continuous phase of this emulsion is the possibility of incorporation of this emulsion into other hydrophobic mediums such as butimen, enhancing mechanical strength and durability. The silica nanoparticles used here not only potentially stabilize the emulsions but also introduce

additional benefits such as improved mechanical property, and allows for controlled release of KCOOH through the internal phase domains and through the particle shells. To the best of our knowledge, this is the first report of the preparation of a surface coating polymer membrane formed by the combined system of Pickering emulsion and solvent evaporation. This method is expected to be a potential candidate for the design and synthesis of functional surface coating polymer membranes [34].

3.2. Materials and Methods

3.2.1. Materials

Potassium formate (KCOOH) salt (99 %) and Sodium dodecyl sulfate (SDS) was purchased from Sigma in powder form. Agarose powder was purchased from Sigma-Aldrich. Silica nanoparticles (AEROSIL 816 ®) with particle diameter of 12 nm were kindly supplied by Degussa in powder form. Cyclohexane (99.9 %), acetone (99 %), ethanol (99 %) were purchased from Merck. Glass Petri-dishes and glass microscope slides were purchased from Nunc. Deionized water with an electrical resistance of 17 MΩcm was used in our experiments (Purelab Option, ELGA).

3.2.2. Preparation of Functional polymer Composite

3.2.2.1. Preparation of Silica Nanoparticle and SBS solutions

Silica AEROSIL 816 ® nanoparticles were dispersed in cyclohexane with three different concentrations 0.7, and 1.0 gram in 100 mL cyclohexane. The dispersion was carried out by high energy application via ultra-sonication tip (73 MS, 50 % amplitude, 50 Hz frequency) for 3 minutes. Ice bath was applied every 45 seconds to avoid excessive temperature rises. During the period between nanoparticle dispersion and emulsion preparation, the nanoparticle suspension is kept in ultrasonic bath in order to avoid agglomerations that may arise from steady positioning. The SBS stock solution is prepared by mixing 110 mg/ml SBS in cyclohexane. The mixture is stirred on magnetic stirrer at room temperature.

3.2.2.2. Preparation of the Emulsion without Gelation of the Internal Phase.

The moisture in the solid KCOOH was eliminated through freeze-drying. An aqueous KCOOH stock solution (0.5 g/mL) was prepared by dissolving the salt in

distilled water at room temperature. In order to obtain emulsion templates with just aqueous KCOOH solution in the dispersed phase, 0.5 mL of nanoparticle stock solution was added into aqueous KCOOH solution in the amounts of 0.5 or 0.25 to obtain emulsions with 25 or 14 % (v/v) internal phase fractions, respectively. To this solution 1 mL of SBS stock solution is added to obtain emulsions with SBS in the continuous phase.

3.2.2.3. Preparation of the Emulsion with Gelation of the Internal Phase

Agarose solution was prepared by adding 1% (w/w) agar powder in distilled water. The mixture was cooked in microwave oven until it boiled and all powder was dissolved. Subsequently 0.5 g of KCOOH was dissolved in 1 mL of agarose solution, which yielded 0.5 g/ml KCOOH (s) salt solution in agarose. Three different fractions of internal volume of salty agar solution were added into three different concentrations of nanoparticle-cyclohexane dispersion. The particle dispersion was kept at room temperature. Stock nanoparticle solution concentrations of 0.7% (w/v), 1.0% (w/v), and internal volume fractions of 14 % (v/v) and 25 % (v/v) were prepared. For example, for an internal volume fraction of 25 % (v/v), 0.5 mL of the KCOOH agar solution was added into 0.5 mL of nanoparticle stock solution phase under high shear applied by vortex at maximum speed for 5 seconds. As hot agarose solution was mixed in the cyclohexane, the aqueous solution formed well-dispersed droplets which were stabilized by nanoparticles. The stabilized agarose droplets instantly cooled as they mixed with the nanoparticle solution at room temperature. As agarose solution turned into gel phase, hydrophilic gel droplets that were dispersed in cyclohexane formed an emulsion. Subsequently, 1 ml of the concentrated SBS polymer in cyclohexane (110 mg/ml) was added drop-wise into 1 mL of the KCOOH, agar, and nanoparticle solution with gentle mixing.

3.2.2.4. Casting of Emulsions on Substrate Surfaces

Microscope glass slides were rinsed with ethanol and distilled water. The substrates were dried with nitrogen and 100 µl of each emulsion solution was deposited on glass slides separately. The cast membranes on glass slides were dried at 15 °C. The membranes were considered to be dry when the solvent evaporated from both phases of the emulsion, and membranes appeared elastic.

3.2.2.5. Salt release characterization

The release of anti-icing agent from dry composite membranes was investigated by immersing samples in water and measuring the quantity released into water using Ion Selective Electrode (ISE K800). First of all, the wet emulsions were poured into petri dishes and dried in 24 hours in order to obtain dry templates. Then, dry composite membranes were incubated in 20 ml deionized water for different time periods without changing the water (Figure 3.1). K+ ions were measured using ion selective electrode after each period. The amount of KCOOH (Potassium formate) released was calculated using measured K+ concentrations for each dry composite membrane.

Figure 3. 1: Measurement of K+ ions released from dry composite membranes immersed in water.

3.2.6. Anti-icing property characterization

The anti-icing property of functional composite membranes was investigated with respect to freezing water droplet rate. Freezing of water droplets on composite materials was monitored using temperature and humidity controlled chamber (Figure 3.2). Dry membranes were prepared on glass slides. Then, 10 of water droplets were dropped onto each membrane and incubated in chamber with -14 °C plate and 5 °C ambient temperature. Duration of the freezing of water droplets were recorded. Each experiment were repeated 4 times following to washing and drying of membrane surface to imitate the raining conditions.

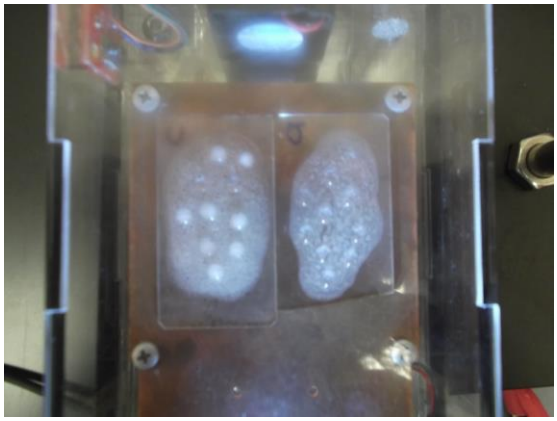

Figure 3. 2: Monitoring of freezing delays on composite membranes in temperature and humidity controlled chamber.

3.3. Results and Discussion

Stable emulsions of aqueous KCOOH solutions were prepared in SBS/cyclohexane solution using semi-hydrophobic silica nanoparticles (Figure 3.1). Addition of semi-hydrophobic nanoparticles resulted in homogenous emulsions 3hich were stable up to three months. Semi-hydrophobic silica nanoparticles have tendency to locate at the aqueous/organic interface and minimize the interfacial energy of the system. The amount of nanoparticle used is critical both for the long-term stability of the emulsion. Next, emulsion templates were formed from the dispersed droplets of the initial emulsion. The method involves an elastic membrane platform based on the continuous polymer phase; and functional domains, where domains are spread on a solid platform at a macroscopically homogeneous order (Figure 3.3). Emulsion stabilization prior to drying offers the possibility to integrate two opposite surface properties in a resultant elastic membrane. Through the design presented in this study, the previously developed emulsion templating studies were combined, where functionally loaded aqueous droplets formed a stable emulsion within the hydrophobic continuous phase with the aid of surface functional nanoparticles [34].

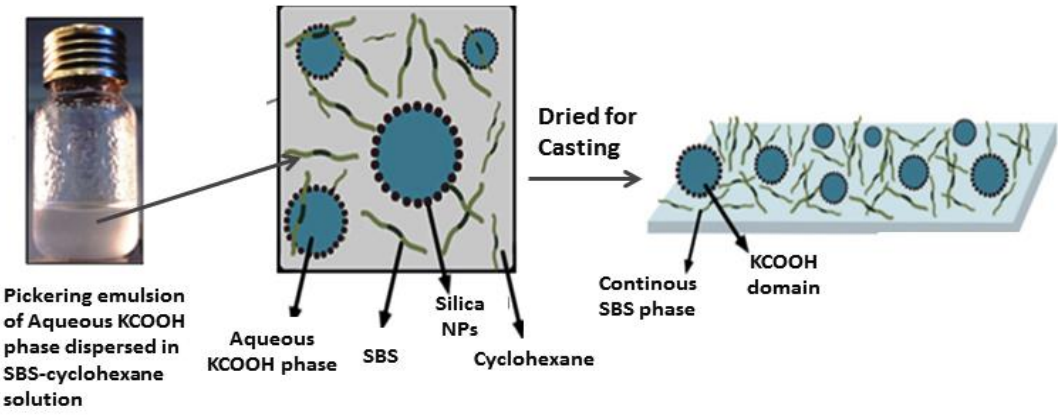

Figure 3. 3: Schematic representation of the steps for casting of solutions prepared with aqueous KCOOH solution suspended in SBS polymer with particle stabilization[34].

3.3.1. Comparison of emulsion stabilization methods

In order to investigate the stabilization potency of different mechanisms, emulsions prepared with different methods were compared. First, emulsions were prepared without any additional stabilization attempt, then they were prepared by a long tailed ionic surfactant SDS and finally surface modified hydrophobic silica nanoparticles (AEROSIL 816H) have been used. Since the main goal was to develop an ideal stabilization technique for the proposed material mixture, initially no gel was introduced into the system. Droplet formation upon shear and phase separation havebeen observed in micro-scale under optical microscope immediatelyand 3 minutes after preparation. (Figure 3.4). The results show that, at the very instant of shear exposure, all emulsions yield to spherically shaped internal phase aqueous KCOOH droplets suspended in the continuous SBS copolymer solution medium. When stabilization agent is not used however, many of the aqueous droplets merge with time. Three minutes after deposition on the surface, unstable internal phase droplets were distorted and swiftly merged upon slightest collusion and yield phase separation (Figure 3.4 a). Next, surfactant material was used to test the effect on emulsion stabilization. SDS was added into the aqueous phase along with KCOOH, before the internal phase was emulsified with the hydrophobic polymeric phase. Introduction of SDS into the system yielded stabilization of wet emulsions to some extent. Droplets with irregular sizes were formed, where many of them were not durable enough to survive beyond 3 minutes. (Figure 3.4 b). As a final approach, particles are

introduced into the continuous phase prior to emulsification in order to obtain robust and stable emulsions in this study. Unlike conventional surfactant molecules, functional nanoparticles were adequate to maintain well dispersed spherical droplets of the internal aqueous phase (Figure 3.4 c). This demonstrated the superiority of the particle stabilization technique over conventional surfactants in our system. Particle self assembly around the droplets has the advantages of being irreversible and energetically more favorable over assembly of surfactant molecules [34].

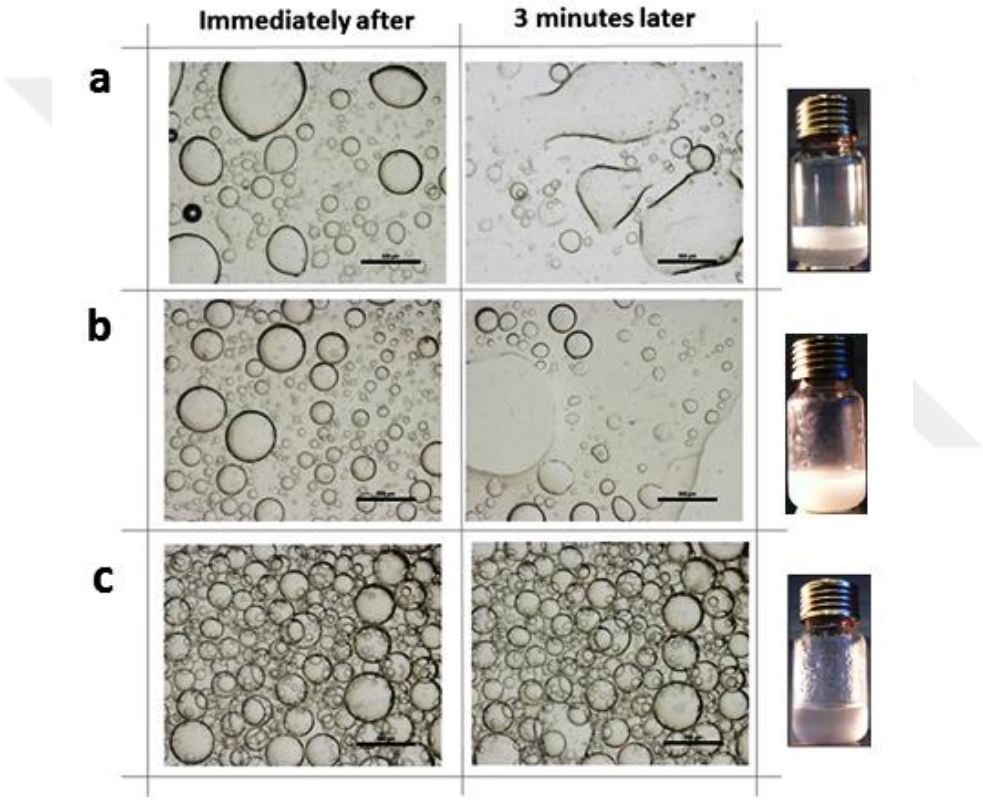

Figure 3. 4: Optical microscope images of wet emulsions and their macroscopic appearance with internal volume fraction Q =25% (v/v) prepared by different stabilization methods for immediately after and 3 minutes after preparation of emulsions. (a) Wet emulsions without stabilizing agent, (b) wet emulsions prepared with SDS surfactant as the stabilizing agent, (c) wet emulsions prepared by nanoparticle stabilization. Scale bar is 500 mm [34].

In Figure 3.5, the dispersions of salt domains in the dry state are compared with those having agar gels in salt domains. The droplets having agar gels were larger compared to those without gel. More importantly, in the dry state droplets with gel maintained their well-defined spherical shapes with slight distortions due to shrinkage during drying. The gel stabilized salt pockets were also much more homogenously dispersed in the dry films compared to those stabilized only by nanoparticles. Furthermore, the salt pockets having gels in the aqueous phase were resistant to being cracked by capillary effects during evaporation of the solvents. The elimination of cracks allows better encapsulation of the salt in the pockets and its controlled release when needed. Better controlled release profile of the functional agent (salt in this case) from the gel domains to the surrounding is important in applications such as preventing ice formation by salt release.

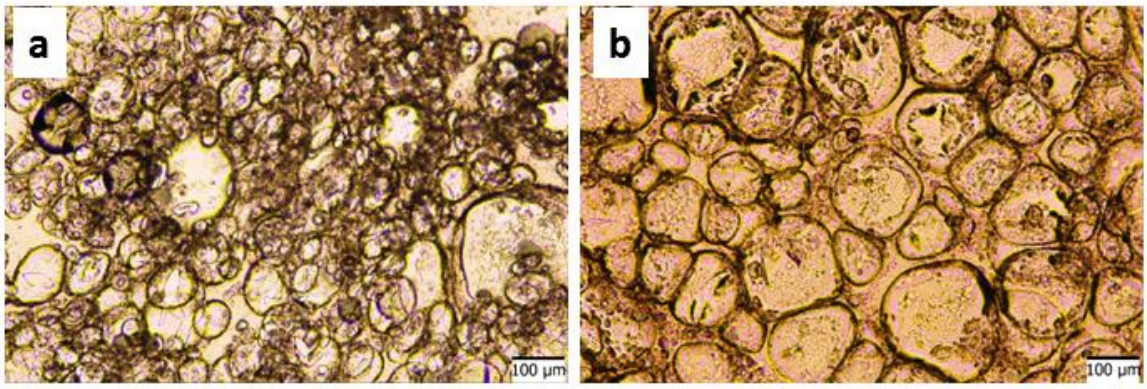

Figure 3. 5: Optical microscope images of dry membranes of emulsions prepared a) without agar gel in the dispersed phase, b) with agar gel in the dispersed phase. Scale bar is 100 µm.

3.3.2 Dynamic Mechanical Analysis

Dynamic mechanical analysis of the composite (Φ=0.25, 1.0% nanoparticle (NP)) with and without agar were undertaken with oscillatory tests using Dynamic Shear Rheometer (DSR). The oscillatory tests were conducted with temperature sweeps (20-100 °C) at constant frequency (1 Hz) and frequency sweeps (0.016-16 Hz) at constant temperature (25 °C). The principal viscoelastic parameters obtained from the temperature sweep oscillatory tests were complex shear modulus (G*), phase angle (δ) and dynamic

viscosity (μ) (Figure 3.4 a-c). Figure 3.6 a shows that complex modulus which is the measure of material resistance to deformation decreases with temperature for both composites with or without agar. However composites with agar gelation have higher complex modulus trend which indicates that gelation of the internal phase enhances the material resistance to deformation. Figure 3.6 b shows the change of phase angle with temperature. It is seen that phase angle which is the ratio of viscous nature to elastic nature decreases with the gelation of internal phases of the composites. This trend indicates the increase of the elasticity of material with gelation of agar. Figure 3.6 c demonstrates that dynamic viscosity increases with gelation of the internal phase.

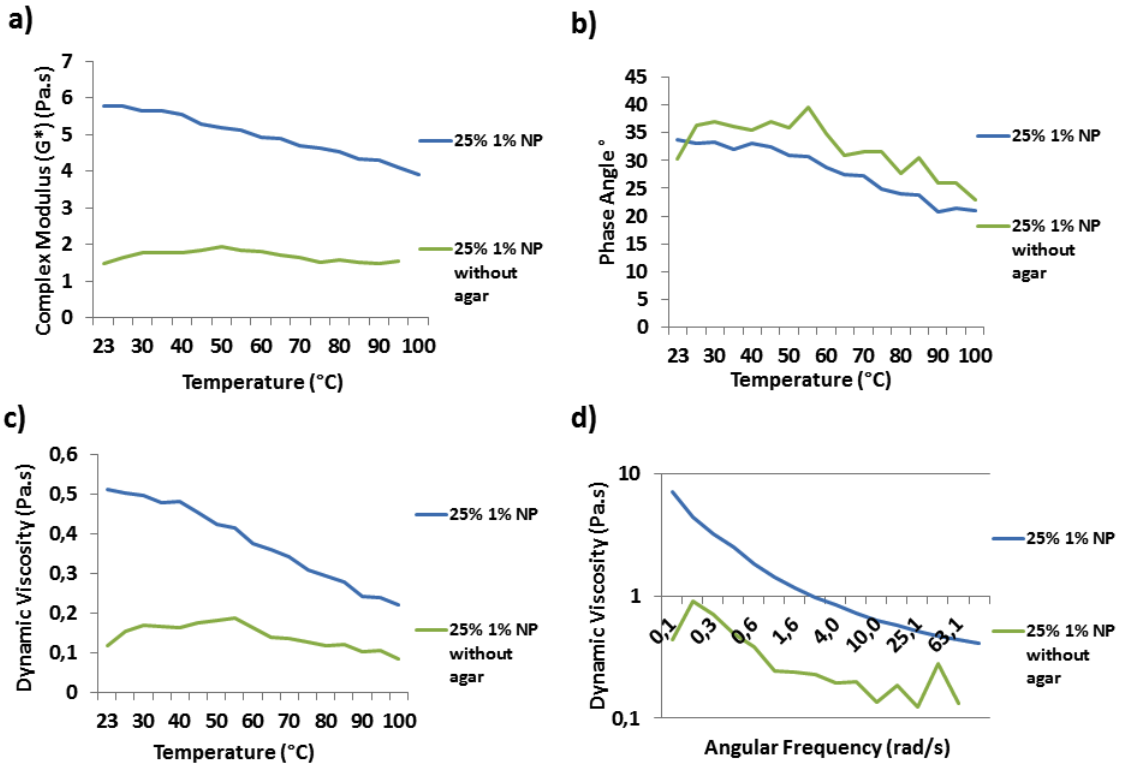

Figure 3. 6: Dynamic mechanical analysis of emulsions prepared with or without agar. Plots of a) Complex modulus, b) Phase angle and c) Dynamic viscosity with temperature ramp at 1 Hz. d) Plots of dynamic viscosity with angular frequency ramp at 25 °C.

The principal viscoelastic parameter obtained from the frequency sweep oscillatory test was dynamic viscosity (μ) (Figure 3.6 d). This figure shows the

enhancement of dynamic viscosity with gelation. It is seen that dynamic viscosity decreases with increase in frequency. This trend is the indication of shear thining behavior of the emulsion similar to the results obtained from flow tests. Figure 3.6 generally shows that there are more smooth trends of decrease in emulsions with gelation of the internal phase due to more uniform and homogeneous structure of the emulsions.

3.3.2. Salt release measurements of functional dry composite membranes

Salt release measurements were applied to the composites with 0.7 and 1.0 % (w/v) of nanoparticle concentration and, ϕ =0.14 and 0.25 with gelation of the internal phase. The release was measured from a sample immersed in water, being the water the same for the whole duration of the test. K+ concentrations measured after 15, 50, 120 and 240 minutes are presented in Table 3.1. The results of salt release measurements is reported in Fig. 3.7.

Table 3. 1: Concentrations of potassium formate in water released from dry composite membranes with geltaion of the internal phase in different time periods

Time (min)	Φ=0.25 and NP 1.0 % (mg/ml)	Φ=0.25 and NP 0.7 % (mg/ml)	Φ=0.14 and NP 0.7 % (mg/ml)	Φ=0.14 and NP 1.0 % (mg/ml)
15	627	505	356	326
50	744	637	414	386
120	925	778	484	489
240	943	806	489	532

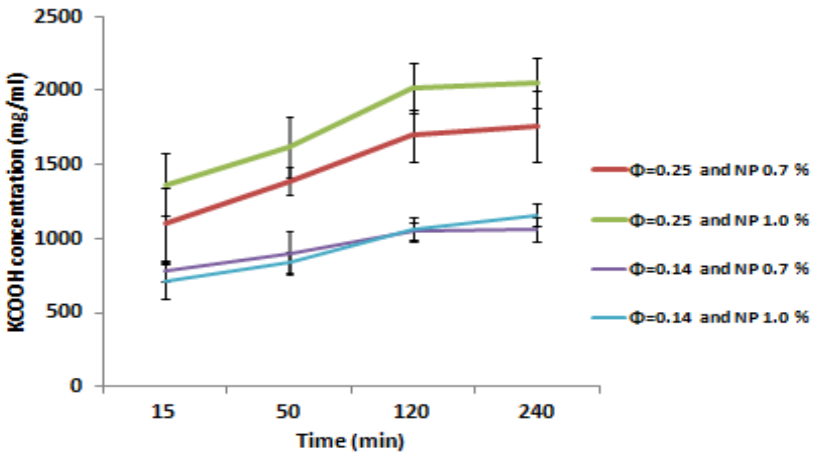

Figure 3. 7: Effect of internal phase volume fraction and nanoparticle concentration on profile of potassium formate release from dry composite membranes with gelation of the internal phase [34].

The graph has a trend shows that there is continous salt release from dry membranes in 2 hours and seems to converge in 4 hours. It is seen that, depending on the initial salt content (Table 3.2), potassium formate concentration increases with the increase of internal phase volume fraction. Higher nanoparticle concentration also results in increase of potassium formate released. From the final concentration of salt in water it can be calculated that the composites with internal phase volume fraction and nanoparticle concentration ((ϕ =0.25, 1.0 %), (ϕ =0.25, 0.7 %), (ϕ =0.14, 0.7 %) and (ϕ =0.14, 1.0 %)) release about 48.9 %, 44.4 %, 41.8 % and 48.3 %, respectively of the potassium formate. This higher release can be explained by the fact that increase of nanoparticle concentration increases the number of droplets and interfacial area which can provides higher release.

Table 3. 2: Initial amounts of potassium formate encapsulated in the dry composite membranes with gelation of the internal phase.

	Φ=0.25 and NP 1.0 %	**Φ=0.25 and NP 0.7 %**	**Φ=0.14 and NP 0.7 %**	**Φ=0.14 and NP 1.0 %**
Initial number of moles of KCOOH (mmol)	0.99	0.99	0.56	0.56

3.3.3. Anti-icing properties of functional dry composite membranes

Measurements of anti-icing properties were performed by measuring the freezing times of water droplets on composite membranes in a homemade temperature and humidity controlled chamber with -14 °C plate and 5 °C medium temperature. The composites with 0.7 and 1.0 % (w/v) of nanoparticle concentration and, ϕ =0.17 and 0.25 with gelation of the internal phase were measured in these experiments. The anti-icing property of the composites membranes with respect to water droplet freezing time is reported in Fig. 3.8.

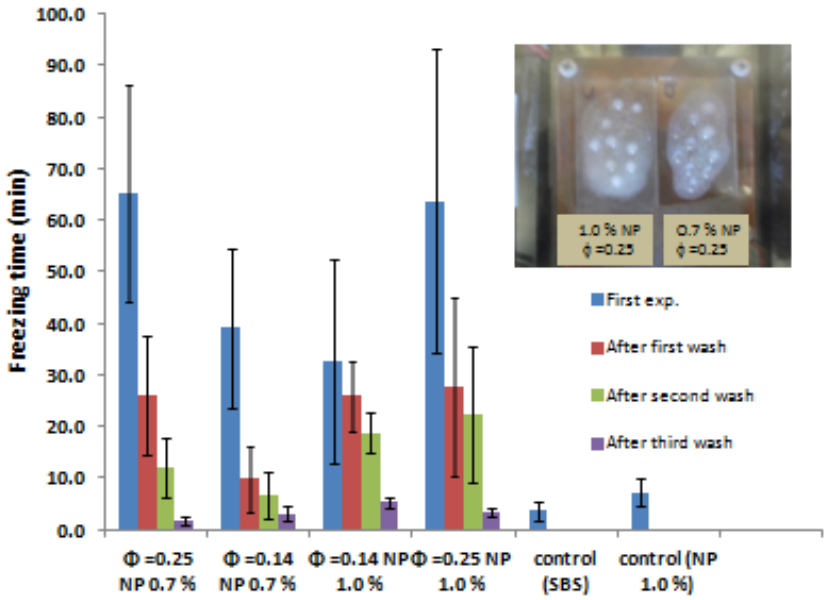

Figure 3. 8: Average freezing times of 10 water droplets on dry composite membranes with gelation of the internal phase, SBS (control) and SBS with 1.0 % nanoparticle

concentration (control).The inset figure is from one of the experiments after 60 minutes where the composite with 1 % (w/v) nanoparticle concentration (left, ϕ =0.25) and 0.7 % (w/v) nanoparticle concentration (right, ϕ =0.25) are monitored in humidity and temperature controlled chamber (plate temperature: -14 °C, ambient temperature: 5 °C) [34].

The bars are showing the results of first and the following experiments after first, second and third wash, respectively for each sample. The freezing time is the average of freezing times of 10 of water droplets on the composite membranes. It can be seen that the nanoparticles with ϕ =25 delayed the freezing about 70 minutes, while the composites with ϕ =0.17 could delay 40 minutes at maximum. Increase in the internal phase volume fraction results in increase of the freezing time as a result of high salt content included. On the other hand, higher nanoparticle concentration has opposite effect by decreasing the freezing time in first experiments. The Fig. 8 inset shows one of the first experiments that two composite membranes are monitored in humidity and temperature controlled chamber with with -14 °C plate and 5 °C medium temperature. It is seen that most of the water droplets on the composite membrane (left, ϕ =0.25) with 1 % (w/v) nanoparticle concentration are frozen, while there are still unfrozen droplets on the composite membrane (right, ϕ =0.25) with 0.7 % (w/v) nanoparticle concentration after about 60 minutes. But another fact obvious in the Fig. 8 is higher nanoparticle concentration leads to higher freezing times in experiments following to washing. This is the indication that higher nanoparticle concentration around the droplets decrease permeability and provides limited salt release while first experiment and washing, and allows for continous salt release for longer time. This is why, in the following experiments after washing, the composites with lower nanoparticle concentration have longer freezing times.

3.4. Conclusion

This study has combined two well established approaches of emulsion templating in order to produce a hydrophobic membrane that can store hydrophilic domains and can provide cpntrolled release of agents. The droplets were functionalized by loading with aqueous KCOOH as a representative hydrophilic agent. The emulsion was

stabilized by solid particle stabilization method using partially hydrophobic silica nanoparticles. The functionalized packages with gel domains were also fabricated and compared to the ones without gel domains. The effect of stabilization method and gelation on the stability of the initial emulsion and morphology of the resultant membrane were investigated.

The embedded hydrophilic domains can serve as functional capsules which store anti-icing agents and are surrounded by nanoparticles. Dry templated emulsion is characterized with respect to permeability to anti-icing agent and water droplet freezing rate. Dry composite membranes released 32 g/m^2 anti-icing agent within 4 hours and delayed freezing of water droplets for about 70 minutes. Salt release and anti-icing properties of dry membranes could be tuned witj nanoparticle concentration and internal phase fraction. Finally, the template emulsion can be designed to serve both as a dry membrane and to be integrated into other hydrophobic mediums such as bitumen.

Chapter 4

DESIGN OF FUNCTIONAL POLYMER COMPOSITE MODIFIED BITUMEN

4.1. Introduction

Anti-icing functionality is desired in many outdoor systems in order to delay ice formation and to prevent adhesion of ice on surfaces, so that mechanical removal of ice from the surface is easier. In industrial applications, such as for wind turbines and on pavements for vehicle transportation during the winter, anti-icing is critical. According to ten-year averages from 2004 to 2013, 41% of crashes that happen on wet pavement occur during snow or on slippery pavements [171, 172].

Until recently, studies on anti-icing surfaces were mainly geared towards achieving super-hydrophobicity on surfaces [173-178]. However, superhydrophobicity is not necessarily appealing on all surfaces that require anti-icing function. Upon exposure to water, superhydrophobic surfaces promote slip, since they reduce drag by trapping gas bubbles between the surface and the liquid using a microscopic texture. Furthermore, surface geometry modification at nano-level is difficult and in most cases not economically feasible [173-175]. Another approach to eliminate ice formation on surfaces is the use of anti-icing agents. Ionic salts are the most commonly employed

agents for this purpose. As ions dissolve in water, they localize between water molecules and retard the crystallization process. As a result of the delay in crystallization, water remains in the liquid phase at lower temperatures than the freezing point of pure water [179, 180].

Sodium chloride, calcium chloride, and sodium acetate have been commonly used as anti-icing agents; however, these salts have a negative impact on the stiffness and viscoelastic properties of asphalt pavements [181-184]. The influence of conventional use of potassium formate on asphalt concrete is also investigated [185-187]. The deterioration effect of acetate [187] and formate [186] based deicers is observed in these studies when asphalt concrete is exposed to deicers solutions. However, polymer modification of bitumen is also suggested in these studies to counterbalance the negative effects of deicers in terms of mechanical properties. Various solutions have been suggested as alternatives to the conventional usage of these agents. One of those strategies involves the addition of levulinic salts into the asphalt mixture to eliminate the need for the common anti-icing agents and to obtain pavements with an anti-icing property [75]. In another study, researchers evaluated the potential of synthetic fillers such as sodium chloride, calcium carbonate, magnesium carbonate in an asphalt mixture to promote an anti-icing property. A delay in frost formation and a decrease in adhesion between ice and the pavement were reported [77] .

Previous studies are important for the development of anti-icing strategies; however, the influence of these synthetic fillers on the thermomechanical properties of the binder in asphalt mixtures still needs to be investigated [77]. The modification of bitumen with a styrene-butadiene-styrene SBS polymer for improved thermomechanical properties has also been considered separately in other studies [88, 89, 188-194]. The hydrophobicity and thermoplastic nature of the SBS polymer allows for incorporation of this composite into bitumen, opening up the possibility of delivering anti-icing agents through bitumen. SBS has been widely used in polymer modified bitumen (PMB) for the construction of asphalt binders and constitutes the continuous phase of the parent emulsion and the membrane base of the composite developed here [195]. Bitumen is a semi-solid hydrocarbon material, generally produced from certain crude oils by distillation (atmospheric/vacuum) units in oil refineries. The majority of bitumen has

been used as a binder in asphalt road pavements [79]. Due to high traffic density, increases in loading and pressure, plus insufficient maintenance, asphalt pavements can deteriorate with time. Distress signs often take the form of rutting and cracking. To minimize the damage and increase the lifetime of asphalt roads, polymer modified bitumens, including those modified with SBS, have been used [88, 89, 188-190, 196].

To our knowledge, no study exists that considers the anti-icing property along with thermomechanical properties for polymer-modified bitumen. The formation of a functional polymer-modified bitumen system is based on the fine dispersion of a polymer-ionic salt composite in bitumen and on the compatibility of the polymer bitumen system [77, 89, 190, 192]. In our previous study, we incorporated an ionic salt, potassium formate (HCOOK) into SBS through a particle stabilized emulsion templating approach. Our design consists of a composite membrane coating, which integrates a hydrophobic polymer adhesive base and a dispersed hydrophilic phase. The hydrophilic phase includes agarose (agar) hydrogel domains to store the anti-icing agent HCOOK. Controlled release of HCOOK from this composite was characterized, and a freezing delay of about 70 minutes was observed on this functional composite surface in a temperature and humidity controlled chamber [1]. In this chapter, we modified bitumen with this functional polymer composite to obtain polymer composite-modified bitumen with anti-icing surface properties. The compatibility of SBS in bitumen opens up the possibility to incorporate this composite system into bitumen for anti-icing functionality as a result of effective incorporation of functional packages. In this chapter, we accomplish proper incorporation of the polymer composite into bitumen and evaluate the morphology, rheology, salt release, and contribution of this modification to anti-icing properties of bitumen surfaces [2].

4.2. Materials and Methods

4. 2.1. Materials

Styrene-butadiene-styrene block copolymer (SBS, S:B weight fraction: 70:30) (Kraton D1101), potassium formate (HCOOK) salt (99 %) (Sigma Aldrich), silica nanoparticles (AEROSIL 816 ®) and cyclohexane (99.9 %) (Merck) were used for the

preparation of particle stabilized emulsions. Agar powder was purchased from Sigma-Aldrich. 50/70 penetration grade bitumen was kindly supplied by TUPRAS. Deionized water was used in the experiments (Purelab Option, ELGA). Glass petri dishes and glass microscope slides were purchased from Nunc.

4.2.2. Preparation of composite-modified bitumen

4.2.2.1. Preparation of emulsions

Particle stabilized emulsions with 0.25 (v/v) internal phase fraction (Φ=0.25), 1.0 % (w/v) nanoparticle concentration with or without gelation in the internal phase were prepared as described in previous chapter [1]. Briefly, 0.5 mL HCOOK (0.5 g/ml) salt solution with or without agar was added to 0.5 mL of 1.0 % (w/v) nanoparticle-cyclohexanone stock solution under high shear applied by a vortex mixer at the maximum speed for 5 seconds. After stabilization of the aqueous droplets by nanoparticles in the stock solution, 1 mL of SBS polymer in cyclohexane (110 mg/mL) was added drop-wise to 1 mL of the HCOOK, agar, and nanoparticle solution by mixing slowly.

4.2.2.2. Preparation of functional composite membranes and incorporation into bitumen

Prepared emulsions were cast in petri dishes to dry and functional composite membranes were obtained. The emulsions were dried in petri dishes for 24 hours at room temperature. The SBS polymer and the composites were chopped up and then incorporated into bitumen using a laboratory scale mixing device. The bitumen composite blends were prepared with a three-blade impeller low shear mixer (RW20, IKA Germany). The composite was mixed into bitumen at a temperature of 170 °C and a rotation speed of 125 rpm for 2.5-3 hours. After processing, the samples were stored at room temperature (Figure 4.1).

Figure 4. 1: A schematic of the preparation of composite polymer-modified bitumen [2].

4.2.3. Surface characterization of composite-modified bitumen

4.2.3.1. Fluorescence Microscopy

Fluorescence microscopy was used to infer SBS morphology in a polymer-modified bitumen. The morphologies of SBS in polymer-modified bitumen and in composite-modified bitumen were investigated under fluorescence microscopy with 520 nm emission and 450-490 nm excitation wavelength range.

4.2.3.2. Atomic Force Microscopy

Atomic Force Microscopy (AFM) experiments were performed in a Bruker Dimension Icon AFM with MPP21100-10 REFSP tips. Typical scans covered areas of 20x20 μm^2 in bitumen samples. Imaging was performed in soft tapping mode (intermittent contact) at room temperature. Both topographic and phase difference microscopy (PDM) images were recorded and analyzed.

4.2.4. Dynamic mechanical analysis

The most commonly used method of fundamental rheological testing of bitumen is a dynamic mechanical method using oscillatory-type testing, generally conducted within the region of the linear viscoelastic (LVE) response. The oscillatory tests were performed using a Discovery Hybrid Series-2 Rheometer (TA), which applies oscillating shear stress and strain to a bitumen sample sandwiched between parallel plates, at different loading frequencies and temperatures. The DHR tests reported in this study were performed at 0.02 Hz constant frequency and temperature sweeps between 20 and 100 °C. The tests were undertaken with a 20 mm diameter, 1 mm gap and parallel plate testing geometry.

4.2.5. Characterization of Functional Properties

4.2.5.1. Salt release characterization

The release of HCOOK from the polymer composite-modified bitumen was investigated by immersing samples in water and measuring the K^+ ions released into water using an ion selective electrode (ISE K800). Dry composite-modified bitumen samples were incubated in 20 mL deionized water for different time periods without changing the incubation water medium. K^+ ions were measured using the ion selective electrode (WTW Potassium Combination Electrode K 800) at specific time points. The amount of HCOOK released was calculated using the measured K^+ concentrations.

4.2.5.2. Anti-icing property characterization

The anti-icing properties of base bitumen and composite-modified bitumen were investigated with respect to the freezing rate of a water droplet on the bitumen surface. Freezing of water droplets on the bitumen surfaces was induced using a temperature and humidity controlled chamber (Teknofil Co.). One hundred μL of water was dropped onto each bitumen surface and incubated in the chamber with a -14 °C plate and 5-6 °C ambient temperature. The durations of the freezing of water droplets were recorded based on the visual observation for disappearance of transparency of the droplets. Incubation of the surfaces with water was repeated three times. For the first part of our experiments, water droplets were removed after each exposure and fresh drops were added after recording freezing times. In the second part, water droplets were kept on the surface after each exposure and subsequently evaporated in place so that the salt would not be lost with the water, and the fresh drops of water were then added onto the surface for the repeat measurements.

4.3. Results and Discussion

4.3.1. Dynamic Mechanical Analysis

Bitumen was modified by the SBS polymer in the dry form as a control. A mixture of HCOOK and bitumen was prepared as an additional control. Therefore, five different samples were examined, and these were listed in Table 4.1.

Table 4. 1: Description of the sets studied for characterization of mechanical and anti-icing properties.

Sample set	Percent polymer in bitumen (wt/wt)	Presence of agar	Presence of KCOOH
Base bitumen	0	No	No
Bitumen + 5% salt	0	No	Yes
Bitumen + 5% solid SBS	5	No	No
Bitumen + 5 % dry composite (no agar)	5	No	No
Bitumen + 5 % dry composite (with agar)	5	Yes	No
Bitumen + 5 % SBS solution	5	No	No
Bitumen + 5 % composite (wet)	5	Yes	Yes

Dynamic mechanical tests were conducted to investigate the viscoelastic properties of bitumen. The viscoelastic parameters measured in the oscillatory tests are the complex modulus (G*) and the phase angle (δ). G* is defined as the ratio of maximum stress to maximum strain and provides a measure of the total resistance to deformation under shear loading. It contains elastic and viscous components, which are the storage modulus (G') and loss modulus (G''), respectively. These two parameters are related to each other through the phase angle (δ), which is the phase lag between the applied shear stress and the shear strain during an oscillatory test. The phase angle is a measure of the viscoelastic balance of the material behavior and is equal to the arctangent of the ratio of loss modulus (G'') to storage modulus (G') [89].

Isochronal plots of the complex modulus G* versus temperature at 0.02 Hz for all samples defined above are shown in Figure 4.2. Modification of the bitumen with the

SBS polymer resulted in only a minor increase in G* at lower temperatures, but there was a significant increase at high temperatures compared to base bitumen. The G* profile reached a plateu region, consistent with a polymer network dominant structure observed in previous studies with SBS polymer-modified bitumen [89]. We also modified bitumen with an SBS solution (SBS dispersed in cyclohexane) and a wet composite (SBS and HCOOK dispersed in cyclohexane) and observed a significant decrease in G* compared with base bitumen at all temperatures, which may be associated with the damage of the binder structure due to the presence of cyclohexane. Since there is no such decrease in the G* versus temperature profile for the dry composite-modified bitumen, we continued to use dry composites rather than wet composites in our experiments. It was observed from the G* profiles that the composite-modified bitumen had very similar G* profiles to the base bitumen and did not have higher values of G*, as was found with the dry SBS modification. This lower G* was due to the lower amount of SBS in the bitumen + dry composite sample compared to the amount in bitumen + solid SBS sample. This result was further supported by the G* values of the salt-modified bitumen sample, where there was a minor decrease in G*. These results suggest that dry composite-modified bitumen has similar mechanical strength despite the presence of the anti-icing agent. In previous studies deterioration effect of acetate and formate based deicers was demonstrated [185, 187]. However, these deicers are applied on asphalt pavements direclty which can cause this kind of deterioration. In our design we incorporate potassium formate into bitumen through SBS polymer that counterbalance the deterioration effects of formate based deicers by establishing a polymer network which increase the resistance of bitumen against deformation. This effect was also discussed in a previous study where asphalt concrete was stored in potassiım formate solution at 19 °C for 48 hours. In that study, authors report that polymer mix modification including SBS polymer counterbalance the negative effects of potassium formate solution in terms of mechanical properties such as indirect tensile strength and fracture and results in reduced susceptibility to anti-icing chemical [186]. However, SBS polymer modification does not contribute to binder-aggregate binding affinity and binder-aggregate affinity decreases in potassium formate solutions which is discussed as contradiction. We observed similar outcomes from dynamic mechanical analysis in terms of mechanical properties (Figure 4.2). Although

salt addition causes a minor decrease in the complex modulus of bitumen, salt including composite modified bitumen have slightly increased complex modulus values compared to base bitumen which shows that adding salt in composite structure do not decrease mechanical strength and resistance of bitumen against to deformation. Additionally, the tests used in previous study imitate the usual usage of salts on asphalt pavements by storing them in salt solutions. However, in our study, we proposed encapsulation of salt in SBS polymer and controlled release of it through bitumen for anti-icing property to replace the conventional usage of salts on asphalt roads for de-icing property.

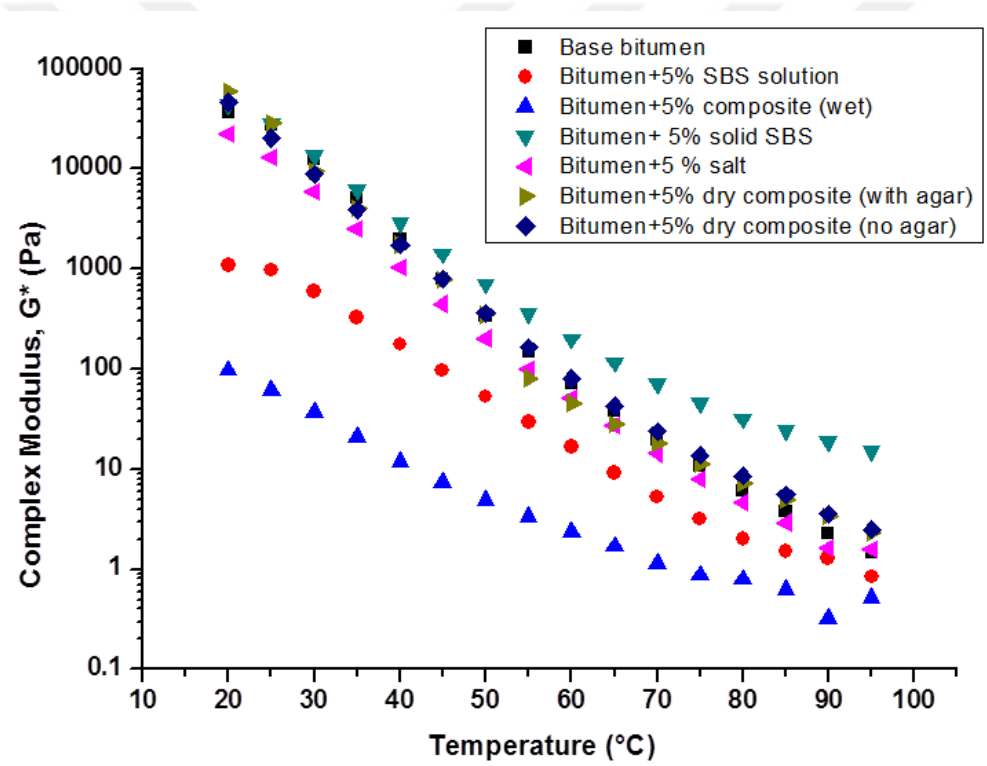

Figure 4. 2: Isochronal plots of the complex modulus, G* at 0.02 Hz for SBS and composite-modified bitumen [2].

Phase angle (δ) versus temperature values for the SBS polymer and composite-modified bitumen groups are shown in Figure 4.3. It can be observed from the figure 4.3 that δ measurements are also sensitive to the modification of bitumen. Tanδ is the ratio of the loss modulus to storage modulus, which corresponds to the ratio of the viscous to

elastic nature of the material. Figure 4.3 shows that the δ values of bitumen samples modified with the dry composite are lower than the base bitumen at low temperatures, but then they increase and reach similar values to the base bitumen at high temperatures. This result suggests that the composite-modified bitumen is more elastic than the base bitumen at temperatures up to about 60 °C. δ values of solid SBS modified bitumen has a decreasing trend with temperature, which is consistent with previous studies and is due to an increase in the elastic nature of the binder from the distribution of polymer [89]. Lower δ values were observed for bitumen samples modified by the wet composite compared to bitumen modified by the dry composite for the entire temperature range. The low δ values can be explained by decreases in viscosity due to the presence of cyclohexane in the medium. This is undesirable for pavement applications, further supporting our decision to focus on dry composites for this work. The δ measurements together with G* measurements also suggest that the dry composite-modified bitumen increases the elasticity at low temperatures, and composite modification does not affect the viscoelastic balance and the strength of bitumen at high temperatures. Hence, it was concluded that, from a viscoelastic property standpoint, the functional composite in the dry form provides sufficient mechanical performance for pavement applications.

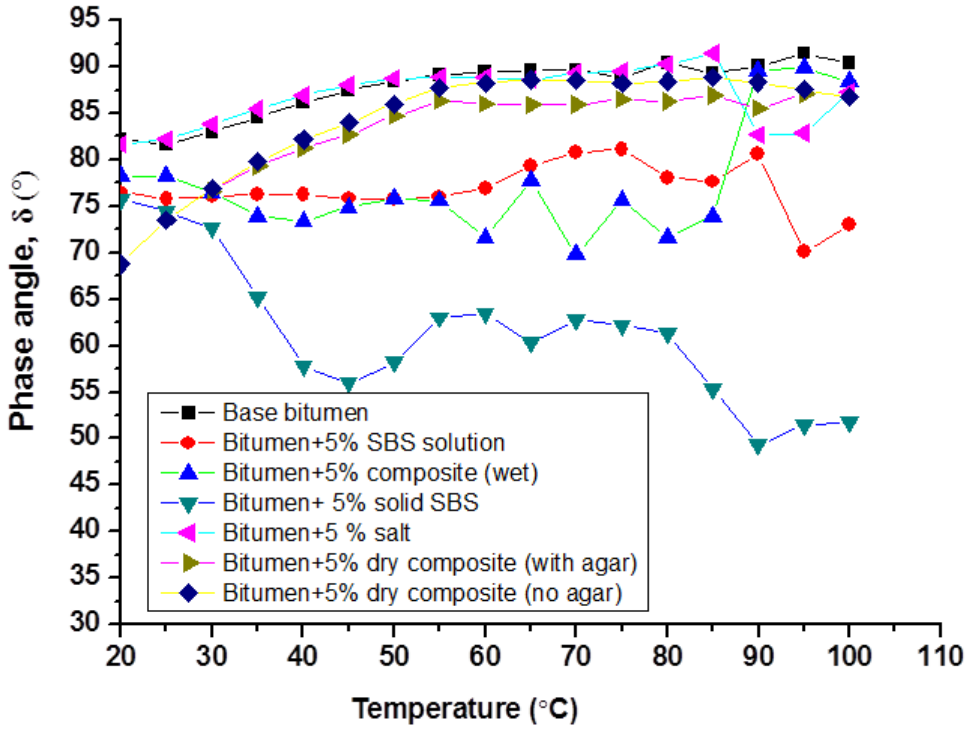

Figure 4. 3: Isochronal plots of the phase angle at 0.02 Hz for SBS and composite-modified bitumen [2].

4.3.2. Morphological characterization of modified bitumen

4.3.2.1. Fluorescence microscopy

The resins and aromatics present in bitumen swell the SBS polymer, and this swelling results in fluorescence of SBS under fluorescence microscopy with 520 nm emission and 450-490 nm excitation wavelength range. The fluorescence behaviour due to swelling has been used to infer the morphology of the SBS and composite in bitumen [189]. Bitumen samples modified with SBS and composite were investigated under fluorescence microscopy to visualize the distribution of the additive throughout the bitumen. Fluorescence microscope images for composite- or SBS-modified bitumen samples are shown in Figure 4.4. It can be observed that solid SBS can form better polymer distribution than composite modified bitumen (Figure 4.4 a). This difference in morphology is consistent with the observed dynamic mechanical properties of solid SBS-modified bitumen, as a uniform distribution of polymer would have a positive influence on the complex modulus and elastic properties of bitumen, which were seen

through the higher G* and lower phase angle of samples modified by solid SBS (Figure 4.2 and Figure 4.3).

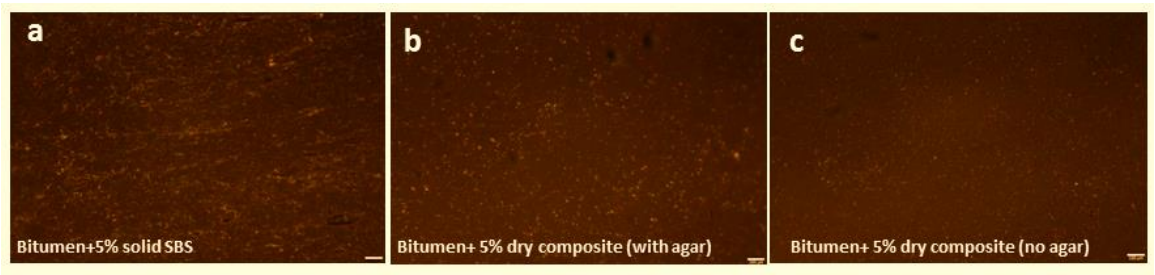

Figure 4. 4 Morphological analysis of SBS and composite-modified bitumen with fluorescence microscopy (scale bar: 100 μm)[2].

4.3.2.2. Atomic Force Microscopy (AFM)

The microstructure of bitumen is usually described by the so-called "colloidal model". According to this model, bitumen is considered as a colloidal system constituted by micelles of asphaltenes dispersed in bitumen [197, 198]. Typical AFM images demonstrate that bitumen is a multiphase material. Asphaltenes and resins behave as solid-like materials, resulting in an increased stiffness [79]. These larger-size molecules seem to form the stiffer parts observed during AFM testing. The soft matrix, on the other hand, contains small-size saturates and aromatics. Masson et al. reported that asphalt contains multiphase bitumen, consisting of a nanostructure phase, defined as "bee-like", and a dispersed phase referred to as the "catana or catanic" phase [199]. The name "bee" comes from the presence of alternating higher and lower parts in the surface topography of bitumen.

Figure 4.5 shows AFM images in three dimensional phase (left) and topography (right) modes for the base and modified bitumen samples. Base and bitumen samples modified by SBS polymer and dry polymer composite with/without agar were investigated using soft tapping mode AFM. Both topographic and phase difference images were recorded and analyzed. In Figure 4.5, the phase images on the left panel demonstrate the soft sections as dark regions, where the rigid domains in the bitumen structure are shown with a light color. In the corrosponding height images on the right

panel (Figure 4.5), the dark areas correspond to valleys and low areas of the surface profile, while the light colored areas correspond to peaks on the surface.

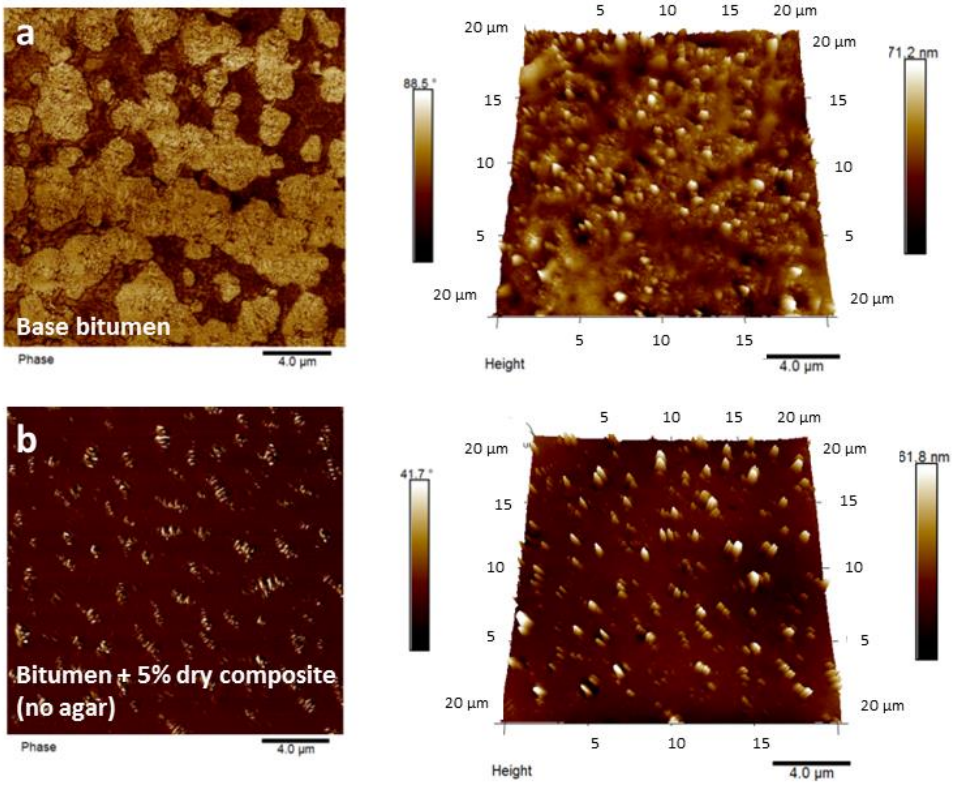

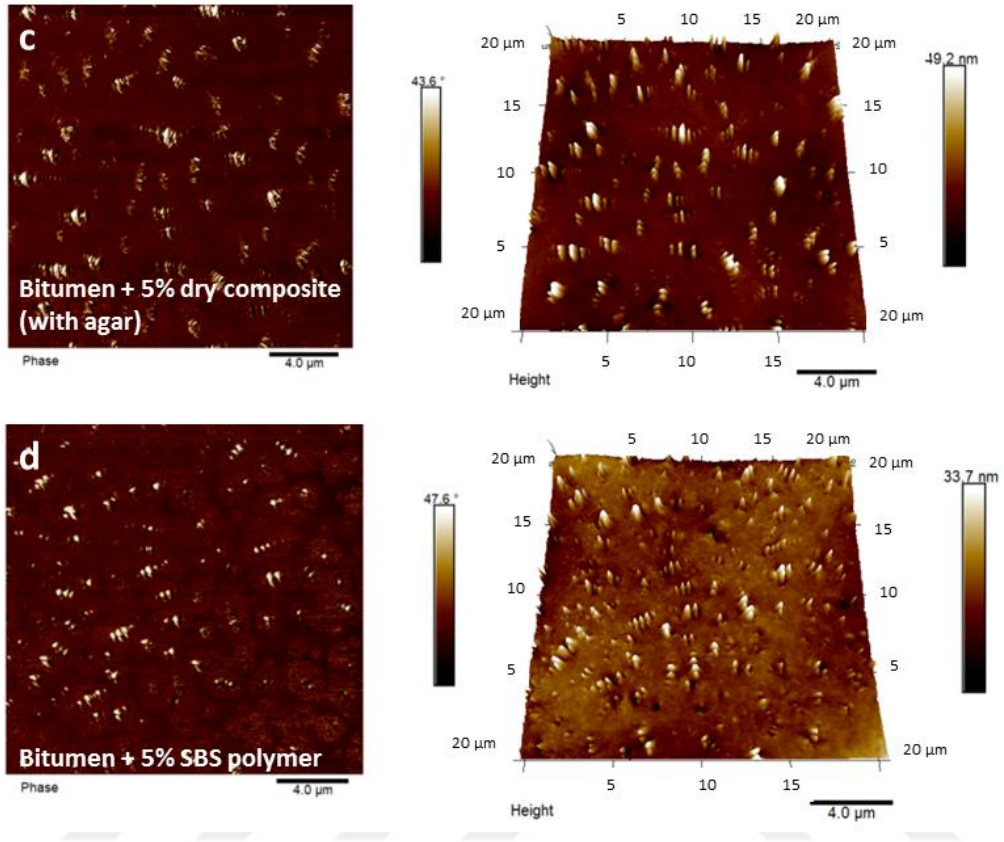

Figure 4. 5: AFM phase difference (left) and topographic image (right) of a) base bitumen b) dry composite (with agar)-modified bitumen (5% (wt/wt)) c) dry composite (without agar)-modified bitumen (5% (wt/wt)) d) SBS polymer modified bitumen (5% (wt/wt)) [2].

Our AFM images qualitatively demonstrate the standard description of bitumen structure. As shown in Figure 4.5 a, two phases can be identified for base bitumen, but the bee-like structures are not clearly distinguishable. More distinctive bee-like structures were observed for bitumen modified by the polymer composite (5% (wt/wt)) and SBS (5% (wt/wt)) demonstrating that modification of bitumen changes the surface topography of bitumen, resulting in more phase and height differences. The bee-like structures become more distinct with the addition of other ingredients into the bitumen.

Figure 4.5 b and 4.5 c show that the composite polymers with or without agar in bitumen are distributed more uniformly than the SBS polymer, which is also consistent with flouresence microscopy characterization (Figure 4.4). Larger bee-like features are

observed in the SBS polymer-modified bitumen. In addition, a new phase is observed around the bee-like features in the SBS and composite (with agar)-modified bitumen, which could be attributed to higher swelling of SBS in those regions (Figure 4.5 c and 4.5 d).

4.3.3. Characterization of anti-icing properties

Anti-icing properties of glass slides coated with base bitumen and composite-modified bitumen were investigated in a temperature and humidity controlled chamber on a -14 °C plate, with ~6 °C medium temperature and 50% humidity conditions. After equilibration at the testing temperature, 100 μL of water was dropped on each sample surface, and the duration of freezing for water droplets was recorded based on the disappearance of transparency. Figure 4.6 shows the images of bitumen coated samples at different time points in the chamber. It can be observed from the Figure 4.6 that the freezing started after 4 minutes on the base bitumen, whereas it took about 9 minutes for water droplets to freeze on the functional composite-modified bitumen. At the end of 27 minutes, all droplets on the base bitumen were completely frozen, while only half of the droplets were frozen on the functional composite-modified bitumen. The average droplet freezing times were calculated as 5 minutes and 15 minutes on the base bitumen and functional composite-modified bitumen surfaces, respectively.

	Base (left) and composite modified bitumen (right)
t=0	
t=4	
t=9	
t=27	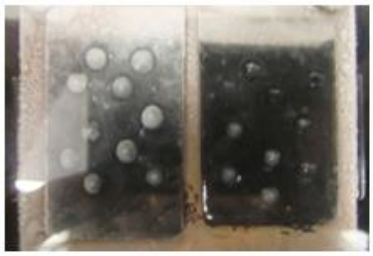

Figure 4. 6: Surface images of base bitumen and composite (with agar)-modified bitumen (7.5% (wt/wt)) in a humidity and temperature controlled chamber at different time points (Plate temperature: -14 °C, medium temperature: 5-6 °C and relative humidity: 50%) [2].

The effect of increasing the salt content of the composite on the anti-icing properties of composite-modified bitumen (5% (wt/wt)) was also investigated by monitoring the freezing of water droplets on polymer composite (without agar)-modified bitumen surfaces with altered salt concentrations. Bitumen was modified with composites

with 1X, 2X, 3X and 4.5X salt content, which corresponded to 0.125 g/mL, 0.25 g/mL, 0.375 g/mL and 0.5625 g/mL salt in wet emulsions, respectively. In order to test salt release from different spots on the bitumen surfaces, subsequent incubations of the surfaces with water droplets were repeated at least three times. The bitumen or composite-modified bitumen surfaces were exposed to water thrice by removing the frozen droplets and subsequently dropping fresh droplets.

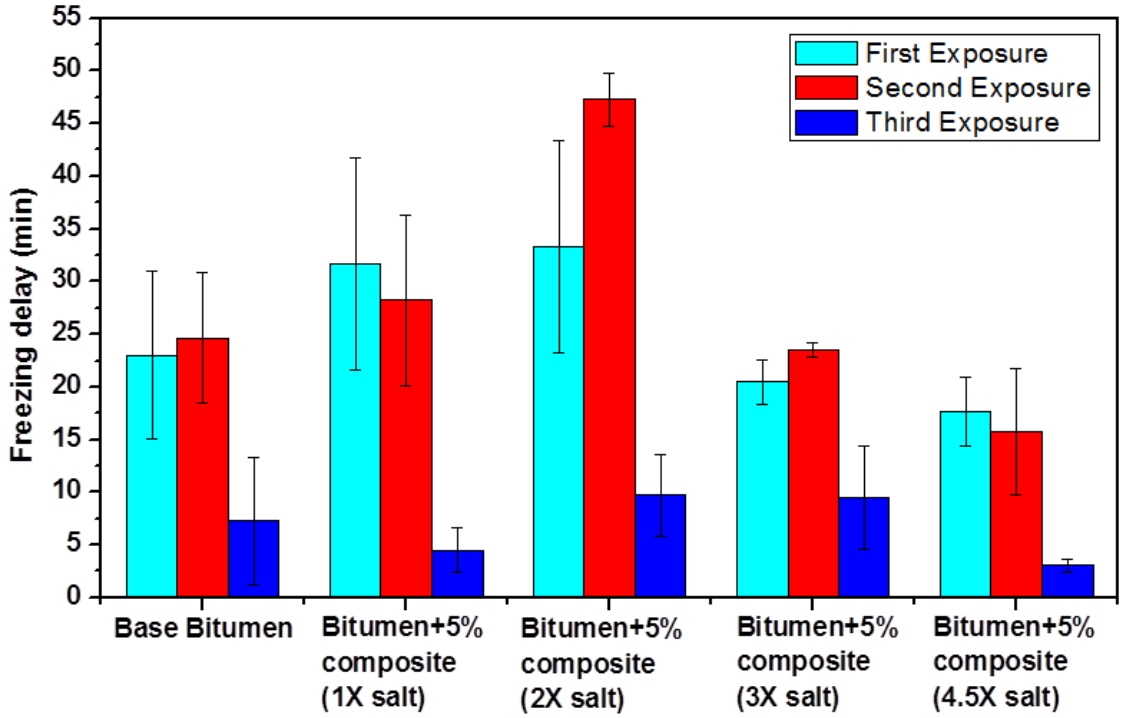

Figure 4. 7: Freezing delays on surfaces of base and composite-modified bitumen (5% (wt/wt)) with different salt content in humidity and temperature controlled chamber (Plate temperature: -14 °C, medium temperature: 5-6 °C and relative humidity: 50%) [2].

Figure 4.7 shows the results of average freezing delay measured on composite-modified bitumen surfaces with 1X, 2X, 3X and 4.5X salt contents. The results suggest that the 2X salt content has the greatest influence on the anti-icing capability, and this effect is more significantly observed after a second exposure. Interestingly, the 3X and 4.5X salt negatively influenced the freezing delay. This result may be due to the low

encapsulation efficiency of high salt within the composite structure, where a significant amount of salt was lost during sample preparation.

The most promising bitumen sample, the composite-modified bitumen with 2X salt content, delayed freezing by approximately 10 minutes higher in the first exposure, and 25 minutes higher in the second exposure compared to base bitumen at the chosen conditions (Plate temperature: -14 °C, medium temperature: 5-6 °C and relative humidity: 50%). These results suggest that 2X salt content in bitumen is the optimum amount of salt that should be used in the polymer composite to study the anti-icing properties of the composite-modified bitumen**.**

Higher freezing delays in second exposures compared to first exposure are expected due to salt release**.** However, it is not sustained in third exposure due to lost salt during the removal of water droplets after each exposure and addition of fresh ones.

The effect of agar within the composite on the anti-icing properties of bitumen was also investigated by monitoring the base and composite-modified bitumen with/without agar (5% (wt/wt)) in a temperature and humidity controlled chamber. The bitumen surfaces were exposed to water three times. However, the method used in previous experiments was improved by keeping water on surface after each exposure, evaporating the water and leaving the salt on the surface between exposures, in order to show only the effect of the composite-modified bitumen, not of salt loss. For these experiments, the 2X salt condition, which corresponded to 0.25 g/ml salt in wet emulsions was used. The average freezing times of water droplets on samples for each exposure using the new method can be observed in Figure 4.8. The results show that the addition of agar into polymer composite increases freezing times of water droplets on bitumen surfaces. This improvement can be explained by the positive contribution of agar to salt-water interactions in bitumen. Agar behaves as bridge in these interactions and helps with the distribution of salt throughout the bitumen.

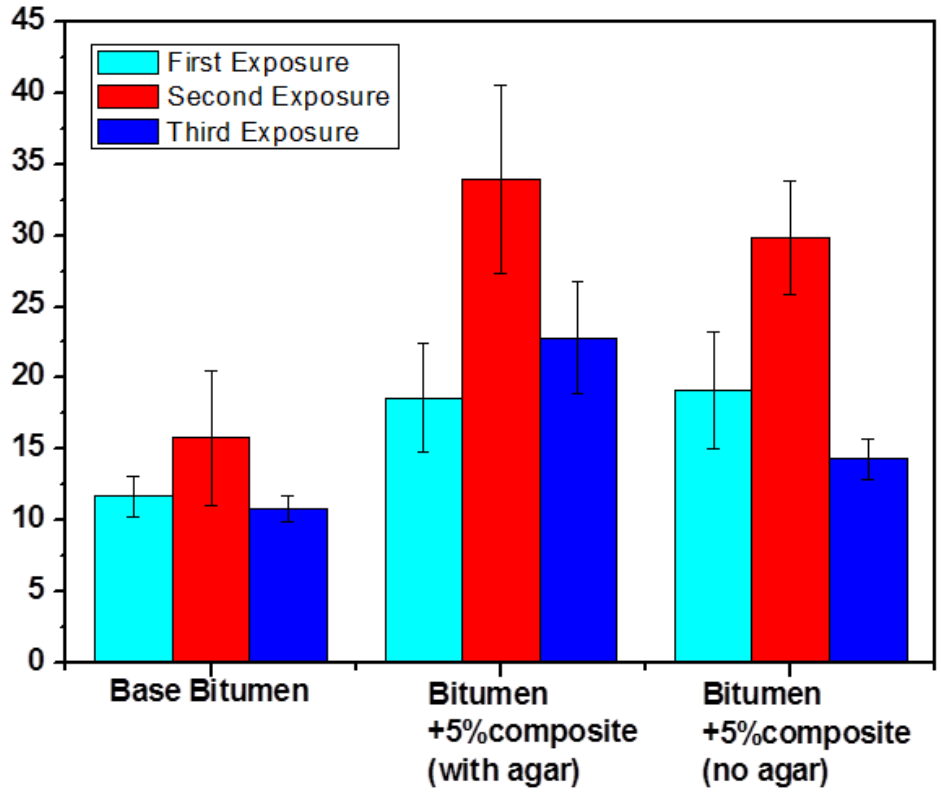

Figure 4. 8: Freezing delays on the surfaces of base, composite (with agar) and composite (no agar)- modified bitumen (5% (wt/wt)) in a humidity and temperature controlled chamber (Plate temperature: -14 °C, medium temperature: 5-6 °C and relative humidity: 50%)[2].

The results also show that the freezing delays in the second exposure are higher than the third exposure, but this difference is less severe than in the experiments in Figure 4.7. This indicates that the change in the experimental method improved salt retention, but did not fully maintain the activity of the salt, likely due to spreading of salt on surfaces during sample handling.

The results of anti-icing experiments suggest that the modification of the bitumen with 5% (wt/wt) functional composite delayed frost formation for 20-25 minutes, depending on the salt content and the presence of agar in the composite at -14 °C plate temperature conditions. Previous studies have shown that asphalt mastics containing 50% (wt/wt) sodium chloride filler in the bitumen delayed frost formation by 20 minutes. We

have shown comparable behavior with composites at a much lower loading (5% (wt/wt)). In this work, we observed significant delay in freezing on composite-modified bitumen surfaces compared to base bitumen surfaces using low composite content (5% (wt/wt)).

4.3.4. Characterization of salt release from composite-modified bitumen

Salt release profiles from polymer composite-modified bitumen were investigated by immersing the samples in water and measuring the HCOOK concentration in water with time. Concentration of HCOOK in water was measured by a potassium ion selective electrode. For salt release experiments, functional composite-modified bitumen with or without agar in the composite was used. Both 5% and 7.5% (wt/wt) composite loadings in bitumen were studied separately. The salt concentration profiles in water are presented in Figure 4.9. The Figure 4.9 shows that the salt was continuously released for 67 days from the composite (with agar)-modified bitumen (5% (wt/wt)), where for other samples, the HCOOK concentration reached saturation at around 47 days. The slow release profiles of HCOOK from the samples demonstrate the potential of this composite for longer periods of use. After 67 days of incubation of the samples in water, 35.8, 7.46 and 5.34 mg of total HCOOK were released from composite (with agar)-modified bitumen (5% (wt/wt)), composite (no agar)-modified bitumen (5% (wt/wt)), and composite (with agar)-modified bitumen (7.5% (wt/wt)), respectively. These values corresponded to 10.8%, 1.07% and 1.5% of the initial salt contents of the composite-modified bitumen samples. Release of that low amount of anti-icing agent is promising for maintanence of the anti-icing property. Since there will be mechanical abrasion on real roads, salt release from underlying layers might provide longer anti-icing effects in real-life conditions. In a previous study, the release of an anti-icing filler from asphalt mixtures was investigated, where 36 % and 47% of sodium chloride was released in two months from two different samples with altered porosity [77]. The salt release profile of polymer composite-modified bitumen obtained in the current study is promising for preparation of pavements with sustainable anti-icing properties.

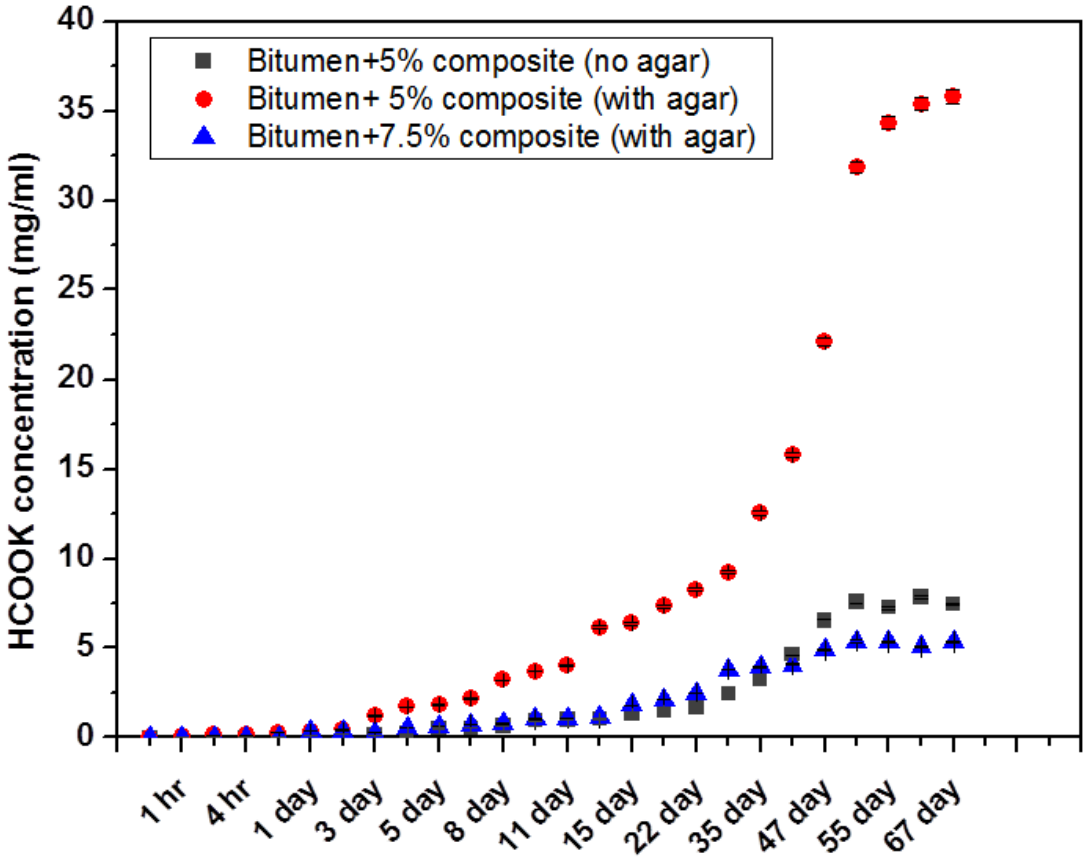

Figure 4. 9: Time dependent release of HCOOK from composite-modified bitumen samples [2].

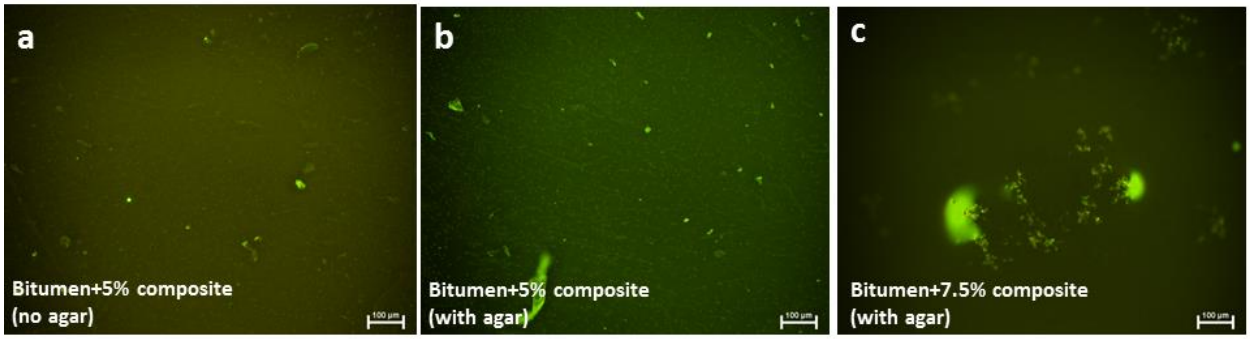

Figure 4. 10: Fluorescent images of a) composite (no agar)-modified bitumen (5% (wt/wt)), b) composite (with agar)-modified bitumen (5% (wt/wt)), c) composite (no agar)-modified bitumen (7.5% (wt/wt)) (scale bar: 100 µm).

Even though the composite (with agar)-modified bitumen (7.5% (wt/wt)) has the highest amount of salt due to highest composite concentration, the highest amount of salt was released from composite (with agar)-modified bitumen (5% (wt/wt)) (Figure 4.9). This result can be explained by the increased aggregation of the polymer composite in bitumen when applied at high concentrations. Aggregation of the polymer composite results in salt retention within the structure and makes it difficult for salt transport to take place towards bitumen surface. In order to explain this result further, the morphologies of the samples were investigated under fluorescence microscopy. The fluorouscent microscopy images of the composite (with agar)-modified bitumen (5% (wt/wt)), the composite (no agar)-modified bitumen (5% (wt/wt)) and the composite (with agar)-modified bitumen (7.5% (wt/wt)) are shown in Figure 4.10. The aggregation of the polymer composite in bitumen modified by 7.5% (wt/wt) composite is clearly observed from the Figure 4.10, where there is a more uniform distribution in bitumen modified by 5% (wt/wt) composite with or without agar in the internal phase (Figure 4.10).

Figure 4.9 also shows that the presence of agar increases the salt release from the composite-modified bitumen. Water swelling of agar increases when placed in salt solutions such as potassium chloride, sodium chloride and calcium chloride. However, this effect decreases when these salts are used in two or three salt combinations [200]. Higher amounts of water can be absorbed from bitumen surface, and higher amounts of salt which is dissolved in water can reach bitumen surface when agar and potassium coexist. The possibility for the better transport of salt to the bitumen surface in the presence of agar was also verified by freezing experiments, where samples with agar in the composite had increased freezing delay on the composite-modified bitumen surface (Figure 4.8).

4.3.5. Characterization of rheological properties in repeating temperature oscillations

Composite-modified bitumen was tested under altered temperature cycles in order to investigate resistance of rheological properties against repeating temperature changes. Complex modulus of composite-modified bitumen was measured for three temperature tcycles of -10, 25 and 70 °C that simulate the extreme temperatures that asphalt can be

exposed in daily and seasonal temperature changes. Figure 4.11 shows that certain complex modulus was measured for certain temperatures. These results show that composite-modified bitumen its rheological properties in temperature changes. This test shows the resistance of mechanical properties of composite-modified bitumen against seasonal temperature changes.

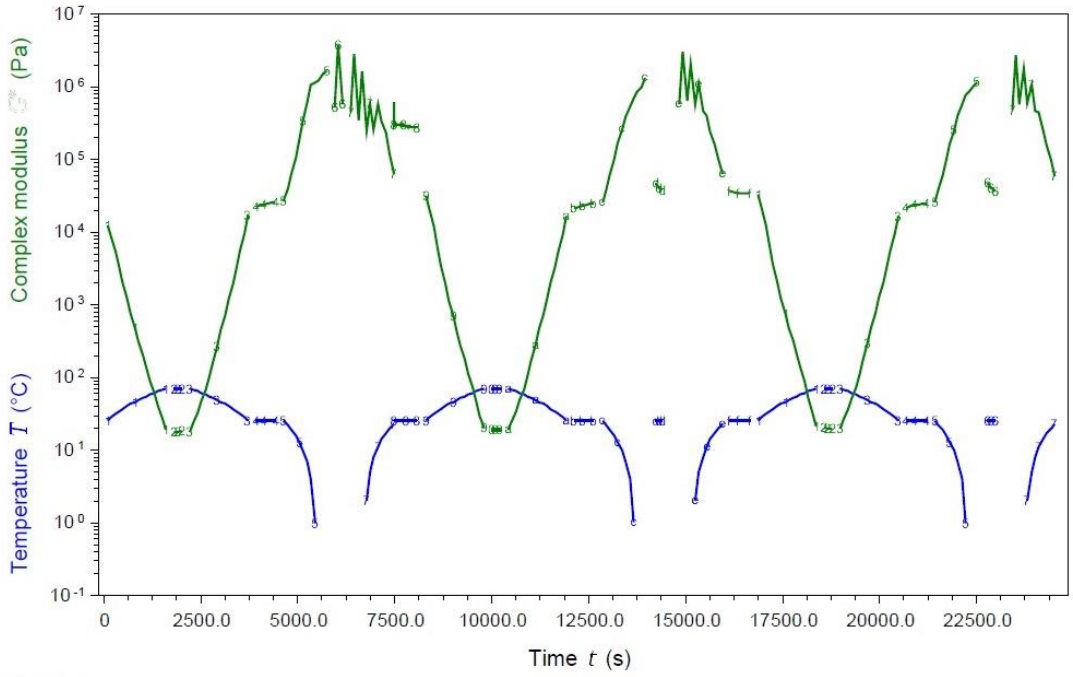

Figure 4. 11: Change of complex modulus of composite modified bitumen with three cycle of temperature changes between -10, 25 and 70 °C.

4.4. Conclusions

In this study, we used a polymer composite containing SBS and HCOOK salt to modify bitumen and to obtain anti-icing surface functionality. In the first part of the work, we investigated the influence of mixing for different functional composites and performed morphology and rheology experiments to evaluate the distribution of the polymer composite in bitumen and characterize the mechanical properties of the final mixture. We achieved a uniform distribution of the polymer composite in bitumen without compromising the mechanical properties.

Next, we conducted freezing experiments to characterize the anti-icing properties of polymer composite-modified bitumen surfaces, where the composite-modified bitumen delayed the freezing time of water droplets by 20 minutes in a temperature and humidity

controlled chamber with a -14 °C plate, 5-6 °C medium temperature and 50 % relative humidity. Salt content was optimized to achieve a maximum delay in freezing, and it was found that the 2X salt condition, or 0.25 g/mL, resulted in the best results in all cases. In addition, we demonstrated controlled salt release over 40-60 days from composite-modified bitumen, and investigated the salt release profiles of modified bitumen with respect to the presence of agar and composite content. We found that agar positively contributes to the release of the salt from the bitumen, potentially due to enhanced water-salt hydrophilic interactions. High composite content decreases the salt release due to the formation of polymer aggregates in bitumen, which prevent salt transport to the surface. Mechanical abrasion might also improve anti-icing property on bitumen surfaces, which will enable more salt release from underlying layers. Since this kind of abbrasion occurs naturally on roads due to moving vehicles in real-life conditions, the expected continuous salt release may allow for sustainable anti-icing property on road surfaces.

In summary, we showed the possibility of incorporation and delivery of anti-icing agents through bitumen using a functional polymer composite. Modification of bitumen with an anti-icing functional composite with preserved mechanical properties has been studied for the first time in the literature. The use of polymer composite-modified bitumen with anti-icing properties is promising for production of functional pavements in industrial applications.

Chapter 5

COMPARISON OF DIFFERENT IONIC SALTS FOR COMPOSITE-MODIFIED BITUMEN

5.1. Introduction

Ionic salts as anti-icing agents have been extensively used to eliminate accumulation of ice on asphalt surfaces. However, salt can be easily removed by rain or automobiles and requires frequent application on roads. Besides this economical consideration, anti-icing agents compromise the mechanical properties of asphalt and have a negative impact on living organisms and the environment when used in large amounts. Incorporation of hydrophilic salts into bitumen, a hydrophobic asphalt binder, and controlled release of specific molecules from this hydrophobic medium can provide an effective solution to reduce ice formation on pavements. For this pupose, we modified bitumen with an anti-icing including polymer composite and investigated the mechanical, morphological and functional properties of modified bitumen in previous section. We used potassium formate salt as anti-icing agent. Although potassium formate is more advantageous compared to other salts due to its high solubility and environmental friendly properties, it is more expensive than other salts such as NaCl, $MgCl_2$ or CaCl.

Investigation of alternative salts for butimen modification is required for obtaining more feasible. Therefore, we investigated potential of different salts in this section. For this purpose, we developed functional polymer composites with salt pockets of altered ionic salts such as KCOOH, NaCl or $MgCl_2$. Ionic salts were dissolved in hydrophilic gel medium and dispersed in hydrophobic SBS polymer matrix as explained in previous sections.

We also changed experimental conditions in this section. In previous section we used temperature and humidity controlled custom-made chamber with -14 °C plate, with 5-6 °C medium temperature and 50% humidity conditions. We could observe freezing delay in funtional bitumen compared to base bitumen even in these challenging conditions. In this part, we conducted freezing experiments of composite modified and coated bitumen surfaces in camera-integrated cold chamber where the temperature (-2 ^{o}C) was uniformly distributed. We investigated effect of that identity of salts on mechanical, morphological and functional properties of the composite incorporated or coated bitumen. These results suggested that freezing delay could be tuned with the type and amount of anti-icing agent incorporation into the composite. This approach is promising for development of polymer composite-modified bitumen with anti-icing function and for industrially relevant applications.

5.2. Methods and Results

5.2.1. Materials

Styrene-butadiene-styrene block copolymer (SBS, S:B weight fraction: 70:30) (Kraton D1101), potassium formate (KCOOH) (99 %), magnesium chloride ($MgCl_{2)}$ (99 %) and NaCl (99 %) from (Sigma Aldrich), silica nanoparticles (AEROSIL 816 ®) and cyclohexane (99.9 %) (Merck) were used for the preparation of particle stabilized emulsions. Agar powder was purchased from Sigma-Aldrich. 50/70 penetration grade bitumen was kindly supplied by TUPRAS. Deionized water was used in the experiments (Purelab Option, ELGA). Glass petri dishes and glass microscope slides were purchased from Nunc.

5.2.2. Preparation of Composite Modified Bitumen

2.2.1. Preparation of Emulsions

Particle stabilized emulsions with 0.25 (v/v) internal phase fraction (Φ=0.25), 1.5 % (w/v) nanoparticle concentration with or without gelation in the internal phase were prepared as described in our previous section. However, concentration of salt used in emulsions was determined based on solubility of NaCl in water. Thus, 0.5 mL KCOOH (0.3 g/ml) salt solution with agar was added to 0.5 mL of 1.0 % (w/v) nanoparticle-cyclohexanone stock solution under high shear applied by a vortex mixer at the maximum speed for 10-15 seconds. After stabilization of the aqueous droplets by nanoparticles in the stock solution, 1 mL of SBS polymer in cyclohexane (110 mg/mL) was added drop-wise to 1 mL of the KCOOH, agar, and nanoparticle solution by mixing slowly.

2.2.2. Preparation of functional composite membranes and incorporation into bitumen

Prepared emulsions were cast in petri dishes to dry and functional composite membranes were incorporated into bitumen as described in the previous section. Briefly, the emulsions were dried in petri dishes for 24 hours at room temperature. The SBS polymer and the composites were chopped up and then incorporated into bitumen using a laboratory scale mixing device. The bitumen composite blends were prepared with a three-blade impeller low shear mixer (RW20, IKA Germany). The composite was mixed into bitumen at a temperature of 170 °C and a rotation speed of 125 rpm for 2.5-3 hours. After processing, the samples were stored at room temperature.

2.2.3. Preparation of composite coated bitumen

Emulsions were coated on bitumen surface via spin coating. Five hundred µl of emulsion is dropped on 4 cm^2 of bitumen slide and coated with 1000 rpm for 60 seconds as schematized in Figure 5.1. Then, emulsion coated bitumen slides were dried overnight to obtain composite coating on bitumen surface.

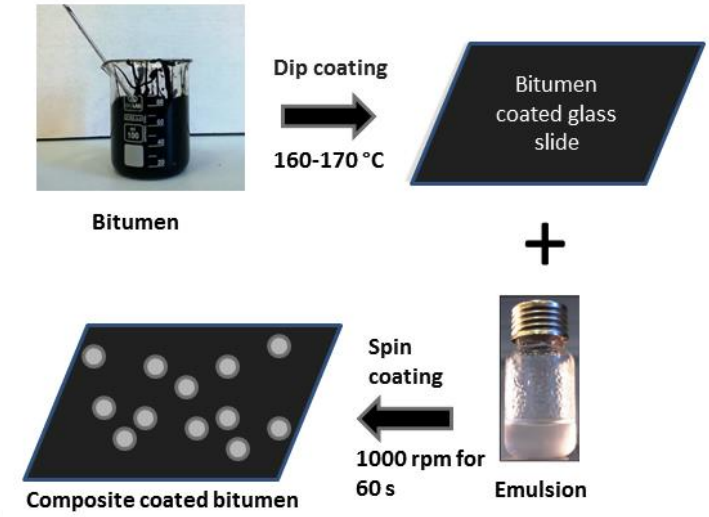

Figure 5. 1: Schematic of composite coating of bitumen surfaces.

5.2.3. Surface characterization of composite-modified bitumen

5.2.3.1. Fluorescence, Light and Scanning Electron Microscope Characterization

Emulsions were prepared by including dispersed aqueous phase of NaCl, $MgCl_2$ and KCOOH. After, emulsions were casted on petri dishes to obtain dry composite membranes. Composite modified bitumen were prepared with incorporation of composite within bitumen or coating on bitumen surface. Fluorescence microscopy was used to infer SBS morphology in composite-incorporated bitumen, while surface morphology of composite-coated bitumen could be investigated with SEM. The morphologies of SBS in composite-modified bitumen were investigated under fluorescence microscopy with 520 nm emission and 450-490 nm excitation wavelength range. Macroscopic appearance of composite membrane are presented with corresponding microscopic image of emulsions, fluorescence microscope images of composite-incorporated bitumen and SEM images of composite-coated bitumen in Figure 5.2. Emulsions prepared with KCOOH or $MgCl_2$ are more stable compared the one prepared by NaCl. This difference leads to formation of more uniform structures in composite membranes when prepared by KCOOH or $MgCl_2$. This difference can be attributed to effects of high concentration of salts on emulsion stability which is also discussed in many studies previously [201-203]. In a previous study, they tested how water-seed oil emulsion stability is affected from differen salts

including NaCl, $CaCl_2$, KCl, $NaCH_3CO_2$ and $NaNO_3$. They found that all salts decrease the stability of these emulsions and causes water separation from oil. In our study, NaCl has the highest concentration compared to other salts since same amount of mass is used for each salt. Thus, higher concentration of NaCl might have affected stability of emulsions in negative way. Another possible reason may be negative effect of high concentrations of Na+ ions on agar gel network. In a previous study, it is discussed that addition of sodium sulphate weakens the gel structure of agarose. In our previous study, we demonstrated that more uniform structure of composite membranes is obtained in presence of agar. Hence, high concentrations of Na+ which effects agar gel formation in negative way can result in non-uniform structure in composite membranes. This result is also consistent with SEM observations. More spherical, gel like and embedded agar domains are seen in bitumen surfaces coated with KCOOH or $MgCl_2$ incorporated composite. On the other hand, more rigids domains are seen in NaCl case which is consistent with inadequate gelation of agar in presence of high amount of Na+. However, these differences in structures of emulsion membrane or composite coated bitumen are not observed in composite incorporated bitumen according to fluorescence microscope observation.

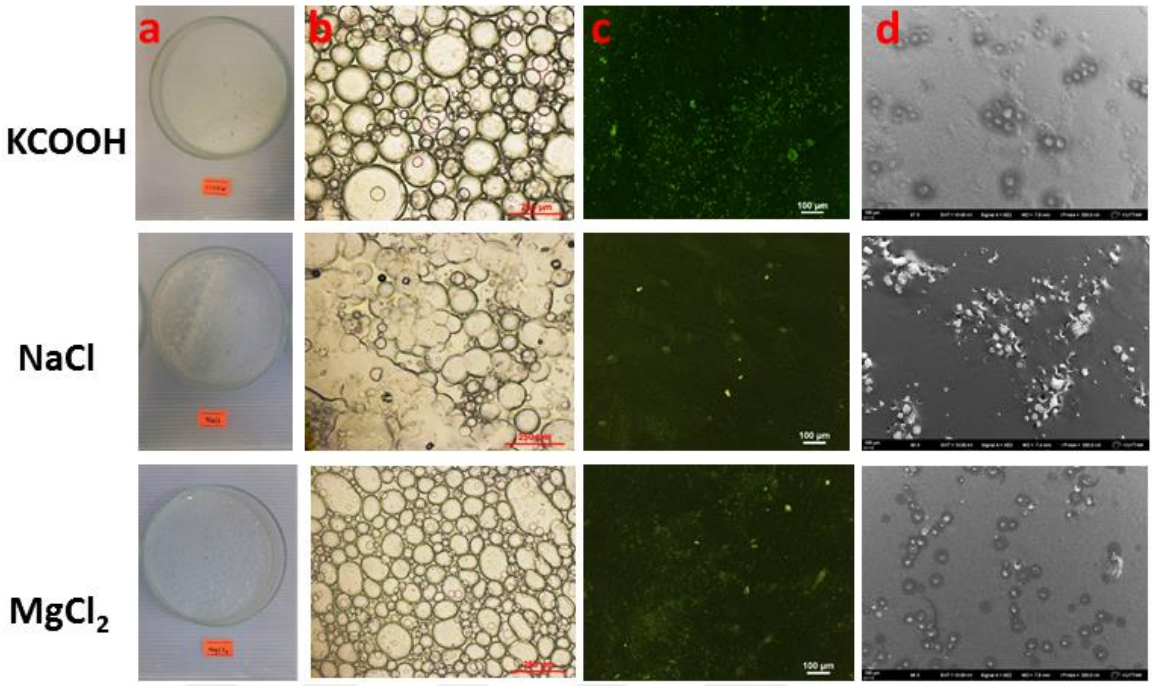

Figure 5. 2: Images of emulsion, composite and composite modified bitumen for different salts. a) Macroscopic appearance of composite membrane b) Microscopic image of emulsions c) Fluorescence microscope images of composite-incorporated bitumen and d) SEM images of composite-coated bitumen.

5.2.3.2. EDX characterization

Composite-coated bitumen surfaces were investigated with EDX for elemental analysis. Sphere-like domains observed on composite-coated bitumen surfaces were analyzed for evidence of presence of salt on surfaces. Both inside and outside of domains were analyzed for tracking the specific element of each salt in order to demonstrate proper encapsulation of salts inside the domains. EDX spectras for inside and outside of domains on bitumen surface coated with emulsions of different salts are presented along with the SEM images of the domains in Figure 5.3. Graphs presented in Figure 5.3 b are obtained from outside of domains and graphs in Figure 5.3 c are for inside of domains. It is seen that K element is detected for KCOOH salt modified surface which is indication of opresence of KCOOH inside the domain. However, K element is not detected from outside of the same domain. Similarly, Na and Cl is observed in domains for NaCl coated bitumen surface and Mg and Cl are detected for MgCl2 coated bitumen surface while these indicators were not seen for outside of domains. This analysis shows that ionic salts

were encapsulated properly in agar domains on bitumen surface so that salts were not spreaded to outside of domain.

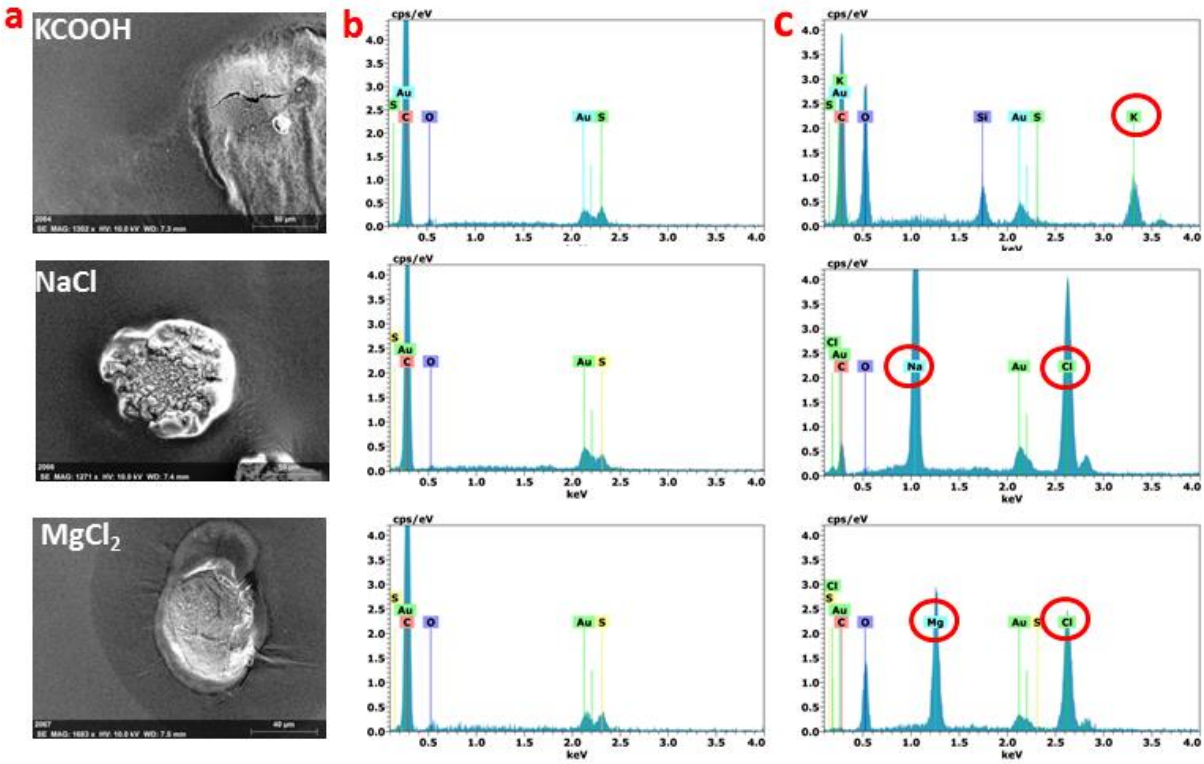

Figure 5. 3: EDX analysis of composite-coated bitumen surfaces prepared with different salts. a) SEM image, b) EDX spectra for inside and c) EDX spectra for outside of domains on bitumen surface.

5.2.3.3. Atomic Force Microscopy

Atomic Force Microscopy (AFM) experiments were performed in a Bruker Dimension Icon AFM with MPP21100-10 REFSP tips. Typical scans covered areas of 20x20 μm^2 in bitumen samples which were prepared via incorporation or coating of composite on the surface of bitumen. Imaging was performed in soft tapping mode (intermittent contact) at room temperature. Both topographic and phase difference microscopy (PDM) images were recorded and analyzed. According to phase images in Figure 5.4, base bitumen is composed of two phases which can be defined as continuous and dispersed phase. Dispersed phase is lighter part which can be composed solutes and

other stiff parts such as asphaltenes, while darker parts are composed of some oils and softer parts. When we compare composite-incorporated bitumen samples (Figure 5.4 a), bee shaped structures are observed in incorporation of each salt. In literature, different conclusions are reported about formation and composition of bee shaped structures. These structures appear as immerged or immersed parts on bitumen surface and related to presence of crystalline wax, asphaltenes or stiffer parts established with modification of bitumen according to different studies. Uniform distribution of these structures can be also related to uniform structure of modified bitumen. These structures also correspond to stiffer parts in bitumen and gives information about mechanical properties, as well. Bee shaped structures are not seen in composite-coated bitumen surfaces since bitumen is not modified by incorporation of an additive in bitumen (Figure 5.4 b). Non uniform structures are seen in coated samples due to hydrophilic-hydrophobic difference between bitumen and ionic salts.

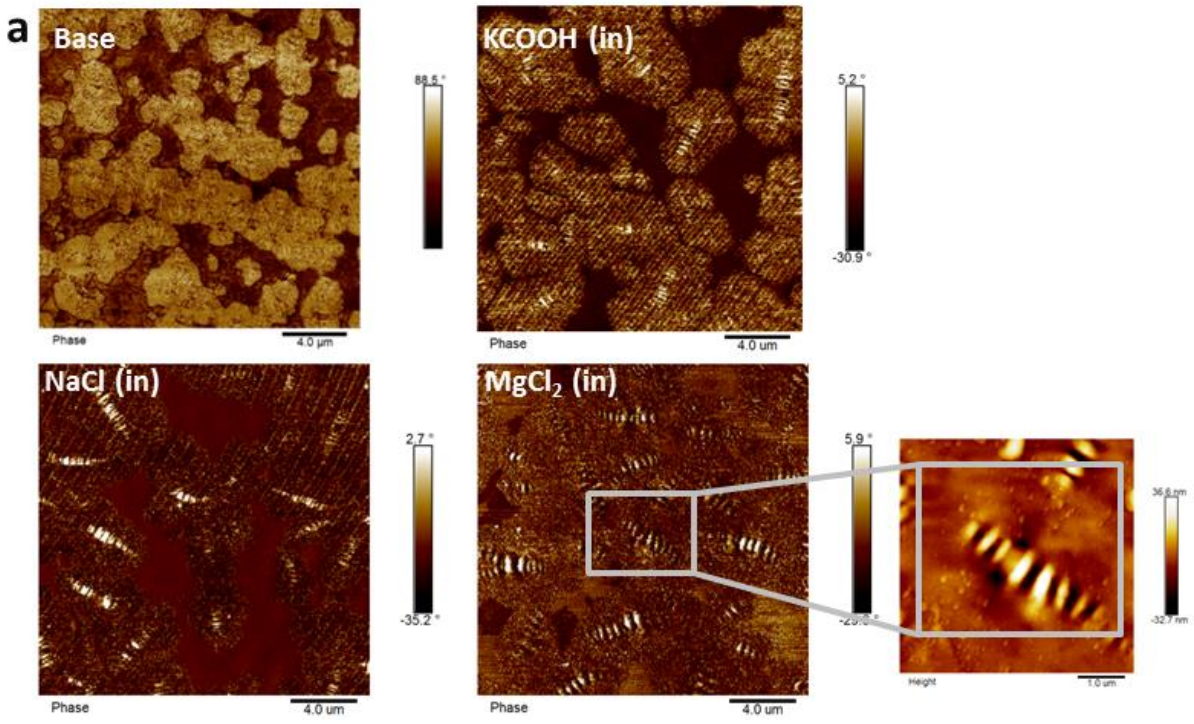

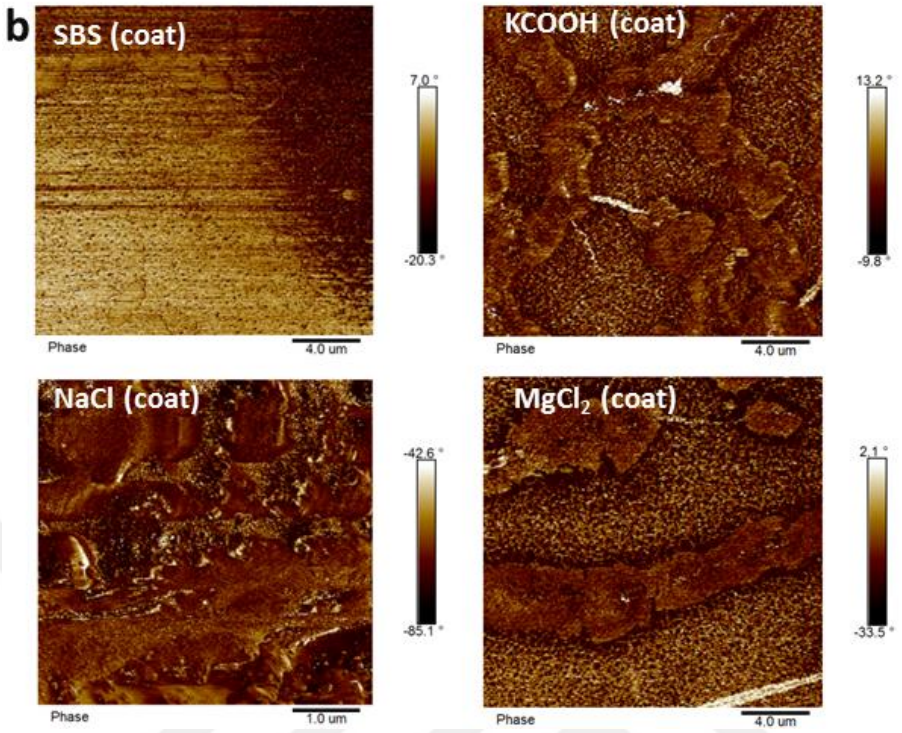

Figure 5. 4: AFM phase difference images of a) base and composite-incorporated b) SBS and composite-coated bitumen surfaces with a topoghraphic zoomed image of bee shaped structures.

5.2.4. Rheological Characterization of composite-modified bitumen

The oscillatory tests were performed using a Discovery Hybrid Series-2 Rheometer (TA), which applies oscillating shear stress and strain to a bitumen sample sandwiched between parallel plates, at different loading frequencies and temperatures. The DHR tests reported in this study were performed at 0.02 Hz constant frequency and temperature sweeps between 20 and 120 °C. The tests were undertaken with a 20 mm diameter, 1 mm gap and parallel plate testing geometry.

Dynamic mechanical tests were conducted to investigate the viscoelastic properties of bitumen. Oscillatory tests were conducted to measure the viscoelastic parameters, complex modulus (G*) and the phase angle (δ). G* gives information about total resistance of material to deformation under shear loading, while δ is measure of viscoelastic balance of the material behavior. δ is the phase lag between the applied shear stress and the shear strain during an oscillatory test and equal to the arctangent of the ratio of loss modulus (G'') to storage modulus (G') [89].

Isochronal plots of the complex modulus G* versus temperature at 0.02 Hz for base and altered salt incorporated composite modified bitumen are shown in Figure 5.5 a. According to Figure 5.5 a, there is no significant difference between G* values of base or composite modified bitumen at high temperatures. However, one order of magnitude difference is observed between NaCl modified bitumen and the others at low temperatures. This decrease is an evidence of a minor decrease in resistance of bitumen at low temperatures with modification of NaCl incorporated composite. Despite the minor differences in G* values, more distinctive decrease is observed in δ values at low temperatures with modification of all composite compared to base bitumen (Figure 5.5. b). Decrease of δ at low temperatures is indication of improved elasticity which is desired property for bitumen for decrease of fractures in real life condition

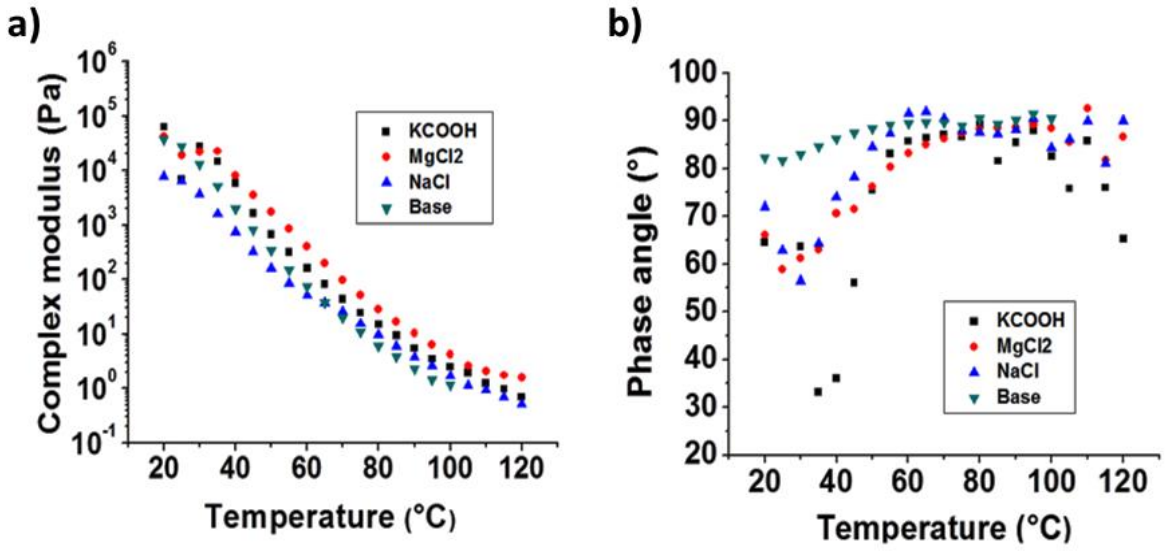

Figure 5. 5: Isochronal plots of a) complex modulus and b) phase angle at 0.02 Hz base and composite-incorporated bitumen for different type of salts

5.2.5. Anti-icing property characterization

The anti-icing properties of base bitumen and composite-modified bitumen were investigated with respect to the freezing rate of a water droplet on the bitumen surface. Freezing of water droplets on the bitumen surfaces was induced using a temperature controlled cold chamber (Figure 5.6). One hundred μL of water was dropped onto each bitumen surface and incubated in the chamber with a -2 °C plate and ambient temperature. The temperatures were also recorded with thermocouples placed in different

parts of chamber. The durations of the freezing of water droplets were monitored with a camera attached system and recorded based on disappearance of transparency of the droplets.

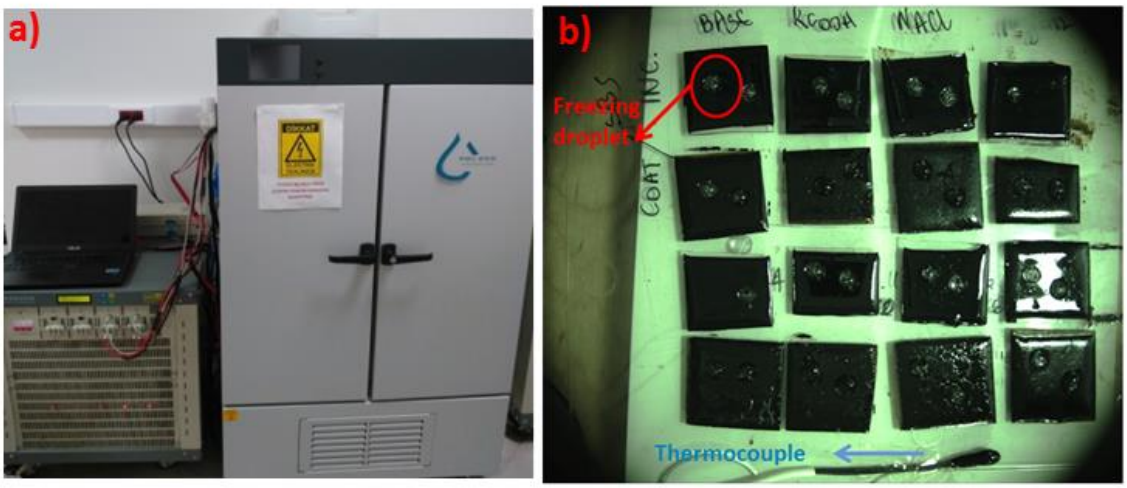

Figure 5. 6: Freezing experiments in cold chamber with a -2 °C plate and ambient temperature a) Camera-attached cold chamber b) Monitoring of freezing of droplets on composite-incorporated and composite-coated bitumen samples in cold chamber.

Incubation of the surfaces with water was repeated two times. Water droplets were kept on the surface after each exposure and subsequently evaporated in place so that the salt would not be lost with the water, and the fresh drops of water were then added onto the surface for the repeat measurements.

Freezing delays on surfaces of base, SBS coated, composite incorporated or coated samples are presented in Figure 5.7. Higher freezing delays were observed in composite coated bitumen surfaces compared to their corresponding composite incorporated ones. Higher freezing delays in coated bitumen is expected result due to direct exposure of water to composite which includes encapsulated salt molecules. Because higher concentration of salt can diffuse from composite layer to water droplets on bitumen surface than the composite incorporated in hydrophobic bitumen medium. Thus, higher freezing point depression effect is seen water droplets directly exposed composite coated bitumen surface.

Table 5. 1: Expected freezing point decrease values of aqueous phase in emulsions with 0.3 g/ml concentration according to Equation 2.7.

Ionic salt	**ΔT (°C)**
KCOOH	8.3
NaCl	12.0
$MgCl_2$	11.1

When we compare coated bitumen surfaces in themselves, highest freezing delay is seen on composite coated bitumen which includes NaCl than MgCl2 or KCOOH. This order of freezing delay is consistent with the freezing point decrease values expected in dispersed phase of parenting emulsions, when same amount of salt used for each salt. These values presented in Table 5.1 were obtained using Equation 2.7 which is based on molality, ionization factor of solute and cryoscopic constant of solvent. However, same order of freezing point effect is not observed in composite incorporated samples due to differences in distribution and diffusion of salts in bitumen which results in that different amounts of salt reach to surface and alters the freezing point depressing effect.

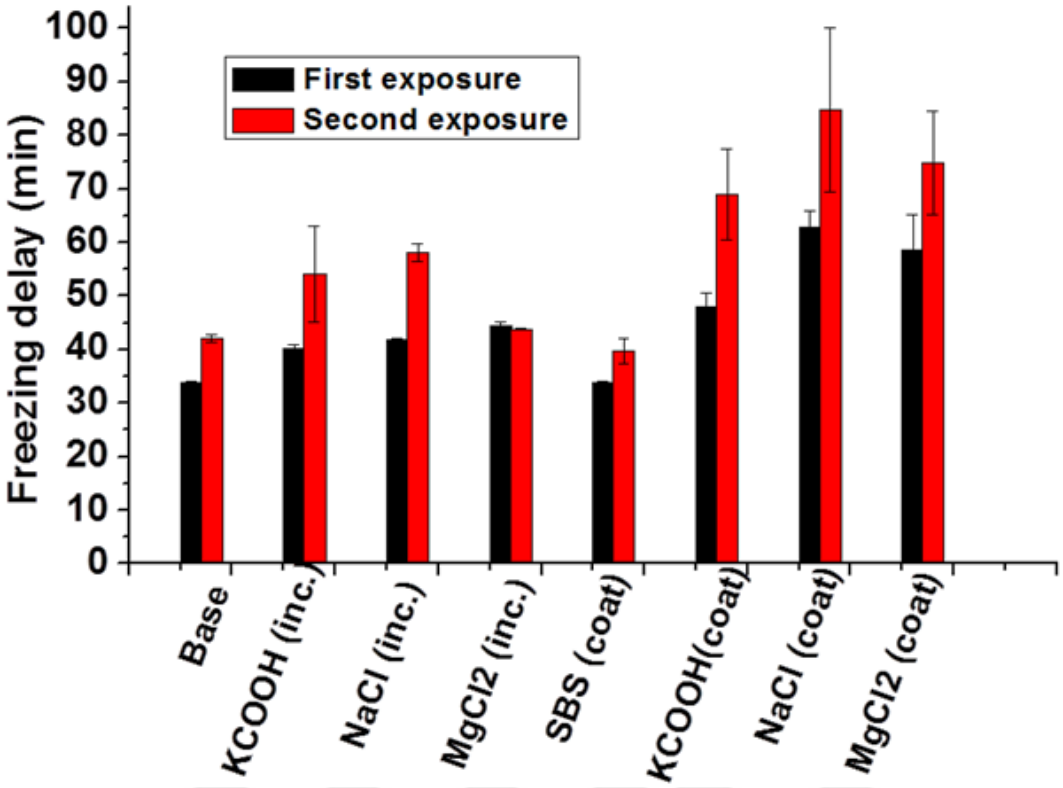

Figure 5. 7: Freezing delays on surfaces of base, composite-incorporated and composite-coated bitumen with different types of salt in temperature controlled chamber (Medium temperature: -2°C).

5.5. Conclusion and Futurework

In this chapter, we investigated the anti-icing properties of different ionic salts for composite-modified bitumen. We did not only incorporate polymer composite in bitumen, we also prepared polymer composite coated bitumen surfaces in order to investigate an alternative use of functional polymer composite for bitumen surfaces.

We performed freezing experiments of composite modified and coated bitumen surfaces in camera-integrated cold chamber with uniform ambient and plate temperature (-2 ^{o}C) which simulates real-life conditions better than previous design. We observed higher freezing delay in composite coated samples compared to composite coated ones. NaCl modified bitumen samples showed higher freezing delay when same amount of salt used for each salt. However, freezing delay performance of KCOOH and $MgCl_2$ can be improved, since more salt can be disolved in dispersed phase for these salts. These results

suggested that freezing delay could be tuned with the type and amount of anti-icing agent incorporation into the composite.

We also observed effect of salt type on mechanical and morphological of the composite incorporated or coated bitumen. We obtained more stable emulsions and more uniform composite membranes with KCOOH and $MgCl_2$. Complex modulus of bitumen was not affected significantly with modification of any salt type. On the other hand, composite modifiedd bitumen samples showed improved elastic property.

Comparison of salts showed the possibility of use of alternative salts for composite modified bitumen. However, optimum freezing point depression performance of each salt for bitumen should be further investigated.

Chapter 6

WATER-IN-WATER EMULSION BASED SYNTHESIS OF NANOSPHERES WITH TUNABLE DRUG RELEASE PROPERTIES

6.1. Introduction

Design and characterization of hydrogels have attracted significant attention in tissue engineering and pharmaceutical applications because of their tunable chemical and three-dimensional physical structure, good mechanical properties, high water content, and biocompatibility [3-6, 99]. PEG-based micro/nano-scale hydrogels have been considered to overcome the problems associated with macroscopic gels, such as small surface area-to-volume ratio, low encapsulation efficiency and longer response time to external stimuli [7, 8, 115]. PEG hydrogel particles still maintain desired characteristics of macroscopic PEG-based hydrogels, such as swelling capacity and biocompatibility [11], furthermore they offer advantages such as a tunable size from nanometers to micrometers, a large surface area for bioconjugation, and an interior network for incorporation and controlled release of molecules [10, 104, 116]. However, several limitations exist for the design and

development of effective hydrogel-based particles as drug delivery carriers for *in vivo* applications [105]. One important requirement involves control over the dimension to be less than 200 nm in diameter, which can improve cellular uptake of particles through cell membranes and reduce nanoparticle uptake through mononuclear phagocytic system [117]. This property can significantly increases the circulation time of particles in blood [9, 10]. For the synthesis of PEG-based hydrogel micro/nanospheres, both solvent evaporation and emulsification methods have been widely used. However, organic solvent or surfactant is often needed in these techniques, and hence further use of obtained particles for biomedical applications is limited [10, 11, 204, 205]. On the other hand, water-in-water (w/w) emulsions are based on polymer–polymer immiscibility in aqueous solutions without the need of surfactants, nanoparticles and organic solvents [1, 44-47]. However, colloidal instability and wide size distribution of w/w emulsion are important considerations that make optimization of synthesis of these particles difficult for further applications [45].

W/W emulsions can be obtained with two-phase aqueous systems, where interfaces occurs between the phases of thermodynamically incompatible aqueous domain [44-47]. Commonly, phase separation is observed between aqueous polymer solutions, such as polysaccharides and proteins. Phase separation occurs due to changes in polymer molecular weight solvent composition and temperature, which can be characterized by the free energy of mixing (ΔF_{mix}) with at least two minima [45, 48]. Phase separation occurs and ΔF_{mix} changes with composition according to free energy of mixing equation of Flory-Huggins theory. This aqueous polymer immiscibility occurs with many combinations of water-soluble polymers (e.g. combinations of dextran, poly(ethylene glycol) (PEG), poly(vinyl alcohol), poly(vinylpyrrolidone), gelatin or soluble starch).The polymers may remain solution; however, above a certain concentration they separate into two aqueous phases [49].

Completely aqueous w/w emulsion technique was first used by Okke et al. as a novel technique for preparation of PEG hydrogel microparticles [46]. In this technique, two-phase aqueous system was obtained where the polymer in the dispersed phase was crosslinked to form hydrogel microparticles. In previous studies, only few reports exist,

where the synthesis of micron-size hydrogel particles via w/w emulsion was considered. In previous report by Murphy and colleagues, dynamic network properties of hydrogel microspheres were characterized and release of proteins such as VEGF and BMP-2 from these microspheres were investigated, where hydrogel microspheres were prepared via w/w emulsion of dextran and PEG prepolymer [44, 47, 118]. Here, we performed optimization for the synthesis of nano-size hydrogel spheres using w/w emulsion and further investigated drug release potential from these nanospheres. We prepared w/w emulsion based on dextran-PEG prepolymer immiscibility and polymerized dispersed PEG phase under visible light to obtain PEG nanospheres. The main differences between the current study and the few previous reports about PEG hydrogel particles synthesized through w/w emulsion involve the uniform distribution and nano-scale size of the particles that could be synthesized here. We studied the influence of polymerization conditions on the morphology and size of PEG hydrogel nanospheres, where loading and release properties of PGB as an anticonvulsant model drug was investigated. We measured pregabalin release from PEG nanospheres and fitted experimental data to a stretched exponential function that described experimental data with high correlation [129]. PEG hydrogel nanospheres promoted sustained PGB release, which can be utilized for various biomedical application with controlled release properties.

6.2. Materials and Methods

6.2.1. Materials

PEG diacrylate (PEGDA) (575 Da) was purchased from Laysan Bio. Triethanolamine (TEA) was purchased from Merck (Germany). Vinyl-2-pyrrolidinone (VP) was purchased from Aldrich. Phosphate buffered saline (PBS) was purchased from Amresco (Solon, Ohio). Dextran was purchased from Sigma. Sodium Phosphate was purchased from Sigma Aldrich. Pregabalin was kindly supplied from Abdi Ibrahim (Istanbul, Turkey). Dulbecco modified Eagle medium (DMEM) was purchased from Gibco Life Tech. Penicillin/streptomycin, L-glutamine and FBS was purchased from Sigma-Aldrich.

6.2.2. Synthesis of Nanospheres

6.2.2.1 Preparation of prepolymer solution

Prepolymer solution was prepared with a concentration of 30 (w/v) PEGDA, 225 mM TEA and 37 mM VP in 10 mM PBS at pH 8. EosinY was added to the prepolymer solution at a final concentration of 0.025 mM.

6.2.2.2. Preparation of w/w emulsions and synthesis of nanospheres:

PEG nanospheres were prepared by w/w emulsion polymerization. 30% (w/v) PEGDA prepolymer solution was prepared with mixture of PEGDA, TEA, NVP and EosinY as explained in previous section. 20% (w/v) dextran solution was prepared in K^+ buffer (0.22MKCl/10mM sodium phosphate/pH 8). The structures of these components and PGB are shown in Figure 6.1. Two polymer solutions were mixed with 1/6 (v/v) volume fraction and aqueous two-phase was obtained. These two phases were mixed for 45 minutes with 1/1250 speed of rotation to obtain an emulsion where PEG prepolymer droplets were dispersed in continuous phase of dextran solution. Dispersed PEG prepolymer droplets were crosslinked with exposure of emulsions to visible light at 514 nm and a flux of 2.5 or 5.0 mW/cm^2 using an argon ion laser (Coherent Inc, Santa Clara, CA). Next, nanospheres were rinsed with distilled water for 20 minutes with 3500 rpm for 3 times and filtered subsequently to remove dextran. Nanospheres were freezed and lyophilized in order to obtain nanospheres particles in dry form. The schematic of the synthesis of the PEG particles is shown in Figure 6.2.

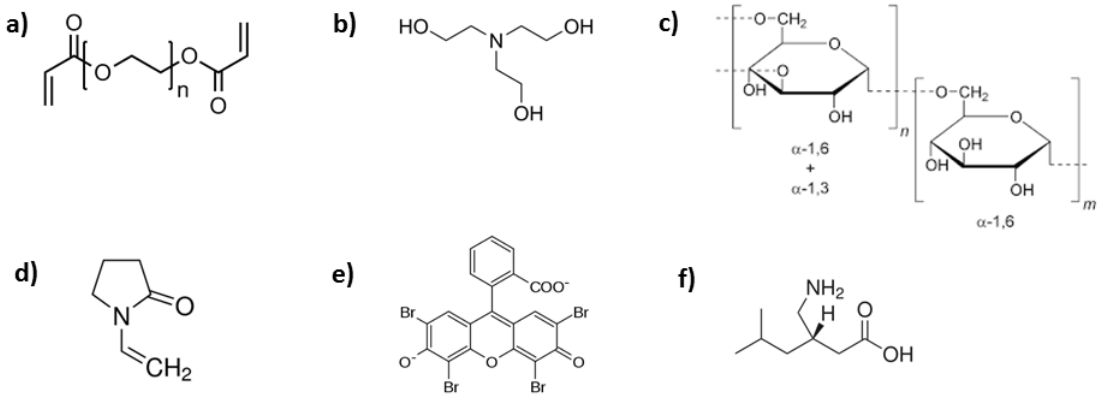

Figure 6. 1: Structures of the components a)PEGDA b)TEA c)dextran d) NVP e) eosinY f) PGB.

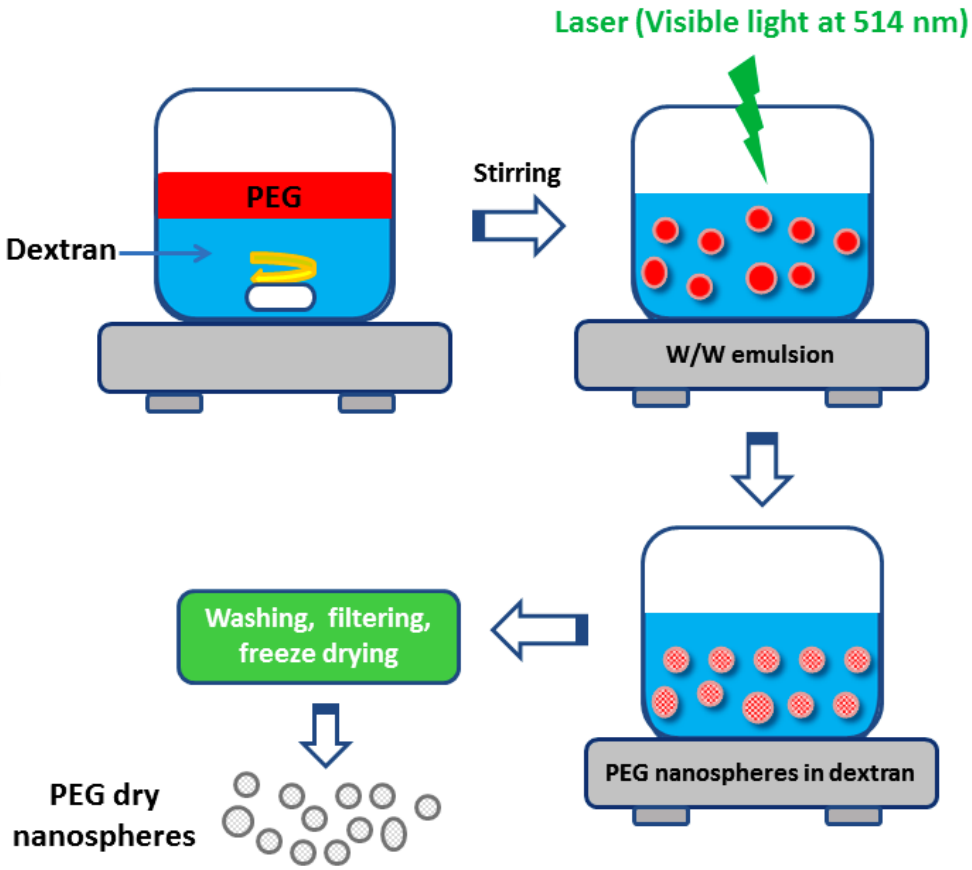

Figure 6. 2: Schematics for the synthesis of PEG nanospheres [12].

6.2.3. Structural, chemical and physical characterization of nanospheres

Nanospheres were characterized in terms of chemical and physical structure, size and morphology. Light microscope and scanning electron microscope (SEM) imaging were used to characterize structure and morphology of the gels. Wet emulsions were investigated under light microscope. Retrieved dry particles were prepared on carbon tape and coated with 10 nm gold for SEM characterization (Zeiss Ultra Plus, Bruker; Optronik Ltd Sti, Ankara, Turkey). Chemical structure of nanospheres was investigated by FT-IR spectroscopy. Hydrodynamic size of the particles was determined using dynamic light scattering (DLS) at 633 nm at room temperature (Malvern zetasizer nano S ZEN 1600, Malvern Instruments, Malvern, UK).

6.2.4. Pregabalin loading and release experiments

Drug loading was carried out with 10 mg of microspheres, where particles were incubated overnight in 1 ml of an aqueous loading solution containing 250 µg/ml concentration of Pregabalin (PGB) (Abdi Ibrahim, Turkey) at room temperature. UV–visible spectrophotometer (Shimadzu UV-3600 – UV–VIS-NIR spectrophotometer) at 210 nm wavelength was used to measure PGB absorption. A standard calibration curve for the absorption of PGB in aqueous solution was generated to determine the concentration in unknown samples. The loading efficiency of PGB into PEG nanospheres was calculated as follows in Equation 6.1:

$$\text{Loading efficiency} = (M_0 - M_f)/M_0 * 100 \quad (6.1)$$

Where M_0 represents the initial PGB mass in the stock solution and M_f is the final PGB mass remaining in the solution. To measure PGB release from nanospheres, PEG nanospheres in dialysis membrane bag were incubated in 20 ml of PBS, and 0.8 ml samples were taken at 0.5, 1, 2, 4, 12, 24, 48 and 72 h time points and sample was replaced with fresh PBS. PGB concentrations obtained from absorption measurements were used to calculate the mass released at time t (M_t) using the following Equation 6.2:

$$M_t = C_t * V + \sum C_{t-1} * V_s \quad (6.2)$$

Where C_t is the concentration of PGB in the release solution at time t, V is the total volume of the release solution (20 ml) and V_s is the volume of the sample taken (0.8 ml). Using M_t values, percent release of cumulative PGB release, Q, was determined as follows in Equation 6.3:

$$Q = (M_t / M_\infty) * 100 \quad (6.3)$$

where M_∞ is the maximal weight of drug released.

6.2.5. Model Fitting

The cumulative release data of PGB was fitted to a mathematical model based on a stretched exponential function (equation 5) developed in a previous study where

controlled release of doxorubicin from Ph-responsive microgels was studied [129]. All data was described by the following model function $Q(t)$, where for cumulative release was dependent on time t as in Equation 6.4:

$$Q(t) = (1 - \exp(-(t/\tau)^b) \qquad (6.4)$$

Here τ is the time when the fraction $(1 - e^{-1}) = 0.632$ of maximum cumulative release, M is achieved and b is the model parameter that defines the stretching of the exponential function. This parameter is expected to be less than 0.5 in a release process and the trend is more flat when it is around 0.25. However, it is unusal to obtain b value around 0.1. On the other hand, there is single relaxation when it approaches to 1.0.

The experimental drug relase data was fitted to this model using non-linear least-squares method [206]. The description of data with this function was carried out using iterative nonlinear regression. This process minimizes the value of the squared sum (SS) of the difference between the data and the fit as shown in Equation 6.5 and 6.6:

$$SS = \sum_{i=1}^{n} r_i^2 \qquad (6.5)$$

$$r_i = y_i - y_{fit} \qquad (6.6)$$

for i=1,2,3…n, where, y_i is the experimental data at specific time, y_{fit} is the value of the curve at that point y_i for a set of n data points. The model equation can also predict the half-time, T when the half of the maximal cumulative release obtained and the change of rate at that time, r which shows how model parameters change with experimental conditions. Half-time, T for the drug can be obtained by rearranging Equation 6.4 as follows:

$$T = \tau(\ln 2)^{1/b} \qquad (6.7)$$

and rate of change at half-time can be obtained as:

$$\left.\frac{dQ}{dt}\right|_{t=\tau} = \frac{M * b * (\ln 2)^{1/b}}{2\tau} \qquad (6.8)$$

The power law,

6.2.6. Biocompatibility tests

To investigate the cell viability of PEG nanospheres *in vitro*, a human dermal fibroblasts (passage number: 16) were used. Cells were cultured at 37 °C with 5% CO2 in an incubator and maintained in DMEM supplemented with 1% penicillin/streptomycin, 2% L-glutamine and 10% FBS. The DMEM was prepared with different concentrations of PEG nanospheres (1, 0.5 and 0.1 mg/ml). Then samples were placed in the incubator and the CellTiter-Glo luminescent cell viability assay (Promega) was used on days 1 and 4 to characterize the metabolic activity of cells. A standard curve was generated using ATP solutions at specific concentrations (1, 0.1 and 0.01 mM) in the cell culture medium. Next, 100 µl from each hydrogel medium was taken and placed in the same amount of CellTiter-Glo Reagent. Both ATP solutions and samples were incubated at 25 °C for 15 min and the luminescence was measured using a plate reader (Biotek, Synergy H1).

6.3. Results and Discussion

The components in PEG nanosphere-dextran system (PEG bulk hydrogel, PEGDA, dextran and PEG nanospheres) were characterized by FTIR spectroscopy to demonstrate the gelation and presence of PEG nanospheres in dextran medium (Fig. 6.3). Weak peak at 1640 cm^{-1} which was assigned to -C=C- stretching [207] occured in PEGDA, while it disappeared in PEG hydrogel and nanosphere due to saturation of double bonds in acrylate groups and formation of a crosslinked polymer network. Strong peaks that appeared between 650 and 1000 cm^{-1} in PEGDA were assigned to =C-H bending of alkenes, where the decrease in the magnitude of these peaks were observed in PEG hydrogel and nanosphere as a result of consumption of double bonds [207]. The result also showed that the FTIR spectra for PEG nanosphere was very similar to that of dextran. This could be explained by the presence of excess dextran in the sample, which could not be completely removed away from the nanosphere particles. The strong peak in nanosphere sample at 1730 cm^{-1} was assigned to C=O stretching [207] and confirmed the presence of PEG nanospheres.

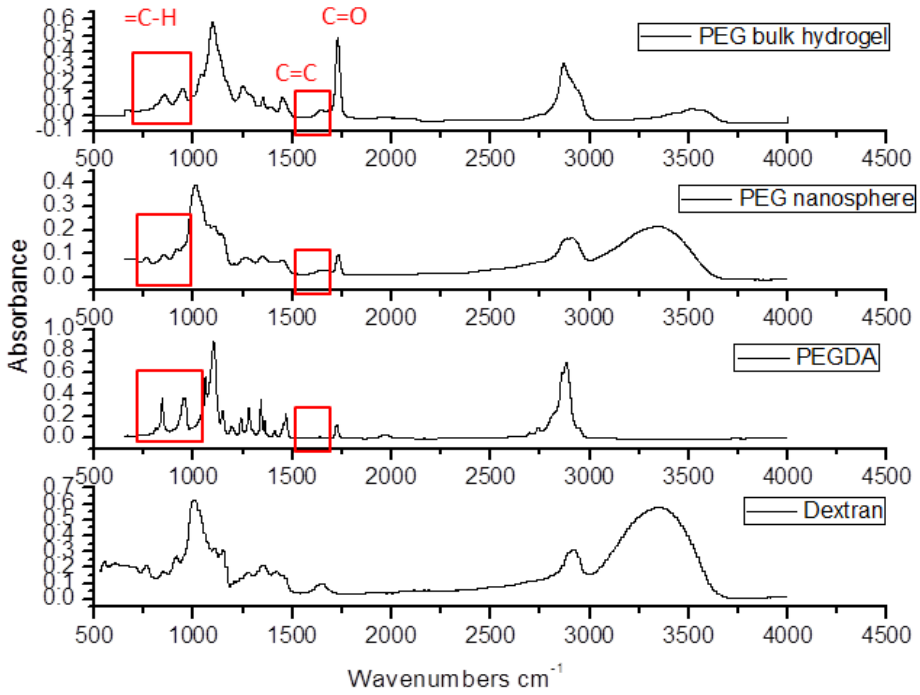

Figure 6. 3: FTIR spectra of PEG hydrogel, PEG nanosphere, PEGDA and dextran.

Morphology of emulsions and PEG hydrogel particles were characterized by light microscope and SEM, where size distribution of PEG hydrogel particles dispersed in water was characterized by DLS. Dextran-PEG prepolymer phase separation was obtained with 30% (w/v) PEGDA prepolymer solution and 20% (w/v) dextran (Fig. 6.3 a). Light microscope image of PEGDA-dexran emulsion demonstrated micron-scale hydrogel spheres, and PEG nanospheres could be visualized by SEM image as were shown in Fig. 6.4. Size of the particles obtained in a dispersed phase of w/w emulsion would change depending on the molecular weight and concentrations of polymer used in each phase, volume fraction of both phases, stirring rate and time used for emulsification [45, 46, 119]. In previous studies, micron size spheres (2.5 to 25 μm) were obtained by emulsification of dimethacrylated PEG (PEG-MA_2; molecular weight: 3400 Da) and dextran (molecular weight: 40 kDa) with a vortex time of 1 min. It was also observed that dispersed PEG hydrogel particles in micron-scale size range would increase with decreased concentration of dextran (from 23 to 15% (w/w)) in continuous phase, probably due to the lower viscosity obtained for the continuous phase [46]. Here, we

could successfully reduce the hydrogel particle size down to nano-scale with high dextran concentration (20% (w/v) and low PEGDA molecular weight (575 Da) using 1/6 (v/v) volume fraction and high stirring time (45 minutes). Decreases in molecular weight of dispersed phase polymer and increases in the viscosity of continuous phase along with stirring time resulted in nano-sized PEG spheres with uniform morphology.

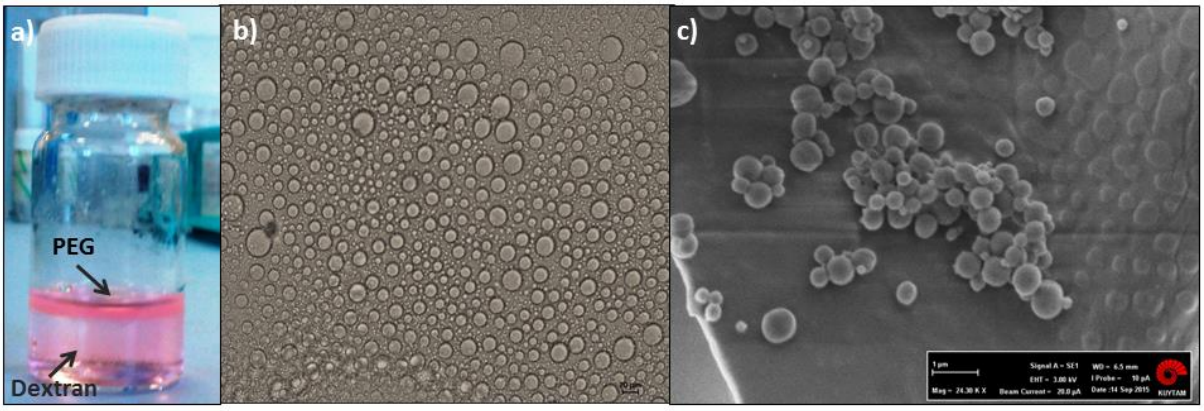

Figure 6. 4: a) Two-phase separation of dextran-PEG polymer b) Light microscope image of dextran-PEG w/w emulsion (scale bar: 20 μm) c) SEM image of dried PEG (scale bar: 1 μm) [12].

Four sets of PEG nanospheres were synthesized through exposure of emulsions to visible light, using altered laser power (100 and 50 mW) and durations (40 and 20 s) (Table 6.1). The influence of polymerization conditions on the morphology, size, drug loading and release properties of hydrogel particles were investigated. Morphology of PEG nanospheres obtained with altered polymerization conditions was characterized by SEM and the results were presented in Figure 6.5. Size distribution of hydrogel particles was determined using DLS as was shown in Figure 6.6. It was observed that uniform and individual particles could be obtained when emulsions were exposed to visible light for 40 seconds (Fig. 6.5a and 6.5c). Some aggregates and non-uniform structures appeared for the polymerization conditions of P100-20s and P50-20s, which were treated with short visible light exposure of 20 seconds (Fig. 6.5 b and 6.5 d). According to DLS characterization, two different size ranges of 5-50 nm and 150-450 nm were obtained in this group. When laser exposure time was reduced from 40 seconds to 20 seconds, non-

uniform structures and polydispersed solution with higher size ranges were observed (Fig. 6.6b and 6.6d). For example, three different size ranges of 5-30 nm, 50-150 nm and 400-850 nm were obtained for P100-20s, where the size distribution for P50-20s sample ranged from 100-600 nm and 5-6 μm (Fig. 6.6b and 6.6d). The reason for higher sizes obtained for P50-20s group was due to the short duration of polymerization time and low power of laser intensity which were insufficient to crosslink all droplets. Insufficient crosslinking could also lead to aggregation of particles causing increases in polydispersity. The DLS results suggested that significant quantity of particles could be obtained in nano-scale with increased laser intensity and polymerization time, and that polymerizaton condition of P50-40s was found as optimum for the synthesis of PEG nanospheres with uniform morphology and size distribution.

Table 6. 1: Description of the sets studied for characterization of size and morphology of PEG hydrogel particles.

Sample Set	Power (mW)	Laser exposure time (s)
P100-40s	100	40
P100-20s	100	40
P50-40s	50	20

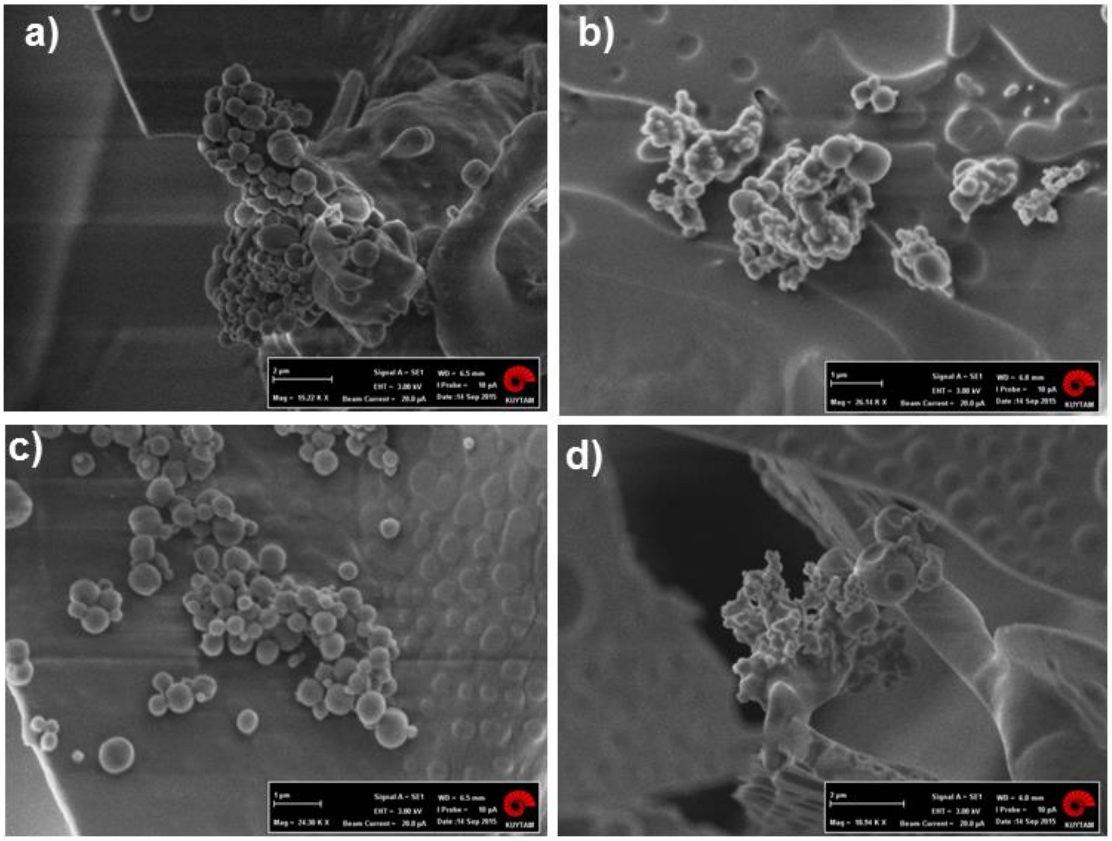

Figure 6. 5: SEM images of PEG nanospheres showing the differences in morphology of a) P100-40s (scale bar: 2 µm) b) P100-20s (scale bar: 1 µm) c) P50-40s (scale bar: 1 µm) and d) P50-20s (scale bar: 2 µm) [12].

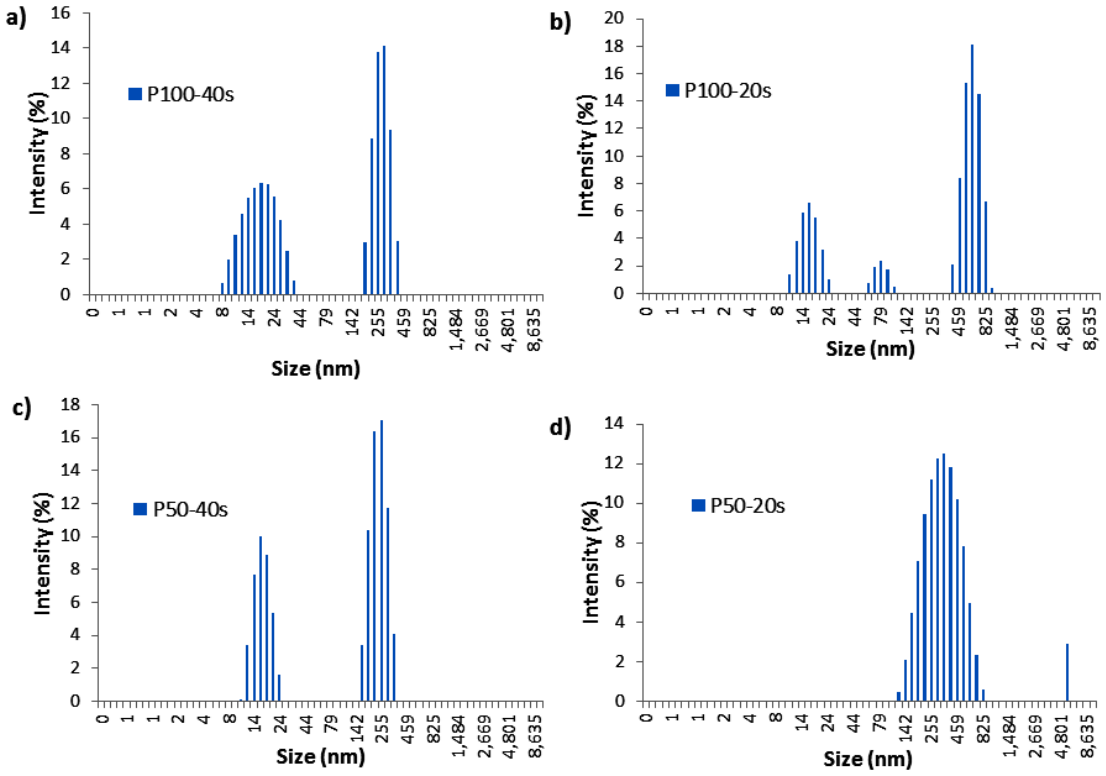

Figure 6. 6: Size distribution of PEG nanospheres a) P100-40s b) P100-20s c) P50-40s d) P50-20s obtained from DLS characterization [12].

6.3.1 PGB loading into PEG nanospheres

PEG hydrogel particles synthesized with altered polymerization conditions were incubated in PGB solution. PGB loading efficiencies into PEG nanospheres were calculated by Equation 6.1, and the results were given in Table 6.2. Depending on the polymerization parameters, different laoding efficiencies were obtained. Loading efficiencies were found as 52.23±1.25, 56.67±3.76, 80.18±3.66 and 67.23±2.66% for P100-40s, P100-20s, P50-40s and P50-20s samples, respectively. Maximum PGB loading efficiency was found in PEG nanosphere for P50-40s condition, where the emulsion was exposed to 50 mW visible light for 40 seconds. PEG nanospheres synthesized with P100-40s and P100-20s conditions had lower PGB loading efficiencies compared to that of P50-40s and P50-20s conditions, probably due to the stiffer hydrogel network structures obtained with high power of visible light. The differences in the loading efficiency between the samples exposed to low power of visible light (P50-40s and P50-20s) can be explained by the formation of non-uniform structures and gel

particle aggregates formed in P50-20s condition, which was observed in SEM and confirmed by DLS characterization. These aggregates could decrease the loading of PGB into gel structure performance due to decreased surface area of particles in PGB solution. On the other hand, PEG nanospheres prepared with P50-40s condition had more uniform individual spherical structures with nano-scale size ranges as was observed in SEM and confirmed by DLS. Small particle size along with uniform structure resulted in increase in the surface area of particles, which promoted the interaction and diffusion of PGB molecules through the pores of hydrogel particles. In our previous study, we investigated PGB loading into ph-responsive composite hydrogels composed of Poly(methacrylic acid-g-ethylene glycol) (P(MAA-g-EG)) hydrogel and cross-linked styrene–butadiene–styrene (SBS) gel [13, 208]. Depending on the composition of the hybrid hydrogels, PGB loading efficiencies as high as 63.5±2.4% could be obtained [208]. Here, we observed higher loading efficiency (80.18±3.66%) of pregabalin into PEG nanospheres prepared with P50-40s condition, which was expected as a result of uniform size and morphology achieved with nano-scale hydrogels obtained in this group.

Table 6. 2: PGB loading efficiencies of the samples.

Sample set	PGB loading efficiency (%)
P100-40s	52.23±1.25
P100-20s	56.67±3.76
P50-40s	80.18±3.66
P50-20s	67.23±2.66

6.3.2. PGB release from PEG nanospheres

PEG nanospheres were incubated in PBS for 72 hours and 0.8 ml samples were taken from each set after 0.5, 1, 2, 4, 12, 24, 48 and 72 h and replaced with fresh PBS. PGB release from each PEG hydrogel particle samples were measured by UV-visible spectrophotometer at 210 nm wavelength. Time dependent mass (equation 6.2) and percent release of PGB (equation 6.3) were calculated based on these measurements. Percent cumulative PGB release from PEG nanospheres is shown in Fig. 6.7. After incubation for 72 hours in PBS, maximum cumulative PGB release of 87.34±2.83,

84.01±0.87, 79.52±3.25 and 66.45±1.18% were obtained for P100-40s, P100-20s, P50-40s and P50-20s conditions, respectively. PEG nanospheres synthesized in P100-40s group had the highest percent PGB release due to high intensity of small size (8-40 nm) nanospheres that lead to high surface area interactions with PBS. In addition, it was observed from the figure that the release rate of PGB increased as the size of micro/nano spherical porous structures decreased due to reduced distances required for the diffusion of drug molecules through the gel network. The lowest maximum cumulative PGB release of 66.45% was observed for P50-20s condition. This result was expected and could be explained with the formation of PEG nanosphere aggregates as was observed and discussed in SEM and DLS characterization (Fig. 6.5d and 6.6d). PEG hydrogel particles synthesized through P50-20s condition resulted in a slower PGB release rate and lower maximum cumulative PGB release compared to the particles prepared in remaining groups. This can be attributed to increases in hydrogel size and decreased surface area to volume ratio, which compromised the delivery of PBG molecules from bulk hydrogel structure.

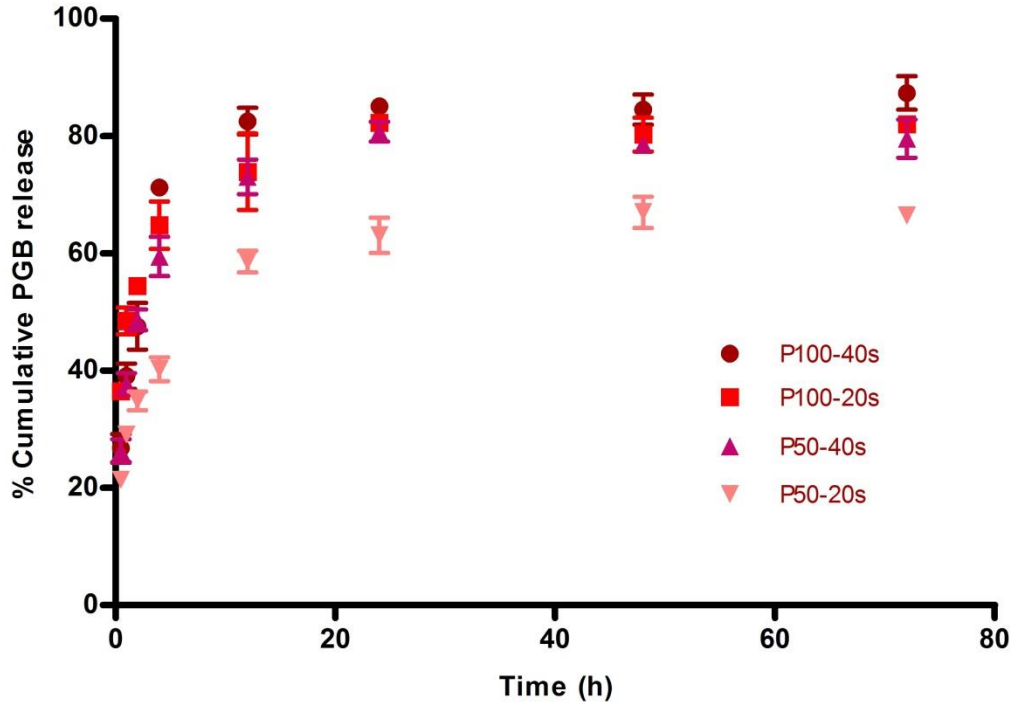

Figure 6. 7: Percent cumulative PGB release from PEG nanospheres [12].

6.3.3. Model Fitting Results

Cumulative PGB release data was fitted to a stretched exponential function model (Equation 6.4) [129]. All data was well described with this model with R^2 (correlation coefficient between the fits and the experimental data) values higher than 0.99, which suggested the goodness of fitting. Experimental release data and estimated cumulative % PGB release curve obtained from fitting of the experimental release data is shown in Fig. 6.8. As a result of the least-squares fittings from the model, R^2 values, estimated *M* (maximum release), *T* (half time), r (rate of change at half time), Ƭ (time for 63.2% cumulative release) and b (the model parameter that defines the stretching of the exponential function) were obtained and these values were listed in Table 6.3. According to the model results, Ƭ and r values obtained from the model equation were directly correlated to the experimental value of *M*. It was found that Ƭ values decreased and r values increased with high experimental values of M. Exponential correlation showing a decrease in Ƭ with increase of experimental cumulative release was observed (R^2=0.98).

A linear correlation showing an increase in the half time slope with experimental cumulative release was also observed (R^2=0.96). The highest release rate in half time and lowest ζ coefficient was observed for P100-40s that had the highest intensity of smaller size nanospheres. The lowest release rate in half time and highest ζ coefficient was observed for P50-20s which contained micron-size particles with decreased surface area and PGB release. Since estimated half time release rate was directly related to ζ (Equation 6.8), it was possible to correlate ζ coefficient with the size of nanospheres. ζ increased with increased size of PEG nanospheres which reduced PGB release. A relation was also observed between experimental conditions and model parameter of the stretched exponential function, b. According to model results shown in Table 6.3, b values are between 0.25 and 0.5 for drug release trends of all conditions studied for synthesis of PEG nanospheres. These values demonstrate the good fitting of the model to experimental data. It was seen that higher b values were obtained for longer polymerization times in which stiffer hydrogel network was obtained and can be related to more diffusion dominated release mechanism.

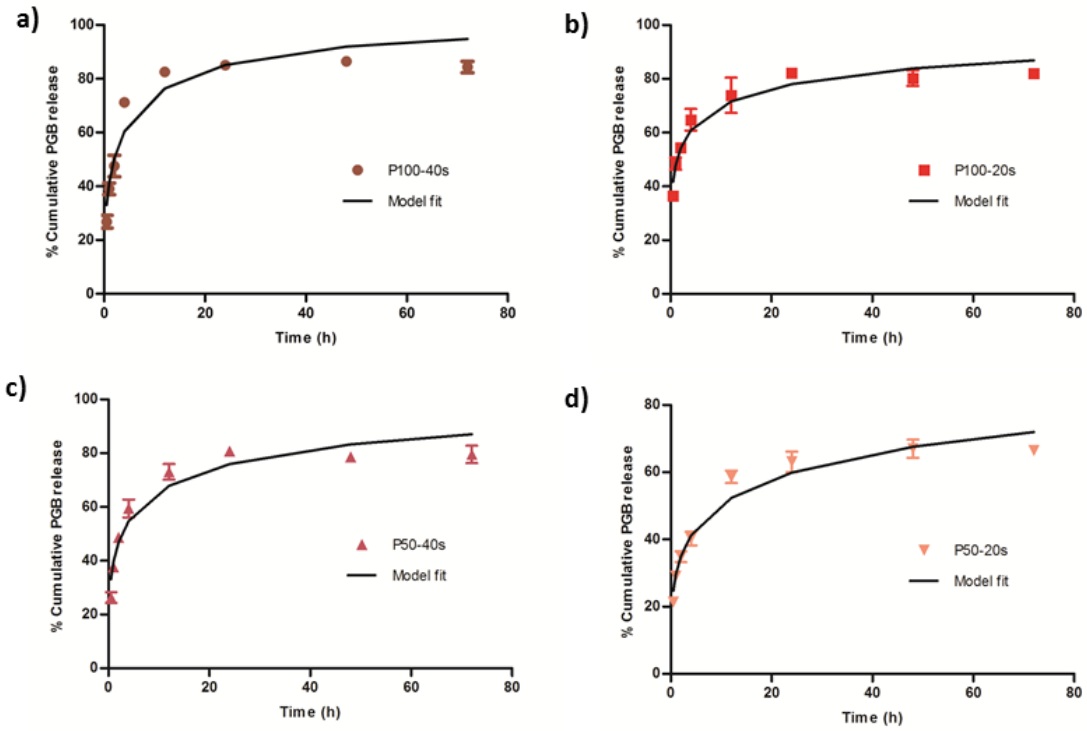

Figure 6. 8: Experimental percent cumulative release of PGB from PEG nanospheres and model fit (solid curves) provided by the model (equation 6.4) [12].

Table 6. 3: Model fit results of PGB release data estimated from stretched exponential model (equation 6.4).

PEG nanospheres	R^2	M (maximum release)	T (half time, hours)	Ƭ (time for 63.2% release)	r (half time slope)	B
P100-40s	0.9923	95.48	1.95	4.71	6.84	0.42
P100-20s	0.9976	87.48	1.29	4.95	6.17	0.27
P50-40s	0.9936	87.01	2.65	8.12	3.56	0.33
P50-20s	0.9953	71.97	9.63	32.42	0.73	0.30

6.3.4. Biocompatibility test of PEG nanospheres

Human dermal fibroblast cells were cultured with PEG nanospheres using altered concentrations of particles (1, 0.5 and 0.1 mg/ml). Cell survival was measured after incubation of cells for 1 and 4 days. *In vitro* percent cell viability results showed that PEG nanospheres do not have toxic effect on cell growth (Fig. 6.9). All samples had higher cell survival of above 80% compared to control groups, except 1 mg/ml concentration of P50-20s (72%) (Fig. 7c). PEG nanospheres synthesized in P50-20s group at 1 mg/ml concentration included some aggregates and these aggregates probably compromised cell growth as a result of sedimentation of larger hydrogel structures and subsequent mechanical stress on cells [209]. Among the sample sets used, highest viability was obtained for the condition of P50-40s after 4 days of incubation. This result could be due to appropriate morphology and size distribution of particles, which did not cause any mechanical stress on cell survival. Slight decrease in cell viability was observed with PEG nanospheres prepared with P100-40s and P100-20s conditions, which were polymerized with high power of visible light. Similarly, precipitation of rigid nanospheres prepared with high intensity might cause mechanical stress and hence influenced the cell growth [209]. Overall, significant negative influences of particles on cell survival were not observed.

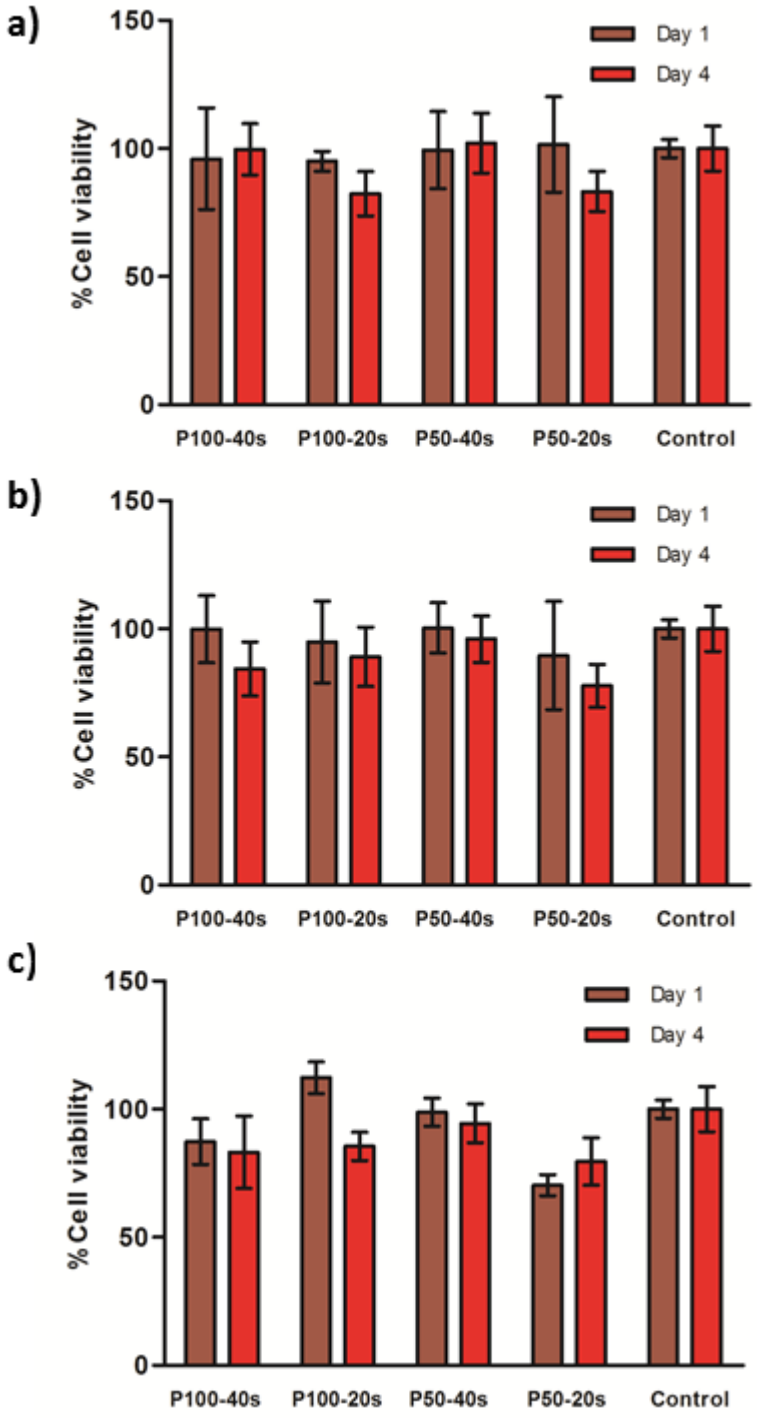

Figure 6. 9 Percent cell viability of fibroblast cells cultured with a) 0.1 b) 0.5 and c) 1 mg/ml concentration of PEG nanospheres [12].

6.4. Conclusion

W/w emulsions based on phase separation of liquids have been promising for synthesis of biocompatible hydrogel particles in drug delivery systems. In this study, the synthesis of nano-scale PEG nanospheres was succesfully carried out through photopolymerization of hydrophilic emulsions based on PEG-dextran emulsion system. PEG nanospheres polymerized with altered laser power and duration of visible light were characterized in terms of morphology, size distribution and PGB drug loading and release properties. Optimum polymerization conditions promoted the morphology of nanospheres, where differences in the size and morphology of PEG nanospheres influenced PGB loading and release profiles. The amount of PGB released with time *in vitro* was fitted to an exponential function model with high correlation coefficients. PEG nanospheres synthesized with low power and high duration of polymerization condition was found as optimum in terms of morphology, size, drug loading and release properties. Furthermore, biocompatibility of PEG nanospheres were tested on fibroblast cells and no toxic effect was observed. PEG hydrogel nanospheres synthesized via dextran-PEG w/w emulsion can be utilized for drug/ligand delivery in biomedical applications, where specific targeting could be achieved through functionalization of nanospheres.

Chapter 7

CROSS-LINKED SBS-PEG HYBRID GELS FOR SUSTAINED DRUG RELEASE PURPOSES

7.1 Introduction

SBS is a synthetic triblock copolymer, commonly used as a rubber substitute due to its high tensile strength, high elongation and resilience [133, 134]. Due to its desirable properties, SBS has been used in a variety of industries, ranging from construction (as an additive to bitumen to enhance road resilience) to biomedicine. However, the potential of SBS for biomedical applications has only been considered in limited earlier reports.

SBS can be used to create slightly hydrophobic networks analogous to hydrogels such as poly ethylene glycol (PEG). While hydrogels have been widely studied as biomaterials due to their controllable swelling, molecule loading and release properties, their hydrophobic counter parts have not received the same attention, especially in relation to biomaterials research [16]. However, it is also possible to obtain covalently crosslinked hydrophobic networks, such as SBS, through appropriate use of crosslinking molecules [133, 139, 145, 147]. Crosslinked SBS network can be synthesized through the addition of radicalized thiol groups onto the double bonds found in the poly(butadiene blocks). This mechanism, also known as “click chemistry”, is relatively simple, versatile and has been extensively studied and used to control molecular weight in radical

polymerization reactions [151]. The eosin Y and TEA initiator system has also been widely used in the crosslinking of poly(ethylene glycol) (PEG) hydrogels and is capable of producing radicals to drive the crosslinking under visible (wavelength ~500nm) or UV light [3, 152, 153]. We combined these two systems for the first time, where SBS polymer was crosslinked via UV photoinitiated thiol-ene reactions using dithiothreitol (DTT) as crosslinker, and eosin Y-TEA photoinitiation system to initiate crosslinking reactions with TEA radicals.

In this chapter, we investigated sustained drug release from SBS-PEG hybrid gels. For this purpose, we aim to synthesize PEG particles embedded SBS hybrid gels for extended delivery of model drugs. The reasons for wishing to achieve slow release are to decrease the number of daily administrations, improve compliance and minimize side effects [14, 15]. Sustained drug release is important for efficacious treatment of diseases such as periodontitis and severe bacterial infections since these physiological processes require repeated administration of drugs. Sustained release of drugs from gel network depends on hydrophilic-hydrohobic nature of the drugs and the gel matrix, network properties of gel matrix and degradability of the components [14]. Here, we use SBS for gel matrix since SBS is a hydrophobic, biocompatible co-polymer and can be cross-linked to obtain a gel network with very low mesh size [13]. In literature, SBS was used in few biomedical applications [17] and drug release kinetics of this rubber elostomer is unknown. PEG is a well-known biocompatible polymer and can be crosslinked via photopolymerization to obtain a hydrophilic gel network [12]. Thus, our objective is to design a novel hybrid gel for sustained release of a model drug with amphiphilic property, by using styrene-butadiene-styrene (SBS) hydrophobic polymer network as matrix where hydrophilic polyethylene glycol (PEG) hydrogel particles were embedded. For synthesis of SBS-PEG hybrid gels, we firstly synthesized PEG particles via particle stabilized emulsion method to be able to distribute hydrophilic PEG particles in hydrophobic SBS polymer uniformly. We characterized surface properties of SBS-PEG gels via SEM and contact angle measurements. The mechanical properties of gels were investigated with nanoindentation tests. Next, we investigated release of an anti-rheumatoid arthritis drug from PEG particles and SBS-PEG hybrid gels prepared with normal SBS and crosslinked SBS. The results showed that SBS-PEG gels have potential for sustained drug delivery applications.

7.2. Materials and Methods

7.2.1. Materials

SBS D1101 (S:B wt fraction 70:30) was purchased from Kraton; DL-Dithiothreitol (DTT); eosin Y and ethanol (99.8%) were purchased from Sigma-Aldrich; Triethanolamine (TEA) and Cyclohexanone (99.9%) were purchased from Merck (Darmstadt, Germany) and Phosphate-buffered saline (PBS) tablets were purchased from Amresco (Solon, Ohio). Silica nanoparticles (AEROSIL 816) were used for preparation of emulsions. PEG diacrylate (PEGDA) (575 Da) was purchased from Laysan Bio. Triethanolamine (TEA) was purchased from Merck (Germany). Vinyl-2- pyrrolidinone (VP) was purchased from Aldrich. AZ11657312 was kindly supplied from Aztra Zeneca (Istanbul, Turkey). Dulbecco modified Eagle medium (DMEM) was purchased from Gibco Life Tech. Penicillin/streptomycin, L-glutamine and FBS was purchased from Sigma-Aldrich.

7.2.2. Synthesis of PEG particles and SBS-PEG gels

Prepolymer solution was prepared with a concentration of 30 (w/v) PEGDA, 225 mM TEA and 37 mM VP in 10 mM PBS at pH 8. EosinY was added to the prepolymer solution at a final concentration of 0.025 mM. 25 % (v/v) fraction of internal volume of prepolymer solution is added into silica nanoparticle dispersion (1.5 wt %) in cyclohexanone. The particle dispersion was kept at room temperature. Stock nanoparticle solution concentration of 1.5% (w/v) was prepared. 0.5 mL of the PEGDA prepolymer solution was added into 1.5 mL of nanoparticle stock solution phase under high shear applied by vortex at maximum speed for different times. As prepolymer solution was mixed in the cyclohexanone, the aqueous solution formed well-dispersed droplets which were stabilized by silica nanoparticles. The synthesis of an PEG particles was carried out using a TA Instruments AR/DHR series rheometer (New Castle, DE) with UV light attachment. 600 µl of stabilized prepolymer emulsion in vial was illuminated with UV light at 365 nm, with a flux of 100 mW cm^{-2} for 900 s. Next, PEG-cylohexane emulsion were washed with ethanol and distilled water, filtered and dried to obtain organic solvent removed dry PEG particles. PEG hydrogel particles were incubated in AZ11657312 solution for drug loading. A prepolymer solution containing 7.5 wt% SBS, 2.5 wt% DTT, 0.075 mM eosin Y, and 225 mM TEA was prepared in cyclohexanone. PEG particles

loaded with AZ11657312 were dried and dispersed in cylohexane with 10 mg/ml concentration. PEG particle dispersion was added to SBS prepolymer solution with 0.16 (v/v) volume fraction. The mixture was then exposed to UV light at 365 nm, with a flux of 150 mW cm^{-2} under 1% strain, at a frequency of 10 Hz for 3000 s. The crosslinked SBS networks were synthesized in the shape of a disk over a quartz sensor surface covered with a rotating plate with a diameter of 2 cm, and a fixed gap size of 1000 μm. The synthesis of PEG particles and encapsulation of particles in crosslinked SBS is schematized in Figure 7.1.

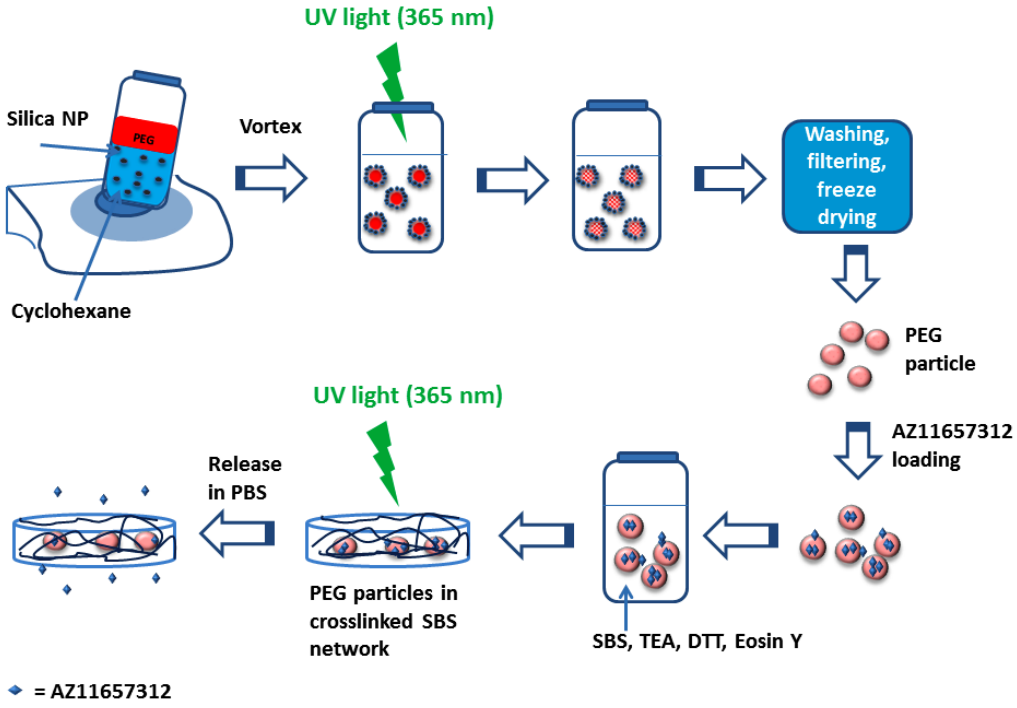

Figure 7 1: Schematic for synthesis of SBS-PEG gels.

7.2.3. Morphological characterization of emulsions, PEG particles and SBS-PEG gels

Emulsions were investigated under light microscope. SEM imaging was used to characterize structure and morphology of PEG particles and SBS-PEG gels. Static water contact angle measurements were performed on a Dataphysics OCA 35 instrument at

room temperature (24 ± 2 °C) to investigate the wettability of surfaces. 10 mL deionized, triple distilled water was used for measurements.

7.2.4. Nanoindentation tests

Depth sensing nano-indentation test (Agilent G200, USA) with Berkovich diamond indenter tip was used to characterize the mechanical properties of SBS and SBS-PEG gels. During nano-indentation test tip penetrates onto sample surface with indentation load P (N) and indentation depth h (m). Each indentation consists of loading and unloading phase. The hardness and elastic modulus of samples were obtained from the instrument calculating from load–displacement curves by using Oliver-Pharr method [210, 211]. The hardness of the material is obtained from loading phase and defined as:

$$H = \frac{p_{\max}}{A_C} \qquad (7.1)$$

Where, P_{max} is the applied maximum load and A_c is the horizontal projection of the contact area of tip at the end of loading phase, in this case a Berkovich pyramidal tip ($A_c = 24.5h^2$, h being the depth). The initial slope on the unloading branch (stiffness, S) is to the reduced elastic modulus (Er) by the following relationship:

$$S = \left(\frac{\partial P}{\partial h}\right)_{\max} = 2\frac{E_R}{\sqrt{\pi}}A_C \qquad (7.2)$$

And E_r is related to elastic modulus [210], E with the following equation:

$$E_r = \frac{E}{\left(1-\nu^2\right)} \qquad (7.3)$$

Where, v is Poisson's ratio of the samples. In addition, the elastic recovery parameter is calculated as follow:

$$ERP = \frac{h_{\max} - h_f}{h_{\max}} \qquad (7.4)$$

Where, h_{max} is the maximum indentation depth and h_f is the non-recovered depth of the indenter inside the sample. The maximum depth applied in each indentation was 22μm.

7.2.4. Drug loading and release experiments

Drug loading was carried out with 10 mg of PEG particles, where particles were incubated overnight in 1 mL of an aqueous loading solution containing 200 µg/mL concentration of AZ11657312 at room temperature. UV–visible spectrophotometer (Thermoscientific Nanodrop ND100) at 233 nm wavelength was used to measure AZ11657312 absorption. A standard calibration curve for the absorption of AZ11657312 in aqueous solution was generated to determine the concentration in unknown samples. The loading efficiency of AZ11657312 into PEG particles was calculated as follows:

$$\text{Loading efficiency} = (M_0 - M_f)/M_0 * 100 \qquad (7.5)$$

where M_0 represents the initial AZ11657312 mass in the stock solution and M_f is the final AZ11657312 mass remaining in the solution. To measure AZ11657312 release from particles, PEG particles in dialysis membrane bag were incubated in 20 mL of PBS, and 0.2 mL samples were taken at 0.5 h, 1 h, 2 h, 4 h, 12 h, 24 h, 48 and 72 h time points and sample was replaced with fresh PBS. AZ11657312 concentrations obtained from absorption measurements were used to calculate the mass released at time t (M_t) using the following Equation 7.6:

$$M_t = C_t * V + \sum C_{t-1} * V_s \qquad (7.6)$$

where Ct is the concentration of AZ11657312 in the release solution at time t, V is the total volume of the release solution (12 mL) and Vs is the volume of the sample taken (0.8 mL). Percent of cumulative AZ11657312 release, Q, was determined as follows:

$$Q = (M_t / M_\infty) * 100 \qquad (7.7)$$

where M_∞ is the total weight of AZ11657312 loaded in particles.

For investigation of drug release from SBS-PEG hybrid gels, drug loaded PEG particles were encapsulated in SBS membrane or SBS gels. SBS membrane-PEG and SBS-PEG hybrid gels were incubated in 12 ml of PBS, and 0.2 mL samples were taken for 28 days and samples were replaced with fresh PBS. AZ11657312 concentrations obtained from absorption measurements were used to calculate the mass released (Eqn.7.6) and percent of cumulative AZ11657312 release was determined using Eqn. 7.7.

7.3. Results and discussion

7.3.1. Synthesis and characterization of PEG particles

PEG-cyclohexanone emulsions were prepared via silica particle stabilized w/o pickering emulsion. PEG prepolymer droplets were dispersed in continuous phase of cyclohexanone with internal volume fraction (ϕ) of 0.25. Size of droplets in particle stabilized PEG-cylohexane emulsions with 1.5 % nanoparticle concentration was optimized by changing the vortexing time and emulsions were investigated under light microscope. The smallest size was obtained with 8 min vortexing (Figure 7.2). Figure 7.2 shows the effect of vortexing time on size of droplets in PEG-cyclohexanone pickering emulsion.

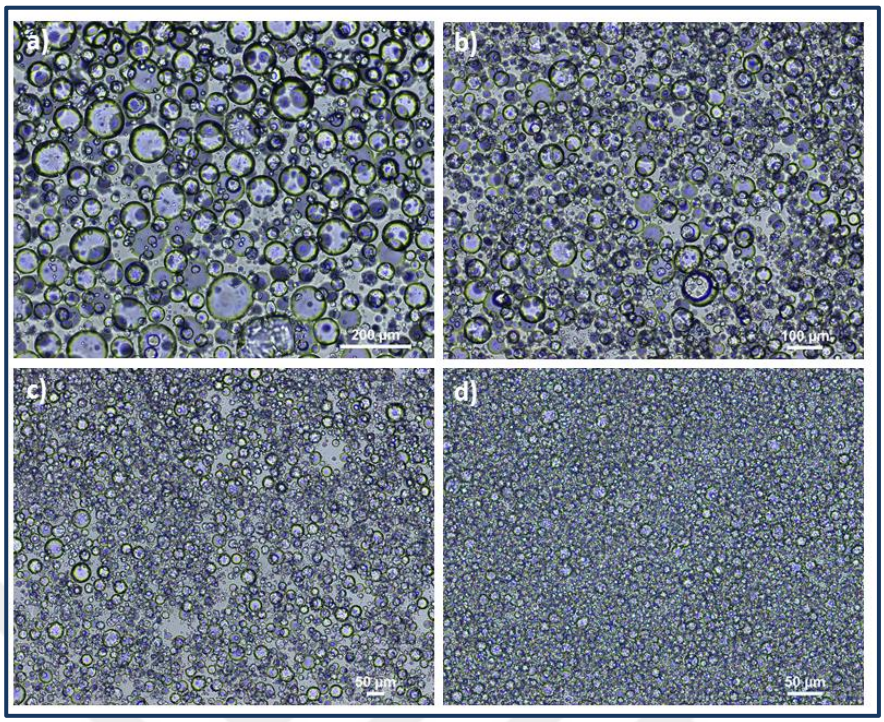

Figure 7 2: Light microscope images of PEG-cyclohexanone (ϕ= 0.25) water in oil silica nanoparticle (1.5 %) stabilized pickering emulsions prepared by vortexing times of a) 30 s b) 60 s c) 2 min d) 8 min.

Next, PEG-cylohexane pickering emulsions were exposed to UV light and PEG prepolymer droplets were gelated via UV initiated photo-crosslinking. Emulsions were washed and dried to obtain dry PEG particles. Morphology of PEG particles were characterized with SEM. PEG particles for SEM characterization were prepared via two different methods. Size of PEG particles in dry powder (Figure 3a) and casted form (Figure 3b) change from 200 nm to 2 µm.

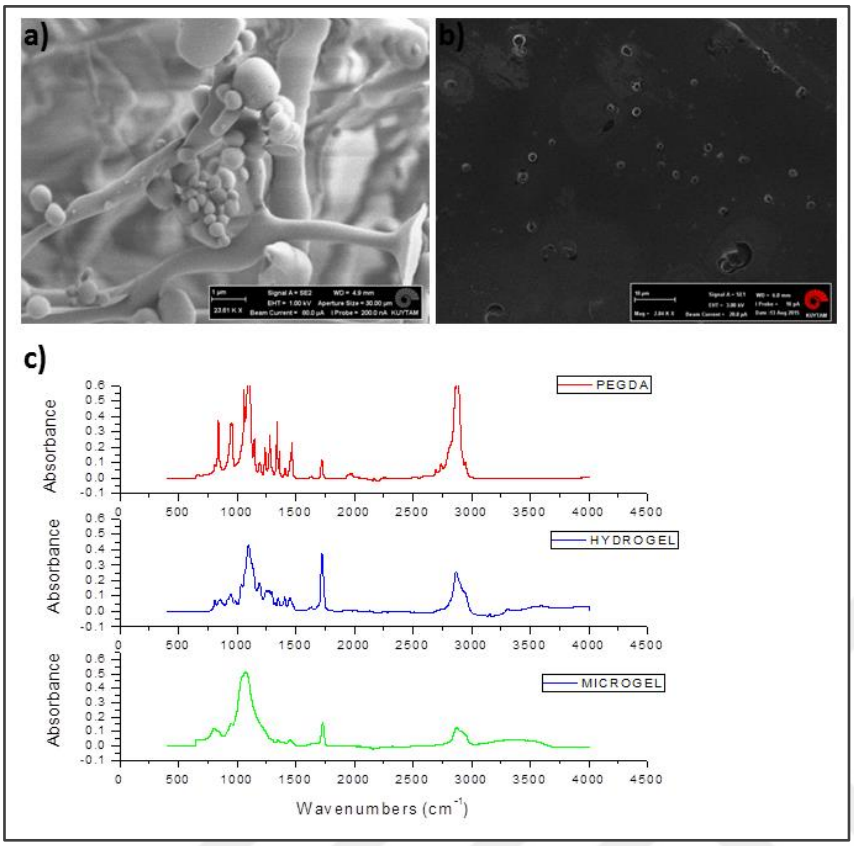

Figure 7. 3: Structural characterization of PEG particles. a) SEM image of powder PEG particles (scale bar: 1 µm) b) SEM image of casted PEG particles (scale bar: 10 µm) c) FTIR spectra of PEGDA, PEG bulk hydrogel and PEG microgel.

PEG particles were also characterized by FTIR spectroscopy to demonstrate the gelation (Figure 7.3c). Weak peak at 1640 cm^{-1} which was assigned to -C=C- stretching occured in PEGDA, while it disappeared in PEG hydrogel and microgel due to saturation of double bonds in acrylate groups and formation of a crosslinked polymer network. Strong peaks that appeared between 650 cm^{-1} and 1000 cm^{-1} in PEGDA were attributed to =C–H bending of alkenes, where the decrease in the magnitude of these peaks were observed in PEG hydrogel and microgel as a result of consumption of -C=C- double bonds.

7.3.2. Synthesis and characterization of SBS-PEG hybrid gels

Crosslinked SBS network was synthesized with the addition of radicalized thiol groups onto the double bonds found in poly(butadiene blocks). Double bonds in the polybutadiene block can remain in a variety of conformations. Among these, alkene

groups existing in the form of vinyl are the most reactive and suitable for the click reaction. Thiol-ene polymerization occurs between thiol and pendant vinyl double bonds arising from 1-2 polymerization of butadiene more efficiently than with the backbone 2-butene double bonds of the polybutadiene chain. Thus, vinyl content of SBS largely determines the extent of the thiol-ene crosslinking reactions. Eosin Y-TEA photoinitiation system is used to initiate crosslinking reactions with TEA radicals. TEA acts as co-initiator and free radicals are originated from TEA with irradiation of eosine contributes to polymerization. We combined these two systems where SBS polymer was crosslinked via UV photoinitiated thiol-ene reactions using DTT as crosslinker, and eosin Y-TEA photoinitiation system to initiate crosslinking reactions with TEA radicals.

The polymer network is formed in the elastomeric phase upon UV irradiation through the vinyl group disappearance and the polymer insolubilization [133, 148]. In SBS copolymer, ends of polybutadiene chains are polystyrene segments which form rigid domains and act as junctions which make SBS copolymer physically crosslinked [134]. This explains the behaviour of a block copolymer at ambient temperatures. However, the situation changes at high temperatures. At about 100°C the styrene end-blocks melt, and the physically crosslinked structure of the material breaks down. With photoinitiated thiol-ene crosslinking, polybutadiene chains are covalently crosslinked with di-thiol crosslinker, DTT. The schematic of the reactions that occurred during crosslinking with photoinitiated radical thiol-ene chemistry, proposed SBS/DTT crosslinked network and the formation of the polymeric network in the elastomeric phase have been demonstrated in Figure 7.4. Similar reactions were suggested for the synthesis of SBS-trifunctional thiol networks in a previous study [212]

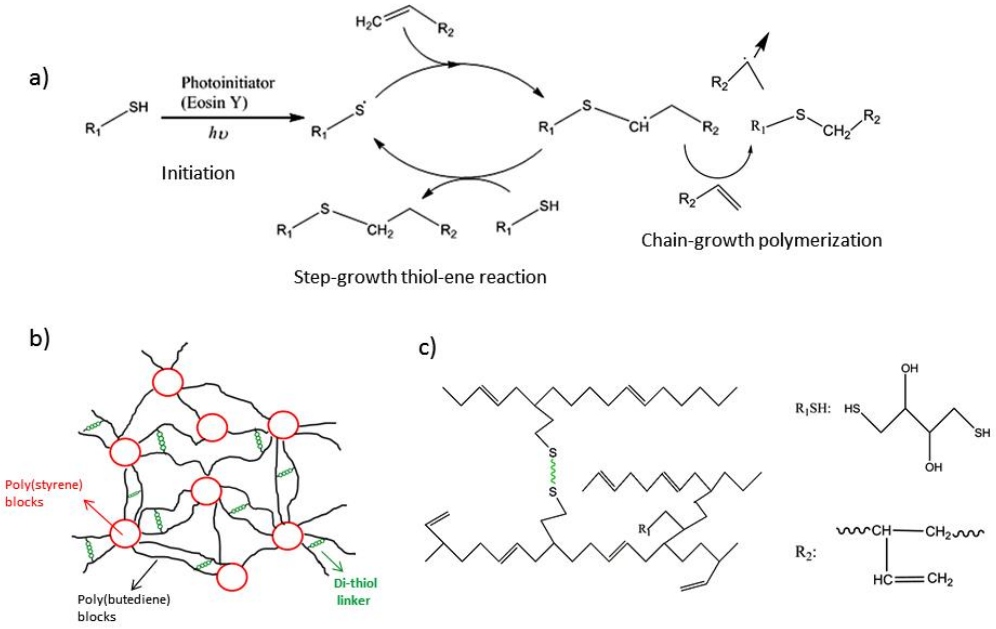

Figure 7. 4. a) Mechanism of UV-light mediated thiyl-ene photopolymerization. Schematic representation of; b) the photocrosslinked SBS triblock copolymer network including DTT, c) the photocrosslinked SBS/DTT polymer network formed in the elastomeric phase [13].

Figure 7.5 demonstrates in-situ rheological measurements, and shows how the moduli of the gels change with time during the crosslinking reactions. The expected behaviour during gelation was the constant increase in G', where solid-like properties during crosslinking reactions dominated up until 1250 seconds of UV exposure (Figure 2). G' eventually settled in a plateau, while loss modulus (G") demonstrated a decreasing trend beyond 750 seconds of polymerization. The behaviour of both G', and G" provides insight into the progress of crosslinking reactions.

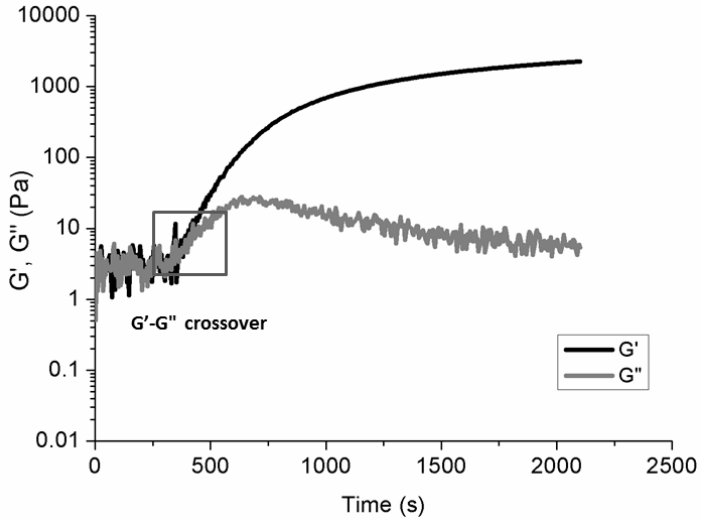

Figure 7. 5: Storage and loss moduli of SBS versus photopolymerization time [13].

SBS-PEG hybrid gels were prepared by incorporation of PEG particles in SBS solution including TEA, DTT and Eosin Y and then photo-initiated crosslinking of SBS solution under UV-light with 365 nm wavelength. The components and schematic of SBS/DTT polymer network structure and PEG particles in SBS gel network is shown in Figure 7.6.

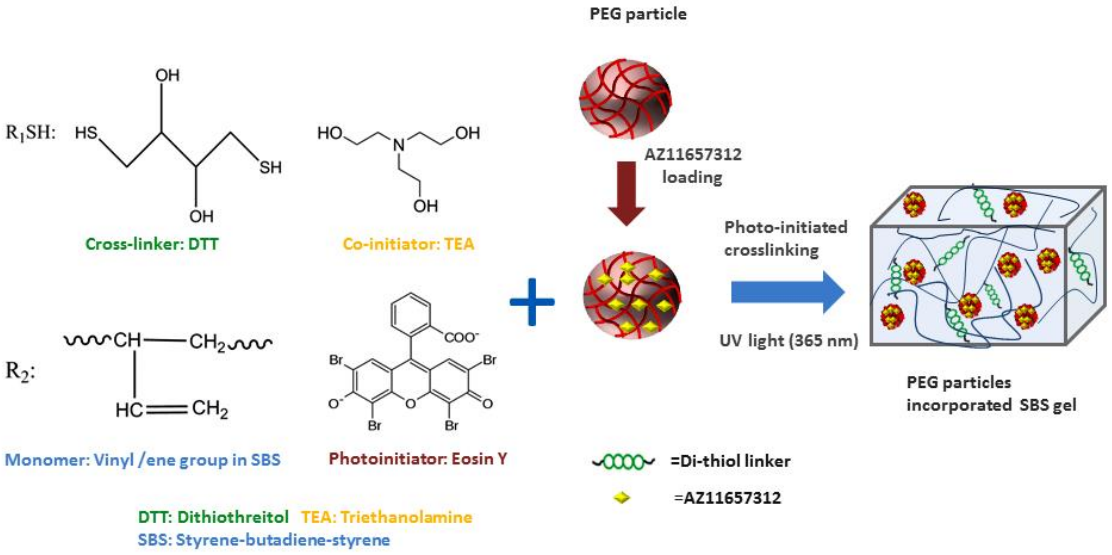

Figure 7 6: Schematics of the components and the PEG particles incorporated photo-crosslinked SBS polymer network structure.

SBS membrane-PEG gels were prepared by incorporation of PEG particles in SBS solution and casting the PEG particle incorporated SBS polymer solution on glass slide. SBS gel and SBS membrane samples were prepared following similar procedure with the hybrid gels without incorporation of PEG particles. Morphology of SBS membrane and SBS gel with or without PEG particles were investigated with SEM imaging (Figure 7.7). A rough surface was observed in SBS membrane and SBS gel coming from physical crosslinked structure of SBS composed of rigid styrene domains and butadiene chains with 30-70 styrene-butadiene composition (Figure 7.7a and b). When styrene amount in SBS is less than 50 (wt) %, styrene is distributed as domains in continuous butadiene matrix. Uniform distribution of PEG particles is observed in SBS-PEG samples in SBS membrane and SBS gel (Figure 4c and d). PEG particles are more distinguished in SBS membrane (Figure 7.7c) than in SBS gel due to hydrophilicity difference between SBS and crosslinked SBS. Since crosslinked SBS is more hydrophilic than normal SBS polymer, PEG particles are more embedded in crosslinked SBS due to hydrophilic nature of PEG.

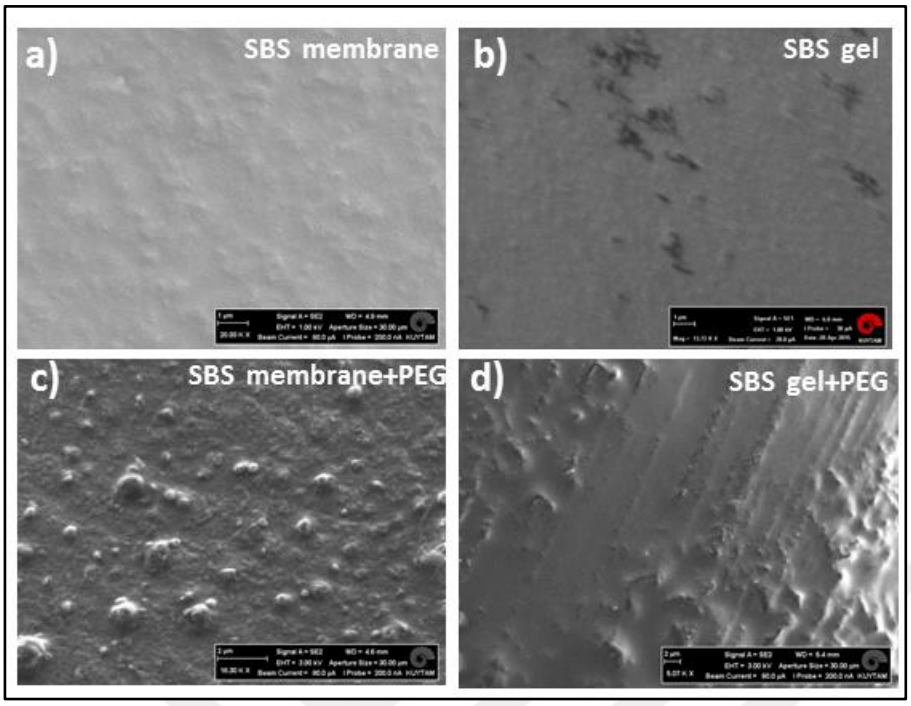

Figure 7 7: SEM images of a) SBS membrane (scale bar 1 μm) b) SBS gel (scale bar 1 μm) c) SBS membrane+PEG (scale bar 2 μm) and d) SBS gel+PEG (scale bar 2 μm). SBS membrane-PEG gels were prepared by casting SBS solution after incorporation of PEG particles. SBS SBS gel+PEG were prepared by crosslinking of SBS solution after incorporation of PEG particles. Hybrid gels were dried in vacuum oven overnight before analysis with SEM.

This difference was investigated with water contact angle measurements. Droplet shapes and water contact angles on surfaces were presented in Figure 6. Water contact angles decrease with crosslinking of SBS and incorporation of PEG particles (Figure 7.8 b). This is expected because incorporation of DTT in SBS for crosslinking increases the hydrophilicity. Similarly, incorporation of PEG particles contributes to hydrophilicity of hybrid gel which can be attributed to hydrophilic property of PEG.

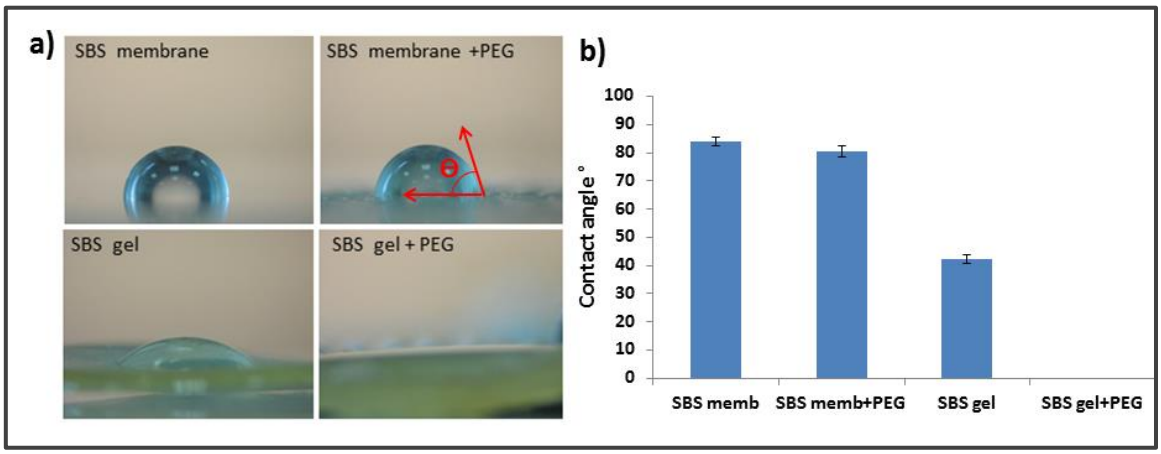

Figure 7 8 Water contact a) images and b) angles (Θ) of SBS membrane, SBS gel, SBS membrane+PEG and SBS gel+PEG surfaces. 10 µl of deionized, triple distilled water was injected on surfaces to obtain water droplets for measurement of contact angles.

7.3.3. Nano-indentation tests

Depth sensing nano-indentation test was conducted to investigate the mechanical properties of dry SBS and SBS-PEG gels. Nano-indentation is a useful tool that allows the direct measurement of the mechanical properties of materials. By indentation of a material to a desire depth followed by retraction of the tip, a load–displacement curve which is a

Characteristic of the material being tested is obtained. Maximum depth of 22 µm was applied in each indentation. Average elastic modulus and hardness were calculated based on these curves by using Oliver-Pharr method. Reduced elastic modulus and stiffness of the gels were calculated using Eqn. 7.2 and 7.3, respectively. Calculations were done using Poisson's ratio as 0.5. Non-recovered depth h_f obtained from load-displacement curves were 4.028 and 3.848 µm for SBS and SBS-PEG, respectively and ERP of the gels were calculated based on these values using Eqn. 7.4. Average elastic modulus, hardness, stiffness and ERP values are shown in Table 7.1. The load-displacement curve in Figure 7.9 shows that the load measured for maximum depth of indentation is in range of 5-6 mN for dry SBS and SBS-PEG gels. Characterization of SBS or crosslinked SBS by means of nano-indentation was not reported previously. Mechanical characterization of hydrogels using nano-indentation is also challenging compared to metals or ceramics [213]. So, there is limited data obtained from nano-indentation analysis of gels. In a

previous study load-displacement curves of epoxy hydrogels was investigated by nano-indentation tests and load of 1.5-2 μN was applied for 1.2 μm of maximum indentation depth [214]. In another study the load applied for maximum indentation was 2.0-2.5 mN for dry PHEMA hydrogels while it is only 0.5 mN for hydrated ones [215]. Here, SBS and SBS-PEG were investigated in dry form and they have stiffer structure compared to mentioned hydrogels. So it is expected to obtain the load in range of 5-6 nM for SBS and SBS-PEG samples. According to load-displacement, a slight increase occurs in applied load to reach same indentation with addition of PEG particles into SBS gel matrix. Average elastic modulus obtained from these curves is 0.233 and 0.267 GPa for SBS and SBS-PEG gels. Hardness, stiffness and ERP values (Table 7.1) which show the mechanical properties of gels are slightly higher for SBS-PEG gels compared to SBS gels, as well. This increase comes from incorporation of particles in polymer system. Because incorporation of nanoparticles or nanotubes in materials can result in enhanced ultimate tensile strength [216, 217].

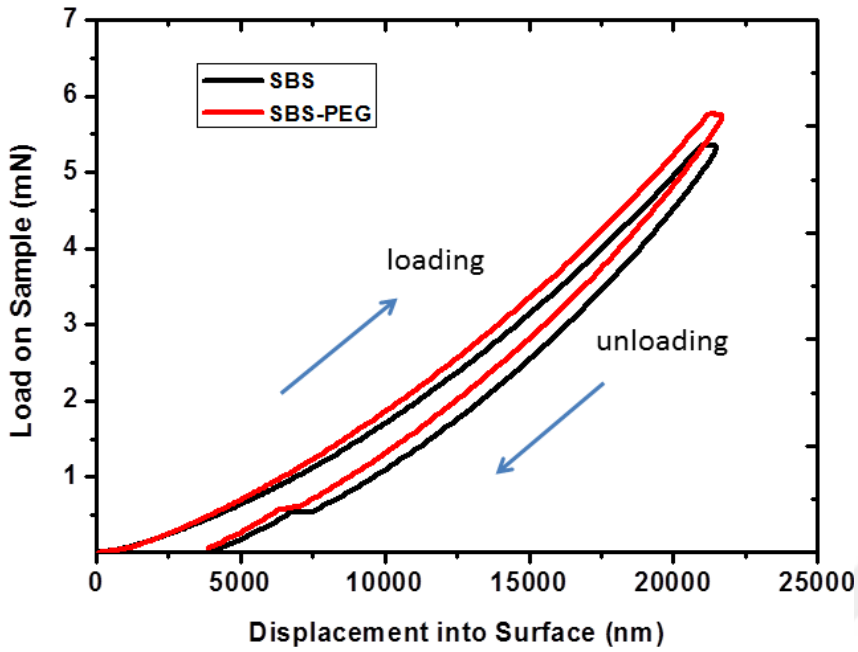

Figure 7 9: Nano-indentation load-displacement curves for SBS and SBS-PEG gels. Maximum indentation depth applied was 22 µm.

Table 7. 1: Average modulus and average hardness of SBS and SBS-PEG gels calculated from load-displacement curves by using Oliver-Pharr method.

	Average Elastic Modulus (E) (GPa)	Average Hardness (H) (GPa)	Average Stiffness (S) (kN/m)	ERP
SBS	0.233	0.080	26.0	0.817
SBS-PEG	0.267	0.103	29.7	0.825

7.3.4. AZ11657312 release from PEG particles and SBS-PEG gels

PEG hydrogel particles were incubated in AZ11657312 solution and percent loading efficiency into PEG particles was calculated as 85±4.2% using Eqn.7.5. For release experiments, PEG particles were incubated in PBS for 72 h and 0.2 mL samples were taken from each set after 0.5 h, 1 h, 2 h, 4 h, 12 h, 24 h, 48 h and 72 h and replaced

with fresh PBS. AZ11657312 release from PEG hydrogel particles samples were measured by UV–visible spectrophotometer at 238 nm wavelength that we determined previously using a set of AZ11657312 solutions with different concentrations. Time dependent mass (Eqn. 7.6) and percent release of PGB (Eqn. 7.7) were calculated based on these measurements. Percent cumulative AZ11657312 release from PEG particles is shown in Figure 7.10. Maximum cumulative AZ11657312 release of 95.5±3.5% was obtained after incubation for 72 h in PBS, however cumulative release was already 91.9±5.8% in 8 hours which can be called as burst release.

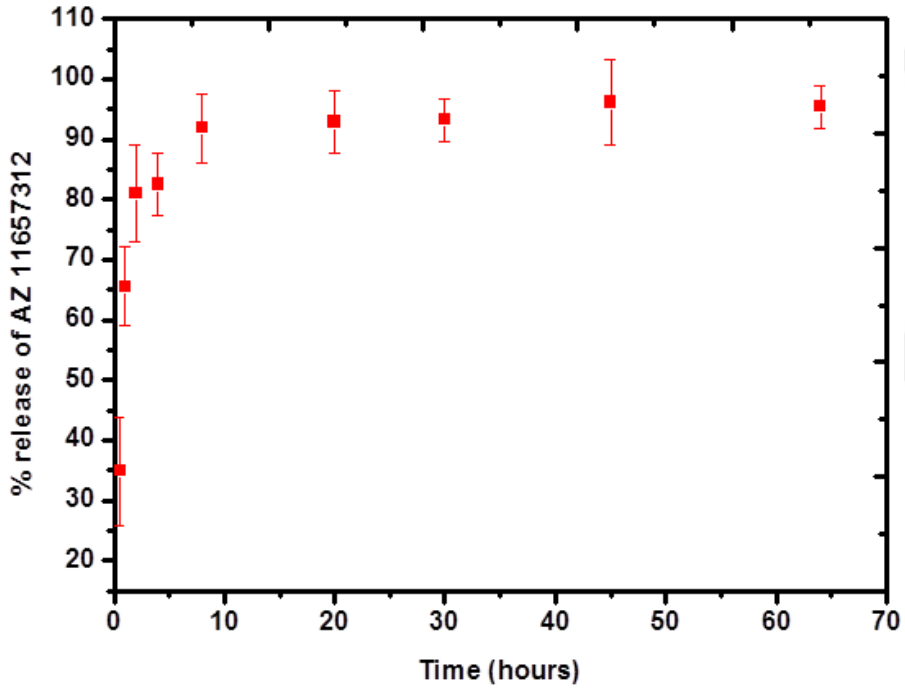

Figure 7 10: Cumulative percent release of AZ11657312 from PEG particles.

Next, PEG particles were incubated in 1000 and 2000 µg/ml concentrations of AZ11657312 and loading efficiencies were found as 61.1±11.0 % and 57.7 ±7.0 %, respectively. After drying, drug loaded PEG particles were encapsulated both in SBS membrane and SBS gels with 0.5 mg/300 µl SBS solution to obtain SBS membrane-PEG and SBS-PEG gels. AZ11657312 was also encapsulated in PEG particles as an alternative option to loading in order to investigate effect of drug encapsulation method on release profile. Amounts of AZ11657312 encapsulated in SBS solutions were calculated based on the amounts of AZ11657312 incorporated PEG particles.

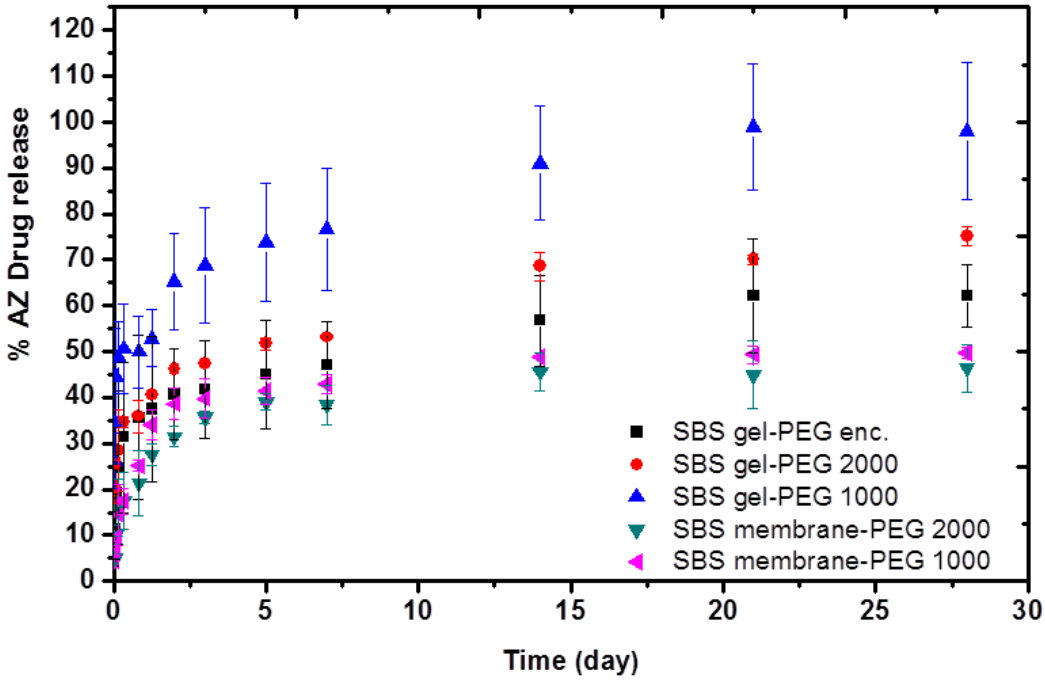

Figure 7 11: Cumulative percent release of AZ11657312 from SBS-PEG membrane and gels

SBS-PEG gels were incubated in PBS for 28 days and AZ11657312 release from SBS-PEG samples were measured by UV–visible spectrophotometer at 233 nm wavelength. The percent release of AZ11657312 for each condition is seen in Figure 7.11. Continuous drug release is observed up to 28 days in all samples due to including SBS membrane or crosslinked SBS in system. This sustained release can be attributed to difference in hydrophobic-hydrophilic nature of SBS-PEG and amphiphilic property of AZ11657312. AZ11657312 prefers to locate on the interface of PEG particle and SBS matrix and this phenomena decreases the diffusion rate of AZ11657312 through SBS matrix to the PBS. The second reason for achieved sustained release is low mesh size of SBS network which slows down the diffusion of AZ11657312. Figure 7.11 shows that crosslinked SBS containing systems provides higher percent drug release compared to only casted SBS membrane due to having a gel network. This crosslinked network structure enhances diffusion of drug and less drug is entrapped in the system than membrane. The more hydrophilic structure obtained in crosslinked SBS gels also

contributes the interaction of PBS with drug through the gel and enhances diffusion of drug to the surface. Higher percent drug release is seen in SBS gel-PEG1000 and SBS gel-PEG2000 drug loaded system compared to SBS gel-PEG encapsulated system where drug is encapsulated in PEG particles instead of loading. This higher release occurs due to fact that drug is not only located inside the PEG particle but also adsorbed on the surface of the PEG particle during loading. So, drug molecules adsorbed on the surface diffuse more easily through SBS matrix which leads to increase in drug release. Another significant observation is higher percent drug release is observed in SBS-PEG loaded in 1000 μg/ml drug solution compared to ones loaded in 2000 μg/ml as a result of more intense drug-drug interactions and aggregations in higher concentrations. Overall, drug release continue up to 28 days in SBS containing hybrid gels is significantly long period for sustained drug delivery. Previous studies focused on extended release profiles of altered drug through various network. Researchers synthesized various materials such as composite polymers and hydrogels for years and showed that matrix systems that include nanoparticles are promising for this purpose [14, 15, 218]. In one of these studies PLGA nanoparticles are incorporated in chitosan scaffolds to control BSA delivery and observed continuous release of BSA up to 25 days [219]. However, release of a drug from hydrophilic hydrogel-rubber elastomer hybrid system was not investigated previously. Our results demonstrate the potential of this SBS-PEG hybrid gels for extended drug release.

7.3.5. Biocompatibility tests of SBS and SBS-PEG gels

To investigate the cell viability of SBS and SBS-PEG gels *in vitro*, a human embryonic kidney (HEK 293) (passage number: 9) were used. Cells were cultured at 37 °C with 5% CO2 in an incubator and maintained in DMEM supplemented with 1% penicillin/streptomycin, 2% L-glutamine and 10% FBS. $1x10^4$ cells per gel were dynamically seeded on the model SBS and SBS-PEG network samples. Then samples were placed in the incubator and the CellTiter-Glo luminescent cell viability assay (Promega) was used on days 1, 3 and 5 to characterize the metabolic activity of cells. Percent cell viability of each sample was found by mormalizing to control cells. In vitro percent cell viability results showed that SBS and SBS-PEG nanospheres do not have significant toxic effect on cell growth (Figure 7.12). All samples had higher cell

survival of above 80% compared to control groups, except SBS-PEG on day 1. Lower cell viability of this group can be attributed to insufficient washing of these samples. Overall, significant negative influences of SBS-PEG and SBS gels on cell survival were not observed.

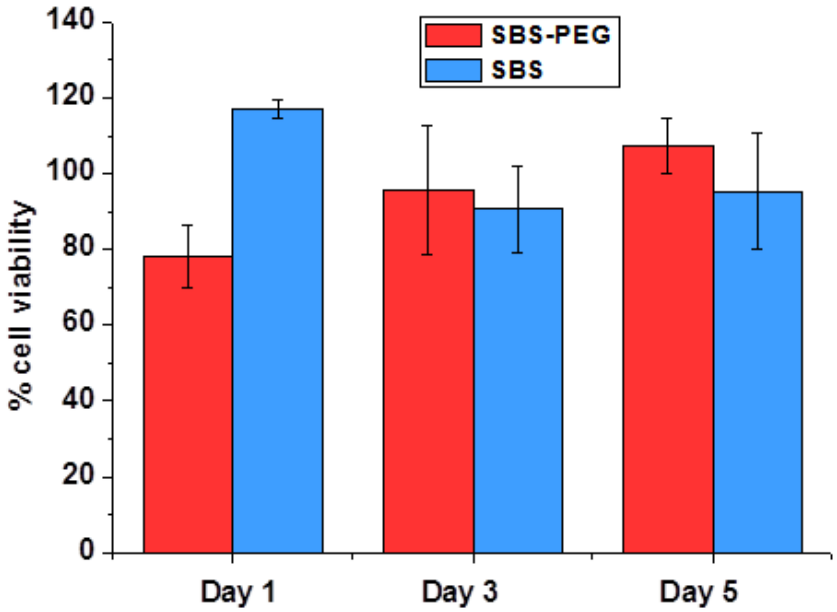

Figure 7 12: Percent cell viability of SBS and SBS-PEG gels.

Chapter 8

CONCLUSION AND FUTUREWORK

In this thesis, we investigated synthesis and characterization of novel functional materials using different emulsion methods for energy and biomedical applications. We designed composite polymer materials in which hydrophilic functional agents can be homogeneously dispersed and controllably released such as anti-icing agents for surfaces, biomolecules or drugs for therapeutic applications.

In the first part of this thesis, we combined the two emulsion templating approaches through particle stabilization to design a functional polymer composite that includes an anti-icing agent. We synthesized a composite membrane coating, which integrates a hydrophobic polymer adhesive base and hydrophilic aqueous phase that incorporates ionic salts using Pickering emulsion and gelation of the aqueous phase. The functional membrane consists of a base which is non-polar SBS block copolymer, and can be compatible with most non-polar surfaces. The hydrophilic domains include spherical droplets that store and induce controlled release of the anti-icing agent potassium formate salt. Dry composite membranes released 32 g/m^2 anti-icing agent within 4 hours and delayed freezing of water droplets for about 70 minutes.

The hydrophobicity and thermoplastic nature of SBS polymer composite allowed us for incorporation of the composite into bitumen, so that it provided possibility of delivering anti-icing agents through bitumen which would otherwise not be compatible. We modified bitumen with this polymer composite to obtain functional bitumen with

anti-icing properties. We investigated the incorporation of this polymer composite into bitumen and demonstrated proper distribution of the composite within bitumen through morphological and rheological analysis. We characterized the anti-icing properties of modified bitumen surfaces and demonstrated significant increases in freezing delay of composite-modified bitumen compared to base bitumen in a temperature and humidity controlled chamber with -14 °C plate and 5 °C medium temperature. In addition, we characterized the release of HCOOK salt from polymer composite-modified bitumen and observed salt release within the range of 1.07-10.8% (w/w) in 67 days, depending on the composite content. These results showed the potential of functional composite modified bitumen for anti-icing properties on roads.

For further investigation of composite modifed bitumen, we investigated the anti-icing properties of different ionic salts for composite-modified bitumen. We did not only incorporate polymer composite in bitumen, we also prepared polymer composite coated bitumen surfaces in order to investigate an alternative use of functional polymer composite for bitumen surfaces. We investigated effect of salt type on functional, mechanical and morphological properties of the composite incorporated or coated bitumen. We performed freezing experiments of composite modified and coated bitumen surfaces in camera-integrated cold chamber with uniform ambient and plate temperature (-2 ^{o}C). Higher freezing delay is observed for composite coated samples compared to composite incorporated bitumen. NaCl modified bitumen samples showed higher freezing delay when same amount of salt is used for each salt. However, freezing delay performance of KCOOH and $MgCl_2$ can be improved, since more salt can be disolved in dispersed phase for these salts. These results suggested that freezing delay could be tuned with the type and amount of anti-icing agent incorporation into the composite. We obtained more stable emulsions and more uniform composite membranes with KCOOH and $MgCl_2$. On the other hand, composite modified bitumen samples showed improved elastic property for each salt type. Comparison of salts showed the possibility of use of alternative salts for composite modified bitumen.

Overall, our results demonstrated the potential of this polymer composite-modified bitumen for anti-icing functionality, and for industrially relevant applications. However, optimized freezing point depression performance and mechanical properties of

each salt for bitumen should be further investigated. Moreover, mechanical properties of composite modified bitumen can be improved with use of cross-linked SBS. Plant scale tests of functional bitumen which include both aggregates and binder should be also conducted before application on roads.

In second part, we investigated synthesis of PEG nanospheres via water-in-water emulsion templating method for biomedical applications. We synthesised nano-scale PEG hydrogel particles using w/w emulsions using phase separation of dextran and PEG prepolymer. DLS and SEM results demonstrated that nano-scale hydrogel spheres could be obtained with this approach. We investigated the release kinetics of a model drug, pregabalin (PGB) from PEG nanospheres and demonstrated the influence of polymerization conditions on loading and release of the drug as well as the morphology and size distribution of PEG nanospheres. The experimental drug release data was fitted to a stretched exponential function which suggested high correlation with experimental results to predict half-time and drug release rates from the model equation. The biocompatibility of nanospheres on fibroblasts using cell-survival assay suggested that PEG nanospheres with altered concentrations are non-toxic, and can be considered for controlled drug/molecule delivery. This method is promising for the synthesis of PEG micro/nanospheres for biological systems, since the emulsion is aqueous and do not require organic solvents or surfactants. PEG hydrogel nanospheres synthesized via dextran-PEG w/w emulsion can be utilized for drug/ligand delivery in biomedical applications, where specific targeting could be achieved through functionalization of nanospheres.

In last part of this thesis, we used SBS for biomedical applications and demonstrated an effective approach to designing a photocrosslinked SBS network. Rheological analysis has been conducted for the investigation of the storage modulus of the resultant network. Further, we could incorporate PEG hyrdogel particles into SBS gels in order to have hybrid gels with sustained drug release properties. We synthesized a novel hydrophobic-hydrophilic hybrid gel for sustained release of a model drug with amphiphilic property, by using styrene-butadiene-styrene (SBS) hydrophobic polymer network as matrix where hydrophilic polyethylene glycol (PEG) hydrogel particles were embedded. SBS-PEG gels were characterized through SEM, water contact angle

measurements and nanoindentation tests. We investigated release of an anti rheumatoid arthritis drug from these SBS-PEG gels and observed sustained drug release up to 28 days. We demonstrated the effect of hydrophilic-hydrophobic nature and crosslinking of SBS on drug release properties. Cell survival analysis with HEK293 revealed that these networks are non-toxic. These results showed that SBS-PEG gels could be considered for a variety of biomedical applications such as drug delivery, wound dressings and 3D printing systems due to their elastic polymer network properties.

BIBLIOGRAPHY

1. Kanyas, S., et al., *Nanoparticle and gelation stabilized functional composites of an ionic salt in a hydrophobic polymer matrix.* PLoS One, 2014. **9**(2): p. e88125.
2. Aydın, D., et al., *Gelation-Stabilized Functional Composite-Modified Bitumen for Anti-icing Purposes.* Industrial & Engineering Chemistry Research, 2015. **54**(50): p. 12587-12596.
3. Bal, T., et al., *Mesenchymal stem cells and ligand incorporation in biomimetic poly(ethylene glycol) hydrogels significantly improve insulin secretion from pancreatic islets.* J Tissue Eng Regen Med, 2014.
4. Brandl, F., F. Sommer, and A. Goepferich, *Rational design of hydrogels for tissue engineering: impact of physical factors on cell behavior.* Biomaterials, 2007. **28**(2): p. 134-146.
5. Crescenzi, V., et al., *Novel hydrogels via click chemistry: synthesis and potential biomedical applications.* Biomacromolecules, 2007. **8**(6): p. 1844-1850.
6. Peppas, N.A., et al., *Hydrogels in biology and medicine: from molecular principles to bionanotechnology.* Advanced Materials-Deerfield Beach Then Weinheim-, 2006. **18**(11): p. 1345.
7. Wu, X.S. and N. Wang, *Synthesis, characterization, biodegradation, and drug delivery application of biodegradable lactic/glycolic acid polymers. Part II: biodegradation.* Journal of Biomaterials Science, Polymer Edition, 2001. **12**(1): p. 21-34.
8. Tan, G., et al., *Preparation, characterization, and drug-release properties of PEG-DA-based copolymer hydrogel microspheres.* Journal of Applied Polymer Science, 2012. **125**(5): p. 3509-3516.
9. Seymour, L., et al., *Effect of molecular weight (Mw) of N-(2-hydroxypropyl) methacrylamide copolymers on body distribution and rate of excretion after subcutaneous, intraperitoneal, and intravenous administration to rats.* Journal of biomedical materials research, 1987. **21**(11): p. 1341-1358.
10. Sultana, F., et al., *An Overview of Nanogel Drug Delivery System.* Journal of Applied Pharmaceutical Science Vol, 2013. **3**(8 Suppl 1): p. S95-S105.
11. Zhu, H. and M.J. McShane, *Synthesis and functionalization of monodisperse poly (ethylene glycol) hydrogel microspheres within polyelectrolyte multilayer microcapsules.* Chem. Commun., 2006. **2**: p. 153.
12. Aydın, D. and S. Kızılel, *Water-in-Water Emulsion Based Synthesis of Hydrogel Nanospheres with Tunable Release Kinetics.* JOM, 2016: p. 1-10.
13. Gidon, D., D. Aydin, and S. Kizilel, *Photocrosslinking of styrene-butadiene-styrene (SBS) networks formed by thiol-ene reactions and their influence on cell survival.* Biomedical Materials, 2015. **10**(6): p. 065001.
14. Maderuelo, C., A. Zarzuelo, and J.M. Lanao, *Critical factors in the release of drugs from sustained release hydrophilic matrices.* Journal of controlled release, 2011. **154**(1): p. 2-19.
15. Sun, L., et al., *Preparation and evaluation of sustained-release azithromycin tablets in vitro and in vivo.* Asian Journal of Pharmaceutical Sciences, 2014. **9**(3): p. 155-161.
16. Jagur-Grodzinski, J., *Polymeric gels and hydrogels for biomedical and pharmaceutical applications.* Polymers for Advanced Technologies, 2010. **21**(1): p. 27-47.

17. Yang, J.M., et al., *Preparation of heparin containing SBS-g-VP copolymer membrane for biomaterial usage.* Journal of Membrane Science, 1998. **138**(1): p. 19-27.
18. Stubenrauch, C., *Microemulsions: background, new concepts, applications, perspectives*. 2009: Wiley.
19. Kenar, J., *FOOD EMULSIONS: PRINCIPLES, PRACTICES, AND TECHNIQUES.* Review Article, 2005. **12**(12): p. 760.
20. Ikem, V.O., et al., *Highly permeable macroporous polymers synthesized from pickering medium and high internal phase emulsion templates.* Advanced Materials, 2010. **22**(32): p. 3588-3592.
21. Imhof, A. and D. Pine, *Ordered macroporous materials by emulsion templating.* Nature, 1997. **389**(6654): p. 948-951.
22. Silverstein, M.S., *Emulsion-templated porous polymers: a retrospective perspective.* Polymer, 2014. **55**(1): p. 304-320.
23. Tadros, T.F., *Emulsion science and technology: a general introduction*. 2009: Wiley-VCH Verlag GmbH and Co. KGaA: Weinheim.
24. Prince, L., *Microemulsions theory and practice*. 2012: Elsevier.
25. Akartuna, I., et al., *General Route for the Assembly of Functional Inorganic Capsules.* Langmuir, 2009. **25**(21): p. 12419-12424.
26. Akartuna, I., et al., *Macroporous polymers from particle-stabilized emulsions.* Polymer, 2009. **50**(15): p. 3645-3651.
27. Cayre, O.J., P.F. Noble, and V.N. Paunov, *Fabrication of novel colloidosome microcapsules with gelled aqueous cores.* Journal of Materials Chemistry, 2004. **14**(22): p. 3351-3355.
28. Menner, A., et al., *Tough reinforced open porous polymer foams via concentrated emulsion templating.* Polymer, 2006. **47**(22): p. 7628-7635.
29. Zoldesi, C.I. and A. Imhof, *Synthesis of monodisperse colloidal spheres, capsules, and microballoons by emulsion templating.* Advanced materials, 2005. **17**(7): p. 924-928.
30. Dai, L.L., R. Sharma, and C.-y. Wu, *Self-Assembled Structure of Nanoparticles at a Liquid− Liquid Interface.* Langmuir, 2005. **21**(7): p. 2641-2643.
31. Lin, Y., et al., *Nanoparticle assembly at fluid interfaces: structure and dynamics.* Langmuir, 2005. **21**(1): p. 191-194.
32. Wu, J. and G.H. Ma, *Recent Studies of Pickering Emulsions: Particles Make the Difference.* Small, 2016. **12**(34): p. 4633-4648.
33. Binks, B.P., *Particles as surfactants—similarities and differences.* Current opinion in colloid & interface science, 2002. **7**(1): p. 21-41.
34. Kanyas, S., et al., *Nanoparticle and gelation stabilized functional composites of an ionic salt in a hydrophobic polymer matrix.* PloS one, 2014. **9**(2): p. e88125.
35. Binks, B. and S. Lumsdon, *Influence of particle wettability on the type and stability of surfactant-free emulsions.* Langmuir, 2000. **16**(23): p. 8622-8631.
36. Paunov, V.N., *Novel method for determining the three-phase contact angle of colloid particles adsorbed at air− water and oil− water interfaces.* Langmuir, 2003. **19**(19): p. 7970-7976.
37. Grigoriev, D., et al., *Contact angle determination of micro-and nanoparticles at fluid/fluid interfaces: the excluded area concept.* Physical Chemistry Chemical Physics, 2007. **9**(48): p. 6447-6454.
38. Lin, Y., et al., *Nanoparticle assembly at fluid interfaces: structure and dynamics.* Langmuir, 2005. **21**: p. 191-194.

39. Wei, Z. and M. Wan, *Hollow microspheres of polyaniline synthesized with an aniline emulsion template.* Advanced Materials, 2002. **14**(18): p. 1314-1317.
40. Stejskal, J., et al., *Polyaniline Dispersions. 6.† Stabilization by Colloidal Silica Particles.* Macromolecules, 1996. **29**(21): p. 6814-6819.
41. Nan, F., et al., *Uniform chitosan-coated alginate particles as emulsifiers for preparation of stable Pickering emulsions with stimulus dependence.* Colloids and Surfaces A: Physicochemical and Engineering Aspects, 2014. **456**: p. 246-252.
42. Binks, B. and S. Lumsdon, *Pickering emulsions stabilized by monodisperse latex particles: effects of particle size.* Langmuir, 2001. **17**(15): p. 4540-4547.
43. Whitby, C.P. and E.J. Wanless, *Controlling Pickering emulsion destabilisation: a route to fabricating new materials by phase inversion| NOVA. The University of Newcastle's Digital Repository.* 2016.
44. King, W.J., M.W. Toepke, and W.L. Murphy, *Facile formation of dynamic hydrogel microspheres for triggered growth factor delivery.* Acta biomaterialia, 2011. **7**(3): p. 975-985.
45. Elbert, D.L., *Liquid–liquid two-phase systems for the production of porous hydrogels and hydrogel microspheres for biomedical applications: a tutorial review.* Acta biomaterialia, 2011. **7**(1): p. 31-56.
46. Franssen, O. and W.E. Hennink, *A novel preparation method for polymeric microparticles without the use of organic solvents.* International Journal of Pharmaceutics, 1998. **168**(1): p. 1-7.
47. Impellitteri, N.A., et al., *Specific VEGF sequestering and release using peptide-functionalized hydrogel microspheres.* Biomaterials, 2012. **33**(12): p. 3475-3484.
48. Dill, K. and S. Bromberg, *Molecular driving forces: statistical thermodynamics in biology, chemistry, physics, and nanoscience*. 2010: Garland Science.
49. Albertsson, P.-Å., *Partition of cell particles and macromolecules: separation and purification of biomolecules, cell organelles, membranes, and cells in aqueous polymer two-phase systems and their use in biochemical analysis and biotechnology*. Vol. 346. 1986: Wiley New York etc.
50. de Freitas, R.A., et al., *Stabilization of water-in-water emulsions by polysaccharide-coated protein particles.* Langmuir, 2016. **32**(5): p. 1227-1232.
51. Balakrishnan, G., et al., *Particles trapped at the droplet interface in water-in-water emulsions.* Langmuir, 2012. **28**(14): p. 5921-5926.
52. Nguyen, B.T., T. Nicolai, and L. Benyahia, *Stabilization of water-in-water emulsions by addition of protein particles.* Langmuir, 2013. **29**(34): p. 10658-10664.
53. Firoozmand, H., B.S. Murray, and E. Dickinson, *Interfacial structuring in a phase-separating mixed biopolymer solution containing colloidal particles.* Langmuir, 2009. **25**(3): p. 1300-1305.
54. Boinovich, L.B. and A.M. Emelyanenko, *Anti-icing potential of superhydrophobic coatings.* Mendeleev Communications, 2013. **23**(1): p. 3-10.
55. Kulinich, S. and M. Farzaneh, *Alkylsilane self-assembled monolayers: modeling their wetting characteristics.* Applied surface science, 2004. **230**(1): p. 232-240.
56. Kulinich, S., et al., *The icephobic performance of alkyl-grafted aluminum surfaces.* Soft Matter, 2015. **11**(5): p. 856-861.
57. Farhadi, S., M. Farzaneh, and S. Kulinich, *Anti-icing performance of superhydrophobic surfaces.* Applied Surface Science, 2011. **257**(14): p. 6264-6269.
58. Kreder, M.J., et al., *Design of anti-icing surfaces: smooth, textured or slippery?* Nature Reviews Materials, 2016. **1**: p. 15003.

59. Cao, L., et al., *Anti-icing superhydrophobic coatings.* Langmuir, 2009. **25**(21): p. 12444-12448.
60. Wang, Y., et al., *Verification of icephobic/anti-icing properties of a superhydrophobic surface.* ACS applied materials & interfaces, 2013. **5**(8): p. 3370-3381.
61. Thomas, S.K., R.P. Cassoni, and C.D. MacArthur, *Aircraft anti-icing and de-icing techniques and modeling.* Journal of Aircraft, 1996. **33**(5): p. 841-854.
62. Kim, B., et al., *Stable superhydrophobic Si surface produced by using reactive ion etching process combined with hydrophobic coatings.* Surface and Coatings Technology, 2013. **232**: p. 928-935.
63. Feng, L., et al., *Super-hydrophobic surfaces: from natural to artificial.* Advanced materials, 2002. **14**(24): p. 1857-1860.
64. Rothstein, J.P., *Slip on superhydrophobic surfaces.* Annual Review of Fluid Mechanics, 2010. **42**: p. 89-109.
65. Liu, Z., et al., *Influence of the chloride-based anti-freeze filler on the properties of asphalt mixtures.* Construction and Building Materials, 2014. **51**: p. 133-140.
66. Parent, O. and A. Ilinca, *Anti-icing and de-icing techniques for wind turbines: Critical review.* Cold regions science and technology, 2011. **65**(1): p. 88-96.
67. Olsen, K., et al., *Wind turbine blade with a system for deicing and lightning protection*. 2003, Google Patents.
68. Giuliani, F., et al., *Effectiveness of sodium chloride-based anti-icing filler in asphalt mixtures.* Construction and Building Materials, 2012. **30**: p. 174-179.
69. Weast, R.C., M.J. Astle, and W.H. Beyer, *CRC handbook of chemistry and physics*. Vol. 69. 1988: CRC press Boca Raton, FL.
70. Strong, C.K., Z. Ye, and X. Shi, *Safety effects of winter weather: the state of knowledge and remaining challenges.* Transport reviews, 2010. **30**(6): p. 677-699.
71. Liu, X. and S. Wu, *Research on the conductive asphalt concrete's piezoresistivity effect and its mechanism.* Construction and Building Materials, 2009. **23**(8): p. 2752-2756.
72. Liu, X. and S. Wu, *Study on the graphite and carbon fiber modified asphalt concrete.* Construction and Building Materials, 2011. **25**(4): p. 1807-1811.
73. Sato, K. and H. Hori. *DEVELOPMENT OF ANTI-ICING ASPHALT PAVEMENTS USING RUBBER PARTICLES*. in *New Challenges for Winter Road Service. XIth International Winter Road Congress*. 2002.
74. Lund, J.W., *Reconstruction of a pavement geothermal deicing system.* Geo-Heat Center Quarterly Bulletin, 1999. **20**(1): p. 14-17.
75. Ganjyal, G., Q. Fang, and M.A. Hanna, *Freezing points and small-scale deicing tests for salts of levulinic acid made from grain sorghum.* Bioresour Technol, 2007. **98**(15): p. 2814-8.
76. Liu, Z., *Anti-freezing materials used in asphalt pavement and its application properties.* Xi'an: Chang'an University, China, 2013.
77. Giuliani, F., et al., *Effectiveness of sodium chloride-based anti-icing filler in asphalt mixtures.* Construction and Building Materials, 2012. **30**: p. 74–179.
78. Liu, Z., et al., *Investigation on the properties of asphalt mixtures containing antifreeze fillers.* Journal of Materials in Civil Engineering, 2014. **27**(6): p. 04014180.
79. Shell-Bitumen-U.K, *The Shell Bitumen Handbook*. Vol. 1. Chertsey: Shell-Bitumen.
80. Stastna, J., L. Zanzotto, and K. Ho, *Fractional complex modulus manifested in asphalts.* Rheologica Acta, 1994. **33**(4): p. 344-354.
81. Ait-Kadi, A., B. Brahimi, and M. Bousmina, *Polymer blends for enhanced asphalt binders.* Polymer Engineering & Science, 1996. **36**(12): p. 1724-1733.

82. Collins, J., et al., *Improved performance of paving asphalts by polymer modification (with discussion).* Journal of the Association of Asphalt Paving Technologists, 1991. **60**.
83. Zhu, J., B. Birgisson, and N. Kringos, *Polymer modification of bitumen: Advances and challenges.* European Polymer Journal, 2014. **54**: p. 18-38.
84. Newman, J.K., *Dynamic shear rheological properties of polymer-modified asphalt binders.* Journal of Elastomers & Plastics, 1998. **30**(3): p. 245-263.
85. King, G., et al., *Additives in asphalt.* Journal of the Association of Asphalt Paving Technologists, 1999. **68**: p. 32-69.
86. Bates, R. and R. Worch, *Styrene–butadiene rubber latex modified asphalt.* Engineering Brief, 1987(39).
87. Oliver, J. and K. Khoo. *Ensuring the quality of SBS modified binders*. in *ARRB Conference, 25th, 2012, Perth, Western Australia, Australia*. 2012.
88. Lu, X., H. Soenen, and P. Redelius, *Rheological characterization of polymer modified bitumens.* Ann Trans Nordic Rheol Soc, 2011. **19**.
89. Airey, G., *Rheological properties of styrene butadiene styrene polymer modified road bitumens.* Fuel, 2003. **82**(14): p. 1709-1719.
90. Lesueur, D., et al., *A structure-related model to describe asphalt linear viscoelasticity.* Journal of Rheology, 1996. **40**(5): p. 813-836.
91. Allen, R.G., D.N. Little, and A. Bhasin, *Structural characterization of micromechanical properties in asphalt using atomic force microscopy.* Journal of Materials in Civil Engineering, 2012. **24**(10): p. 1317-1327.
92. MASSON, J.F., V. Leblond, and J. Margeson, *Bitumen morphologies by phase-detection atomic force microscopy.* Journal of Microscopy, 2006. **221**(1): p. 17-29.
93. McCarron, B., et al., *The Investigation of "Bee-Structures" in Asphalt Binders.* Major Qualifying Project, Worcester Polytechnic Institute, 2012.
94. De Moraes, M., et al., *High temperature AFM study of CAP 30/45 pen grade bitumen.* Journal of Microscopy, 2010. **239**(1): p. 46-53.
95. Jäger, A., et al., *Identification of four material phases in bitumen by atomic force microscopy.* Road Materials and Pavement Design, 2004. **5**(sup1): p. 9-24.
96. Jäger, A., et al., *Identification of microstructural components of bitumen by means of atomic force microscopy (AFM).* PAMM, 2004. **4**(1): p. 400-401.
97. Dourado, E., R. Simao, and L. Leite, *Mechanical properties of asphalt binders evaluated by atomic force microscopy.* Journal of microscopy, 2012. **245**(2): p. 119-128.
98. Sengoz, B. and G. Isikyakar, *Analysis of styrene-butadiene-styrene polymer modified bitumen using fluorescent microscopy and conventional test methods.* Journal of Hazardous Materials, 2008. **150**(2): p. 424-432.
99. Bal, T., B. Kepsutlu, and S. Kizilel, *Characterization of protein release from poly(ethylene glycol) hydrogels with crosslink density gradients.* Journal of Biomedical Materials Research Part A, 2014. **102**(2): p. 487-495.
100. Hoffman, A.S., *Applications of thermally reversible polymers and hydrogels in therapeutics and diagnostics.* Journal of Controlled Release, 1987. **6**(1): p. 297-305.
101. Langer, R., *Drugs on target.* Science, 2001. **293**(5527): p. 58-59.
102. Peppas, N.A., et al., *Hydrogels in biology and medicine: from molecular principles to bionanotechnology.* Advanced materials, 2006. **18**(11): p. 1345-1360.
103. Dadsetan, M., et al., *Characterization of photo-cross-linked oligo [poly (ethylene glycol) fumarate] hydrogels for cartilage tissue engineering.* Biomacromolecules, 2007. **8**(5): p. 1702-1709.

104. Oh, J.K., et al., *The development of microgels/nanogels for drug delivery applications.* Progress in Polymer Science, 2008. **33**(4): p. 448-477.
105. Zhang, H., et al., *Design of biocompatible chitosan microgels for targeted pH-mediated intracellular release of cancer therapeutics.* Biomacromolecules, 2006. **7**(5): p. 1568-1572.
106. Zhu, H. and M.J. McShane, *Synthesis and functionalization of monodisperse poly (ethylene glycol) hydrogel microspheres within polyelectrolyte multilayer microcapsules.* Chem. Commun., 2006(2): p. 153-155.
107. Harris, J.M., *Poly (ethylene glycol) chemistry: biotechnical and biomedical applications*. 2013: Springer Science & Business Media.
108. Zhang, L., et al., *Biocompatible and pH-sensitive PEG hydrogels with degradable phosphoester and phosphoamide linkers end-capped with amine for controlled drug delivery.* Polymer Chemistry, 2013. **4**(4): p. 1084-1094.
109. Singh, S.P., et al., *A peptide functionalized poly (ethylene glycol)(PEG) hydrogel for investigating the influence of biochemical and biophysical matrix properties on tumor cell migration.* Biomaterials science, 2014. **2**(7): p. 1024-1034.
110. Raic, A., et al., *Biomimetic macroporous PEG hydrogels as 3D scaffolds for the multiplication of human hematopoietic stem and progenitor cells.* Biomaterials, 2014. **35**(3): p. 929-940.
111. Yu, J., et al., *In situ covalently cross-linked PEG hydrogel for ocular drug delivery applications.* International journal of pharmaceutics, 2014. **470**(1): p. 151-157.
112. Culver, H.R., J.R. Clegg, and N.A. Peppas, *Analyte-Responsive Hydrogels: Intelligent Materials for Biosensing and Drug Delivery.* Accounts of Chemical Research, 2017. **50**(2): p. 170-178.
113. Shin, D.S., et al., *Sensing Conductive Hydrogels for Rapid Detection of Cytokines in Blood.* Advanced healthcare materials, 2016.
114. Vashist, A., et al., *Recent advances in hydrogel based drug delivery systems for the human body.* Journal of Materials Chemistry B, 2014. **2**(2): p. 147-166.
115. Wu, Y.-H., et al., *Water uptake, transport and structure characterization in poly (ethylene glycol) diacrylate hydrogels.* Journal of Membrane Science, 2010. **347**(1): p. 197-208.
116. Jung, T., et al., *Biodegradable nanoparticles for oral delivery of peptides: is there a role for polymers to affect mucosal uptake?* European Journal of Pharmaceutics and Biopharmaceutics, 2000. **50**(1): p. 147-160.
117. Hobbs, S.K., et al., *Regulation of transport pathways in tumor vessels: role of tumor type and microenvironment.* Proceedings of the National Academy of Sciences, 1998. **95**(8): p. 4607-4612.
118. King, W.J., et al., *Triggered drug release from dynamic microspheres via a protein conformational change.* Macromolecular bioscience, 2010. **10**(6): p. 580-584.
119. Stenekes, R.J., et al., *The preparation of dextran microspheres in an all-aqueous system: effect of the formulation parameters on particle characteristics.* Pharmaceutical research, 1998. **15**(4): p. 557-561.
120. Bon, S.A. and T. Chen, *Pickering stabilization as a tool in the fabrication of complex nanopatterned silica microcapsules.* Langmuir, 2007. **23**(19): p. 9527-9530.
121. Shen, S.-L., et al., *A novel process to synthesize magnetic hollow silica microspheres.* Colloids and Surfaces A: Physicochemical and Engineering Aspects, 2007. **311**(1): p. 99-105.

122. Zhang, K., et al., *Pickering emulsion polymerization: preparation of polystyrene/nano-SiO 2 composite microspheres with core-shell structure.* Powder Technology, 2009. **190**(3): p. 393-400.
123. Xiao, Q., et al., *Preparation and characterization of polyaniline/nano-Fe 3 O 4 composites via a novel Pickering emulsion route.* Synthetic Metals, 2007. **157**(18): p. 784-791.
124. Chen, M., et al., *Synthesis of raspberry-like PMMA/SiO2 nanocomposite particles via a surfactant-free method.* Macromolecules, 2004. **37**(25): p. 9613-9619.
125. He, Y. and X. Yu, *Preparation of silica nanoparticle-armored polyaniline microspheres in a Pickering emulsion.* Materials Letters, 2007. **61**(10): p. 2071-2074.
126. Maeda, H., et al., *Pickering-type water-in-oil-in-water multiple emulsions toward multihollow nanocomposite microspheres.* Langmuir, 2010. **26**(17): p. 13727-13731.
127. Wei, Z., et al., *Facile fabrication of biocompatible PLGA drug-carrying microspheres by O/W pickering emulsions.* Colloids and Surfaces B: Biointerfaces, 2012. **91**: p. 97-105.
128. Andrew K. Fraser , C.S.K., Chien-Chi Lin, *PEG-Based Microgels Formed by Visible-Light-Mediated Thiol-Ene Photo-Click Reactions.* Macromolecular Chemistry and Physics, 2014. **215**: p. 507−515.
129. Dadsetan, M., et al., *Controlled release of doxorubicin from pH-responsive microgels.* Acta biomaterialia, 2013. **9**(3): p. 5438-5446.
130. Liggins, R.T. and H.M. Burt, *Paclitaxel loaded poly (L-lactic acid) microspheres: properties of microspheres made with low molecular weight polymers.* International journal of pharmaceutics, 2001. **222**(1): p. 19-33.
131. Berkland, C., K.K. Kim, and D.W. Pack, *PLG microsphere size controls drug release rate through several competing factors.* Pharmaceutical research, 2003. **20**(7): p. 1055-1062.
132. Mosharraf, M. and C. Nyström, *The effect of particle size and shape on the surface specific dissolution rate of microsized practically insoluble drugs.* International Journal of Pharmaceutics, 1995. **122**(1-2): p. 35-47.
133. C. Decker, T.N.T.V., *High-Speed Photocrosslinking of Thermoplastic Styrene-Butadiene Elastomers.* J Appl Polym Sci, 2000. **77**: p. 1902-1912.
134. Higginbotham, J.E.K.a.C.L., *Synthesis and Characterisation of Styrene Butadiene Styrene Based Grafted Copolymers for Use in Potential Biomedical Applications*, in *Biomedical Engineering, Trends in Materials Science*, A. Laskovski, Editor. 2011, inTech. p. 465-488.
135. Ranade, S.V., R.E. Richard, and M.N. Helmus, *Styrenic block copolymers for biomaterial and drug delivery applications.* Acta Biomater, 2005. **1**(1): p. 137-44.
136. Mark, J.E., *Polymer data handbook*. 2009: Oxford university press.
137. De, S.K. and J.R. White, *Rubber technologist's handbook*. Vol. 1. 2001: iSmithers Rapra Publishing.
138. Yoda, R., *Elastomers for biomedical applications.* Journal of Biomaterials Science, Polymer Edition, 1998. **9**(6): p. 561-626.
139. Dong-Hyuk Lim, H.-S.D., Hyun-Joong Kim, Jung-Suk Bang, Goan-Hee Yoon, *Preparation of SIS-SBS-based UV-cross-linkable pressure-sensitive adhesives using the thiol-ene reaction.* J. Adhesion Sci. Technol., 2007. **21**(7): p. 589-603.
140. Yang, J.M. and S.C. Tsai, *Biocompatibility of epoxidized styrene–butadiene–styrene block copolymer membrane.* Materials Science and Engineering: C, 2010. **30**(8): p. 1151-1156.
141. Ozlem Cevik, D.G., Seda Kizilel, *Visible-light-induced synthesis of pH-responsive composite hydrogels for controlled delivery of the anticonvulsant drug pregabalin.* Acta Biomaterialia, 2014. **11**: p. 51–161.

142. Mateo, J.L., M. Calvo, and P. Bosch, *Physical and mechanical properties of photopolymerized SBS-methacrylic monomer systems.* Journal of Applied Polymer Science, 2003. **89**(10): p. 2857-2864.
143. Roh, D.K., et al., *Proton Conducting Crosslinked Polymer Electrolyte Membranes Based on SBS Block Copolymer.* Journal of Applied Polymer Science, 2011. **121**(6): p. 3283-3291.
144. Bai, J., et al., *A simple approach to preparation of polyhedral oligomeric silsesquioxane crosslinked poly(styrene-b-butadiene-b-styrene) elastomers with a unique micro-morphology via UV-induced thiol-ene reaction.* Polymer Chemistry, 2014. **5**(23): p. 6761-6769.
145. Bai, J., et al., *Tailoring the Morphologies and Mechanical Properties of Styrene-Butadiene-Styrene Triblock Copolymers by the Incorporation of Thiol Functionalized Benzoxazine.* Macromolecules, 2014. **47**(9): p. 2964-2973.
146. Wang, Y.K., et al., *Mechanical and shape memory behavior of chemically cross-linked SBS/LDPE blends.* Journal of Polymer Research, 2014. **21**(4): p. 1-10.
147. Guoliang Wu, Y.J., Lei Ye, Songjun Zeng, Puren Yu, Weijian Xu *A novel UV-crosslinked pressure-sensitive adhesive based on photoinitiator-grafted SBS.* International Journal of Adhesion & Adhesives, 2010. **30**: p. 43-46.
148. Decker, C. and T.N.T. Viet, *Photocrosslinking of functionalized rubbers IX. Thiol-ene polymerization of styrene-butadiene-block-copolymers.* Polymer, 2000. **41**(11): p. 3905-3912.
149. Shih, H. and C.C. Lin, *Visible-light-mediated thiol-ene hydrogelation using eosin-Y as the only photoinitiator.* Macromol Rapid Commun, 2013. **34**(3): p. 269-73.
150. Shih, H., A.K. Fraser, and C.C. Lin, *Interfacial thiol-ene photoclick reactions for forming multilayer hydrogels.* ACS Appl Mater Interfaces, 2013. **5**(5): p. 1673-80.
151. Sandy P. S. Koo, M.M.S., R. Arun Prasath, Andrew J. Inglis, Filip E. Du Prez, Christopher Barner-Kowollik, Wim Van Camp, Thomas Junkers, *Limitations of Radical Thiol-ene Reactions for Polymer–Polymer Conjugation.* Journal of Polymer Science: Part A: Polymer Chemistry, 2010. **48**(8): p. 1699-1713.
152. Nazli, C., et al., *RGDS-functionalized polyethylene glycol hydrogel-coated magnetic iron oxide nanoparticles enhance specific intracellular uptake by HeLa cells.* Int J Nanomedicine, 2012. **7**: p. 1903-20.
153. Kizilel, S., V.H. Perez-Luna, and F. Teymour, *Photopolymerization of poly(ethylene glycol) diacrylate on eosin-functionalized surfaces.* Langmuir, 2004. **20**(20): p. 8652-8.
154. Aranberri, I., et al., *Synthesis of macroporous silica from solid-stabilised emulsion templates.* Journal of Porous Materials, 2009. **16**(4): p. 429-437.
155. Binks, B.P., *Macroporous silica from solid-stabilized emulsion templates.* Advanced Materials, 2002. **14**(24): p. 1824-1827.
156. Busby, W., N.R. Cameron, and A.B.C. Jahoda, *Tissue engineering matrixes by emulsion templating.* Polymer International, 2002. **51**(10): p. 871-881.
157. Dubois, R. and P.Y. Dubois, *Process for preventing formation of black ice on roads by applying a mixture of salt and aqueous fixation composition onto the road surface*. 1984, Selfixat, S. A.: Switzerland.
158. Haibach, K., et al., *Tailoring mechanical properties of highly porous polymer foams: Silica particle reinforced polymer foams via emulsion templating.* Polymer, 2006. **47**(13): p. 4513-4519.

159. Ikem, V.O., et al., *Highly permeable macroporous polymers synthesized from pickering medium and high internal phase emulsion templates.* Advanced Materials, 2010. **22**(32): p. 3588-92.
160. Imhof, A. and D.J. Pine, *Ordered macroporous materials by emulsion templating.* Nature, 1997. **389**(6654): p. 948-951.
161. Imhof, A. and D.J. Pine, *Uniform macroporous ceramics and plastics by emulsion templating.* Chemical Engineering & Technology, 1998. **21**(8): p. 682-685.
162. Pulko, I. and P. Krajnc, *Open cellular reactive porous membranes from high internal phase emulsions.* Chem Commun (Camb), 2008(37): p. 4481-3.
163. Pulko, I., et al., *Ultra-high surface area functional porous polymers by emulsion templating and hypercrosslinking: efficient nucleophilic catalyst supports.* Chemistry, 2010. **16**(8): p. 2350-4.
164. Ruckenstein, E. and C.H. H., *Preparation of a water - permselective composite membrane by the concentrated emulsion method: Its swelling and permselectivity characteristics.* Journal of Applied Polymer Science, 1991. **42**(9): p. 2429–2434.
165. Wei, Z.X. and M.X. Wan, *Hollow microspheres of polyaniline synthesized with an aniline emulsion template.* Advanced Materials, 2002. **14**(18): p. 1314-+.
166. Zoldesi, C.I. and A. Imhof, *Synthesis of monodisperse colloidal spheres, capsules, and microballoons by emulsion templating.* Advanced Materials, 2005. **17**(7): p. 924-+.
167. Melle, S., M. Lask, and G. Fuller, *Pickering emulsions with controllable stability.* Langmuir, 2004. **21**: p. 2158-2162.
168. Dai, L.L., *Self-assembled structure of nanoparticles at a liquid-liquid interface.* Langmuir, 2005. **21**: p. 2641-2643.
169. Pickering, E.C., *Photographs of Faint Stars.* Science, 1907. **25**(637): p. 435-7.
170. Ramsden, W., Proc. R. Soc., 1903. **72**(156).
171. Andrea G. Kraj, E.L.B., *Measurement method and results of ice adhesion force on the curved surface of a wind turbine blade.* Renewable Energy, 2010. **35**: p. 741–746.
172. Cuelho E, H.J., Akin M, Adams E, *Establishing best practices for removing snow and ice from California roadways*. 2010.
173. Kulinich, S.A., et al., *Superhydrophobic Surfaces: Are They Really Ice-Repellent?* Langmuir, 2011. **27**(1): p. 25-29.
174. He, M., et al., *Super-hydrophobic surfaces to condensed micro-droplets at temperatures below the freezing point retard ice/frost formation.* Soft Matter, 2011. **7**(8): p. 3993-4000.
175. Feuillebois, F., M.Z. Bazant, and O.I. Vinogradova, *Effective slip over superhydrophobic surfaces in thin channels.* Phys Rev Lett, 2009. **102**(2): p. 026001.
176. Alizadeh, A., et al., *Dynamics of ice nucleation on water repellent surfaces.* Langmuir, 2012. **28**(6): p. 3180-6.
177. Bahadur, V., et al., *Predictive model for ice formation on superhydrophobic surfaces.* Langmuir, 2011. **27**(23): p. 14143-50.
178. He, M., et al., *Super-hydrophobic film retards frost formation.* Soft Matter, 2010. **6**(11): p. 2396-2399.
179. Hellsten, P.P., et al, *Use of potassium formate in road winter deicing can reduce groundwater deterioration.* Environ Sci Technol, 2005. **39(13)**: p. 5095-5100.
180. Hall, D.L., S.M. Sterner, and R.J. Bodnar, *Freezing point depression of NaCl KCl H20 solutions.* Economic Geology, 1988. **83**: p. 197-202.

181. Shi X, L.Y., Mooney M, Berry M, Hubbard B, Fay L, Leonard AB, *Effect of chloride-based deicers on reinforced concrete structures.* WSDOT Research Report WA-RD 741.1, Washington State Department of Transportation, USA, 2010.
182. Starck P, L.B., *Effect of de-icing agents on the viscoelastic properties of asphalt mastics.* J Mater Sci. **42**: p. 676–85.
183. Testa, D., *Highway operations: progress and products update, SHRP*. 1991, National Research Council, Washington.
184. Penn LS, M., *Ice-pavement bond prevention: fundamental study, SHRP-W/UFR-92-606.* National Research Council, Washington, 1992.
185. Nilsson, F. *Durability problems on Nordic airfields-the influence of deicing agents on asphalt concrete*. in *The XXIInd PIARC World Road Congress*. 2003.
186. Santagata, E., O. Baglieri, and P.P. Riviera. *Effect of anti-icing chemicals on stripping of asphalt concrete mixtures for airport runway wearing courses*. in *Airfield and Highway Pavement 2013@ sSustainable and Efficient Pavements*. 2013. ASCE.
187. Pan, T., X. He, and X. Shi, *Laboratory investigation of acetate-based deicing/anti-icing agents deteriorating airfield asphalt concrete.* Asphalt Paving Technology-Proceedings, 2008. **77**: p. 773.
188. Perezlepe, A., *Influence of the processing conditions on the rheological behaviour of polymer-modified bitumen.* Fuel, 2003. **82**(11): p. 1339-1348.
189. Sengoz, B. and G. Isikyakar, *Analysis of styrene-butadiene-styrene polymer modified bitumen using fluorescent microscopy and conventional test methods.* J Hazard Mater, 2008. **150**(2): p. 424-32.
190. Yildirim, Y., *Polymer modified asphalt binders.* Construction and Building Materials, 2007. **21**(1): p. 66-72.
191. Xiaohu Lu, U.l., *Chemical and rheological evaluation of ageing properties of SBS polymer modified bitumens.* Fuel, 1998. **77**: p. 9-10.
192. Zhu, J., Birgisson, B., Kringos, N., *Polymer modification of bitumen: Advances and challenges.* European Polymer Journal, 2014. **54**: p. 18-38.
193. Bulatović, V.O., V. Rek, and K.J. Marković, *Effect of polymer modifiers on the properties of bitumen.* Journal of Elastomers and Plastics, 2014. **46**(5): p. 448-469.
194. Bulatovic, V., V. Rek, and K. Markovic, *Polymer modified bitumen.* Materials research innovations, 2012. **16**(1): p. 1-6.
195. Airey, G.D., *Styrene butadiene styrene polymer modification of road bitumens.* Journal of Materials Science, 2004. **39**(3): p. 951-959.
196. V. Carrera, A.A.C., M. García-Morales, P. Partal, *Influence of the prepolymer molecular weight and free isocyanate content on the rheology of polyurethane modified bitumens.* European Polymer Journal, 2014. **57**: p. 151–159.
197. Lesueur, D., *The colloidal structure of bitumen: consequences on the rheology and on the mechanisms of bitumen modification.* Adv Colloid Interface Sci, 2009. **145**(1-2): p. 42-82.
198. L. Loebera, G.M., J. Morelb and O. Sutton C *Bitumen in colloid science: a chemical, structural and rheological approach* Fuel, 1998. **77**: p. 1443-1450.
199. Masson, J.F., V. Leblond, and J. Margeson, *Bitumen morphologies by phase-detection atomic force microscopy.* J Microsc, 2006. **221**(Pt 1): p. 17-29.
200. Prat, S., *Antogonistic salt action in relation to the swelling and dyeing of powdered agar.* American Journal of Botany, 1927. **14**: p. 167-186.
201. Adubiaro, H., O. Olaofe, and E. Akintayo, *Effect of Salts on the Emulsifying Properties of Adansonia digitata (Baobab) Seed Flour.* Advance Journal of Food Science and Technology, 2012.

202. Binks, B.P., et al., *Effects of pH and salt concentration on oil-in-water emulsions stabilized solely by nanocomposite microgel particles.* Langmuir, 2006. **22**(5): p. 2050-2057.
203. Jo, Y.-J., et al., *Effect of NaCl Concentration on the Emulsifying Properties of Myofibrilla Protein in the Soybean Oil and Fish Oil Emulsion.* Korean Journal for Food Science of Animal Resources, 2015. **35**(3): p. 315.
204. Freiberg, S. and X. Zhu, *Polymer microspheres for controlled drug release.* International journal of pharmaceutics, 2004. **282**(1): p. 1-18.
205. Kim, T.H., et al., *PEGylated TNF-related apoptosis-inducing ligand (TRAIL)-loaded sustained release PLGA microspheres for enhanced stability and antitumor activity.* Journal of Controlled Release, 2011. **150**(1): p. 63-69.
206. Miller, S.J., *The method of least squares.* Mathematics Department Brown University, 2006: p. 1-7.
207. Socrates, G., *Infrared and Raman characteristic group frequencies: tables and charts*. 2004, West Sussex, England: John Wiley & Sons. 71-72.
208. Cevik, O., D. Gidon, and S. Kizilel, *Visible-light-induced synthesis of pH-responsive composite hydrogels for controlled delivery of the anticonvulsant drug pregabalin.* Acta biomaterialia, 2015. **11**: p. 151-161.
209. Davies, P.F. and S. Tripathi, *Mechanical stress mechanisms and the cell. An endothelial paradigm.* Circulation research, 1993. **72**(2): p. 239-245.
210. Oliver, W.C. and G.M. Pharr, *An improved technique for determining hardness and elastic modulus using load and displacement sensing indentation experiments.* Journal of materials research, 1992. **7**(06): p. 1564-1583.
211. Pharr, G., W. Oliver, and F. Brotzen, *On the generality of the relationship among contact stiffness, contact area, and elastic modulus during indentation.* Journal of materials research, 1992. **7**(03): p. 613-617.
212. Decker, C. and T.N.T. Viet, *Photocrosslinking of functionalized rubbers, 8. The thiol-polybutadiene system.* Macromolecular Chemistry and Physics, 1999. **200**(8): p. 1965-1974.
213. Czerner, M., et al., *Determination of elastic modulus of gelatin gels by indentation experiments.* Procedia Materials Science, 2015. **8**: p. 287-296.
214. Wanasekara, N.D., et al. *Nano-indentation of epoxy hydro gels for soft tissue applications*. in *Bioengineering Conference, 2009 IEEE 35th Annual Northeast*. 2009. IEEE.
215. Kaufman, J.D., et al., *Time-dependent mechanical characterization of poly (2-hydroxyethyl methacrylate) hydrogels using nanoindentation and unconfined compression.* Journal of materials research, 2008. **23**(05): p. 1472-1481.
216. Tang, Z., et al., *Nanostructured artificial nacre.* Nature materials, 2003. **2**(6): p. 413-418.
217. Schneider, A., et al., *Elasticity, biodegradability and cell adhesive properties of chitosan/hyaluronan multilayer films.* Biomedical Materials, 2007. **2**(1): p. S45.
218. Jacobson, G.B., et al., *Sustained release of drugs dispersed in polymer nanoparticles.* Angewandte Chemie International Edition, 2008. **47**(41): p. 7880-7882.
219. Yilgor, P., et al., *Incorporation of a sequential BMP-2/BMP-7 delivery system into chitosan-based scaffolds for bone tissue engineering.* Biomaterials, 2009. **30**(21): p. 3551-3559.

VITA

Derya Aydın was born in Istanbul, Turkey, on March 4, 1985. She received her B.Sc. Degree in Food Engineering from Hacettepe University, Istanbul, in 2008. She worked in INTERKIM as an R&D engineer for 2 years and worked on improvement of formulations for food ingredients. She received her M.Sc. Degree in Computational Sciences and Engineering from Koç University, Istanbul, in 2012. She has worked on "Identifying plant based small molecule inhibitors for biologically important targets in cancer" during her M.Sc. study. From October 2012 to Jue 2017, she worked as teaching and research assistant at Koç University, Istanbul, Turkey where she pursued a Ph.D. study. She worked on "Design of Functional Materials via Emulsion Templating for Energy and Biomedical Application"during her Ph.D.